INFORMATION TO USERS

This dissertation was produced from a microfilm copy of the original document. While the most advanced technological means to photograph and reproduce this document have been used, the quality is heavily dependent upon the quality of the original submitted.

The following explanation of techniques is provided to help you understand markings or patterns which may appear on this reproduction.

1. The sign or "target" for pages apparently lacking from the document photographed is "Missing Page(s)". If it was possible to obtain the missing page(s) or section, they are spliced into the film along with adjacent pages. This may have necessitated cutting thru an image and duplicating adjacent pages to insure you complete continuity.

2. When an image on the film is obliterated with a large round black mark, it is an indication that the photographer suspected that the copy may have moved during exposure and thus cause a blurred image. You will find a good image of the page in the adjacent frame.

3. When a map, drawing or chart, etc., was part of the material being photographed the photographer followed a definite method in "sectioning" the material. It is customary to begin photoing at the upper left hand corner of a large sheet and to continue photoing from left to right in equal sections with a small overlap. If necessary, sectioning is continued again – beginning below the first row and continuing on until complete.

4. The majority of users indicate that the textual content is of greatest value, however, a somewhat higher quality reproduction could be made from "photographs" if essential to the understanding of the dissertation. Silver prints of "photographs" may be ordered at additional charge by writing the Order Department, giving the catalog number, title, author and specific pages you wish reproduced.

University Microfilms

300 North Zeeb Road
Ann Arbor, Michigan 48106

A Xerox Education Company

AXIAL PRESSURE PROFILES IN NON-NEWTONIAN FLOW

by

DAVID BLUM

A dissertation submitted to the Graduate Faculty in Engineering in partial fulfillment of the requirements for the degree of Doctor of Philosophy, The City University of New York.

1972

This manuscript has been read and accepted by the Graduate Faculty in Engineering in satisfaction of the dissertation requirement for the degree of Doctor of Philosophy.

4/26/72
Date

David J. Williams
Chairman of Examining Committee

4/26/72
Date

Jacques E. Benveniste
Executive Officer

Professor Jacques Benveniste

Professor Robert A. Graff

Professor Robert Pfeffer

Professor David J. Williams
Chairman

Supervisory Committee

The City University of New York

SYNOPSIS

Polymeric fluids exhibit interesting and unusual patterns of behavior in capillary flow. This behavior is a direct manifestation of the fluids' viscoelastic character. The capillary rheometer is a particularly important device for studying such behavior from both industrial and theoretical viewpoints. The focus of this research was the measurement of the axial pressure profiles in a capillary rheometer for polymeric fluids in stable flow. Such measurements have received scant attention to date, which is unfortunate inasmuch as they readily yield valuable insight into the mechanisms of viscoelastic flow.

Several regions are defined in the capillary rheometer. The rapid acceleration of the polymeric fluid as it flows from the (a) reservoir, through an (b) entry region, into the capillary generates substantial elastic strains. The attendant elastic energy is dissipated in a (c) relaxation region, after which (d) viscometric flow commences. In the (e) free stream region the polymeric fluid experiences jet swelling. The flow behavior in the first four regions is clearly delineated by the axial pressure profile measurements herein reported.

As an essential preliminary, we examined the effects of

recess transducer mount geometries on the measured stresses in both slits and tubes. This was done to insure the accuracy of the pressure measurements with the recess mount configurations imposed by the physical constraints of current transducer technology. This effort carried additional significance since the literature reports that artifacts could be expected with such recess mount systems. These predictions notwithstanding, no mount geometry errors were observed for either viscoelastic or viscoinelastic fluids over a shear rate range of 1 to 2000 sec^{-1}.

Viscometric flow is described in terms of three material functions: namely, the shear stress, plus the first and second normal stress differences. These parameters were evaluated for a highly viscoelastic fluid (16.5% polyisobutylene in mineral spirits). This study was executed over a wider range of shear rates and with a higher degree of thoroughness than hitherto reported in the literature. Unanticipated patterns in the behavior of the material functions were observed. The first and second normal stress differences were significantly larger than the shear stress. Further, the second normal stress difference rose to a maximum, where it was more than ten-times larger than the first normal stress difference. Finally, the shear stress-shear rate curve exhibited a nearly flat section. All these behaviors were explained with quali-

tative molecular arguments. Less rigorous methods for predicting the material functions were examined, and some were found useful for order of magnitude approximations.

We introduce the concept of excess elastic stress - evaluated by the measured pressures - to characterize flow in the relaxation region. Values of stored elastic energy determined from the excess elastic stress compare favorably with those ascertained from die swell ratios and from entrance correction methods. Furthermore, material relaxation times calculated from excess-elastic-stress relaxation and from die-swell-ratio decay are nearly identical and show an approximate inverse relation to the apparent shear rate from 50 to 5000 sec^{-1}.

ACKNOWLEDGEMENTS

I especially thank Dr. David J. Williams, for his continuous efforts on my behalf throughout this research project, and Dr. Joseph Yerushalmi, for his helpful discussions and suggestions. This research was supported by a grant from The City University of New York under the Faculty Research Award Program - CUNY/RF1018.

TABLE OF CONTENTS

cont.

TABLE OF CONTENTS (cont.)

LIST OF FIGURES

cont.

LIST OF FIGURES (cont.)

cont.

LIST OF FIGURES (cont.)

cont.

LIST OF FIGURES (cont.)

LIST OF TABLES

cont.

LIST OF TABLES (cont.)

I. INTRODUCTION

Laboratory studies of the flow of polymers through capillaries represent a particularly important and valuable approach to process design, as well as an appropriate vehicle for the study of viscoelastic fluids. The flow of polymers in capillaries is complex, and it is convenient to consider first, flows in very long tubes. As shown in Figure 1, a polymer flowing from a reservoir into a capillary is greatly accelerated in the entry region because of the funneling effect. This process generates large elastic strains with a corresponding generation of stresses as the velocity profile rearranges. The establishment of the familiar parabolic profile marks the end of the entry region (which is generally short, being on the order of one tube diameter in length) and marks the beginning of the relaxation region. This region is characterized by fading entrance-borne elastic effects generated in the entry region. This decay is accomplished via a relaxation mechanism and reflects the fading memory of the fluid with respect to past deformations. The point where entrance-borne effects have fully decayed establishes the onset of the viscometric region. Thus, we have two entrance regions: one for the rearrangement of the velocity profile, and a second one for the dissipation of entrance-borne elastic effects. In contrast to the relaxation region, the axial gradient of the

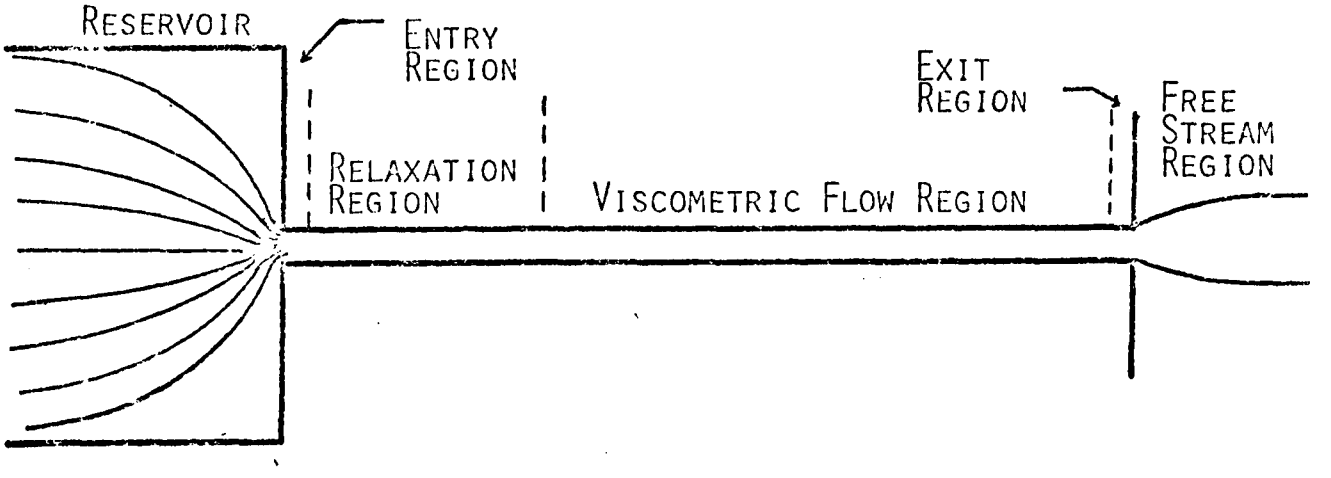

FIGURE 1. SCHEMATIC OF A CAPILLARY RHEOMETER AND THE REGIONS OF FLOW

radial stress in the flow direction is a constant in the viscometric region.

Whereas pressure measurements in the viscometric region have received some attention, published data pertaining to the relaxation region are scarce, and these are often unreliable. This situation is unfortunate since the rate of decay of the excess elastic stress and the length of the relaxation region both provide excellent measures of the extent of fluid memory under extrusion conditions.

Two important phenomena occur in the free stream region: jet swelling in stable flow and melt fracture in unstable flow. As the polymer emerges it exhibits a diameter swell often ranging up to 3 or 4 tube diameters. The swell ratio (free jet diameter/tube diameter) is dependent on the length to diameter ratio of the tube (L/D), and has been observed to decay exponentially with residence time, approaching (for sufficiently long tubes) a final value typically on the order of 1.5 to 2.0. The attainment of a final constant swell ratio indicates the onset of viscometric flow.

Above a certain critical shear stress a polymer may exhibit flow instabilities which result in the extrudate being irregular and distorted. This phenomenon has often been referred to as melt fracture. It remains one of the most puzzling effects observed in polymer fluid systems. The existing

explanations are diverse, seemingly conflicting and often speculative. The present research, however, deals only with stable flow.

We have undertaken a comprehensive experimental research program based primarily on axial pressure profile measurements. Such measurements are the only means available for examining all the regions of capillary flow; and they readily yield a measure of the excess elastic stress in the relaxation region and values for the three material functions in the viscometric region - the shear stress and the first and second normal stress differences. Two fundamentally different fluids were utilized: a viscoinelastic silicone oil and a viscoelastic polyisobutylene solution.

The theoretical concepts underlying our study are reviewed in Section II, and the experimental apparatus is described in Section III. It has been reported that recess transducer mount geometries, such as those required in this study, can cause artifacts to arise in the pressure measurements. This prospect was investigated; and, as reported in Section IV, no regular recess mount effect was observed. The results of our pressure profile studies are presented in Section V. The principal data consists of the variation of the radial stress along the tube, and of the swell ratios over an extended range of shear (1 to 4000 sec^{-1}). These measurements have yielded valuable information concerning the length of the relaxation region and

the rate of decay of the excess elastic stress as well as novel and interesting relationships between the material functions.

II. LITERATURE SURVEY

The funneling of polymer fluids into the capillary generates complex flow patterns both in the reservoir immediately adjacent to the mouth of the tube and in the entry region itself. (Although these flow patterns are closely associated with the problem of melt fracture, we confine our attention to stable entrance flow.) In contrast to the entrance flow of Newtonian fluids for which analytic solutions and well established correlations exist, the corresponding flow of polymer fluids is not well understood. Past researches have yielded visual records of the phenomenon (1-3), and several semi-empirical correlations of the pressure drop in the entrance region (4). Classical boundary layer theory for Newtonian fluids (5) predicts an entrance length for the rearranging velocity profile of $0.02875N_{Re}$ tube diameters. For purely viscous fluids obeying the power law relations Dodge (8) has shown that this entrance length ranges from 0.03 to $0.05N'_{Re}$, where N'_{Re} is the generalized Reynolds number of Metzner and Reed (7). Philippoff and Gaskins (8) and Boger and Ramamurthy (9) conclude that a viscoelastic power law fluid takes even a shorter distance than its purely viscous counterpart. In any event, with the generally small Reynolds number encountered in polymer melt flows, this entrance length may not be measured

reliably with existing techniques.

In the relaxation region the parabolic velocity profile is already established, and the region is characterized by the decay, along the flow direction, of the entrance borne elastic stresses. Thus, contrasting to the viscometric region, the deviatoric stresses in the relaxation region are a function not only of the radial position, but of the axial position as well. (Further, the axial pressure gradient is constant only in the viscometric region.) The length of the relaxation region depends on the extent of the fluid memory with respect to past deformations -- in this particular case, deformations which have occurred in the entrance region.

To date, estimates of the relaxation length are based on insufficient data and are, consequently, not reliable. For polyethylene, Kowalski (10) obtained a relaxation length of 40-60 tube diameters, basing his estimates on swell data. For a similar material, also with swell measurements, Han et al. (11-12) found that only 20 tube diameters were required. Middleman (13) concluded that 40 tube diameters constitutes the length for the flow of 13% polyisobutylene in tetralin. Pressure measurements in tubes by Sakiadis (14-15) and Han (11-12,16) and in slits by Eswaren et al. (17) yield less reliable estimates.

Flow in the viscometric region is one of the few situations for which an exact hydrodynamical solution exists. The more

general constitutive equations, such as Noll's (18-20) simple fluid theory predict the existence of three independent material functions: the shear stress and two normal stress differences -- all functions of the local shear rate. This has been corroborated by experiment (21).

With the velocity components in a tube of radius R and length L, aligned with the z-direction, given by

$$V_z = u(r) \ , \ V_r = 0 \ , \ V_\theta = 0$$

we denote the stress tensor by S_{ij} and consider its decomposition into a pressure p and a deviatoric part T_{ij}.

$$S_{ij} = -p\delta_{ij} + T_{ij}$$

where δ_{ij} is the Kronecker Delta. In the viscometric region the non-vanishing components of T_{ij} are regarded as functions of r only. The stress distribution in this region is given by (21)

(1) $T_{r\theta} = T_{z\theta} = 0$

(2) $T_{rz} = S_{rz} = \tau(K)$

where $K = du/dr$

(3) $T_{zz} - T_{rr} = S_{zz} - S_{rr} = \sigma_1(K)$

(4) $T_{rr} - T_{\theta\theta} = S_{rr} - S_{\theta\theta} = \sigma_2(K)$

The equations of motion reduce to

$$(5) \qquad dT_{rr}/dr + [1/r][T_{rr}-T_{\theta}] = \partial[\rho\psi+p]/\partial r$$

$$(6) \qquad dT_{rz}/dr + T_{rz}/r = \partial[\rho\psi+p]/\partial z$$

$$(7) \qquad 0 = \partial[\rho\psi+p]/\partial\theta$$

where ψ is the gravity potential. In vertical flow, $\psi = -gz$.

From Equations 5 and 6 we conclude that

$$(8) \qquad [\rho\psi+p] = -fz + h(r)$$

and from Equations 6 and 8 it then follows that

$$(9) \qquad T_{rz} = -\frac{1}{2}fr$$

where f represents the driving force in the flow direction since

$$(10) \qquad \partial[\rho\psi+p]/\partial z = \partial[\rho\psi+S_{zz}]/\partial z = -f$$

From Equations 5 and 8 it follows that

$$(11) \qquad dh/dr = dT_{rr}/dr + [1/r][T_{rr}-T_{\theta\theta}]$$

which integrated between r and R yields

$$(12) \qquad h(R) - h(r) = T_{rr}(R) - T_{rr}(r) + \int_r^R [\sigma_2/r]dr$$

Let $T_{rr}(R)-h(R) = C$, then use of Equation 8 yields

$$(13) \qquad -p + T_{rr} = S_{rr}(r,z) = fz + \rho\psi + \int_r^R [\sigma_2/r]dr + C$$

which evaluated at the tube centerline for a downwards

vertical flow reads

$$(14a) \qquad S_{rr}(0,z) = fz - \rho gz + \int_0^R [\sigma_2/r]dr + C$$

At z=L, Equation 14a becomes

$$(14b) \qquad S_{rr}(0,L) = fL - \rho gL + \int_0^R [\sigma_2/r]dr + C = -p(0,L)$$

Along the boundary of the tube, at r=R

$$(15a) \qquad S_{rr}(R,z) = fz - \rho gz + C$$

At z=L, Equation 15a becomes

$$(15b) \qquad S_{rr}(R,L) = fL - \rho gL + C = -P_{RL}$$

$S_{rr}(R,z)$ is the radial normal stress at the tube boundary. Measurements of the profile $S_{rr}(R,z)$ represents one of our primary objectives. These measurements readily yield the value of the constant C and the value of the driving force f. In the viscometric region the variation of $S_{rr}(R,z)$ along the flow direction is linear, whereas upstream in the relaxation region the variation is non-linear. We define the <u>excess elastic stress</u> in the relaxation region as the difference between the actual value of $S_{rr}(R,z)$ and the corresponding value obtained by linear extrapolation from the viscometric region. This is shown graphically in Figure 2. We propose this quantity as a direct measure of the residual entrance borne elastic

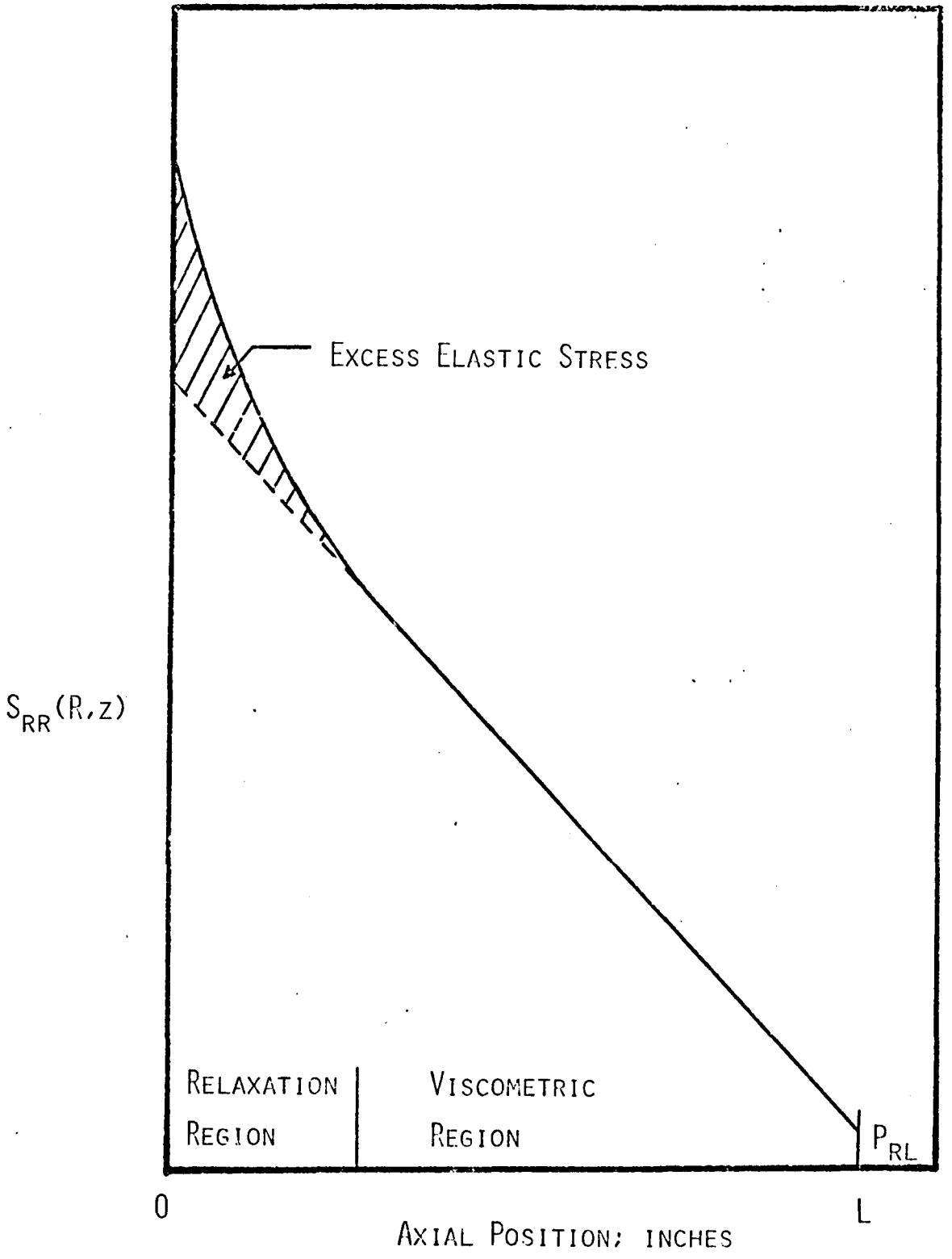

FIGURE 2. SCHEMATIC OF AXIAL RADIAL STRESS PROFILE FOR A VISCOELASTIC FLUID

stresses. The rate at which this stress decays is a measure of the material memory and leads readily to values for the material relaxation time. Correlations of swell decay with residence time should result in a one-to-one correspondence.

A slight manipulation of Equations 14b and 15b yields

$$(16) \qquad -S_{rr}(R,L) = p(0,L) + \int_0^R [\sigma_2/r]dr = -P_{RL}$$

where P_{RL} may be obtained by linear extrapolation of the radial pressure profile to the tube exit (Figure 2). By changing variables from r to fr/2, and following with a differentiation with respect to the upper limit, Equation 16 becomes

$$(17) \qquad \sigma_2(K) = dP_{RL}/d\,\ell n[fR/2] - dp(0,L)/d\,\ell n[fR/2]$$

For many polymer fluids the second term on the right hand side of Equation 17 is negligible and $\sigma_2(K)$ can be approximated by

$$(18) \qquad \sigma_2(K) = dP_{RL}/d\,\ell n[fR/2]$$

Using standard procedures (22-23), we have verified this approximation for our fluids and we wil adopt the use of Equation 18.

(19) By definition: $\sigma_1(K) = S_{zz} - S_{rr}$

Multiplying by rdr and integrating between r=0 and r=R

$$(20) \qquad \int_0^R \sigma_1 rdr = \int_0^R S_{zz}rdr - \int_0^R S_{rr}rdr$$

Integrating the second term on the right hand side by parts

$$(21) \qquad \int_0^R S_{zz} r dr - S_{rr}(R,z)[R^2/2] + \int_0^R [r^2/2][\partial S_{rr}/\partial r]dr$$

But from Equation 5

$$(22) \qquad [\partial S_{rr}/\partial r] = -[1/r][S_{rr}-S_{\theta\theta}] = -\sigma_2/r$$

Substituting Equation 22 into Equation 21 yields

$$(23) \qquad \int_0^R \sigma_1 r dr = \int_0^R S_{zz} r dr - S_{rr}(R,z)[R^2/2] + \int_0^R [\sigma_2/2] r dr$$

Changing the variable r to fr/2, and differentiating with respect to the upper limit, we have

$$(24) \qquad \sigma_1(K) = [1/[fR/2]] \frac{d}{d[fR/2]} \int_0^{fR/2} S_{zz}(\epsilon,L)\epsilon d\epsilon + P_{RL}$$

$$+ \frac{1}{2} dP_{RL}/d\,\ell n[fR/2] - \sigma_2/2$$

Substituting Equation 18 into Equation 24 yields the final expression for the first normal stress difference function,

$$(25) \qquad \sigma_1(K) = P_{RL} + [1/[fR/2]] \frac{d}{d[fR/2]} \int_0^{fR/2} S_{zz}(\epsilon,L)\epsilon d\epsilon$$

It can be readily shown that for the fluids used in this work, omission of the integral term results in an error of less than 10 per cent at shear rates up to 1000 sec^{-1}. Accordingly we have

$$(26) \qquad \sigma_1(K) = P_{RL}$$

If the shear rates are greater than 1000 sec^{-1}, the value of the integral of Equation 25 can be evaluated by standard techniques (24,37). Thus, measurements of the profile of $S_{rr}(R,z)$

(from which the values of f and P_{RL} can be obtained) lead readily to the first and second normal stress difference functions.

Measurements of the normal radial stress profile, $S_{rr}(R,z)$ in stable extrusion of polymer melts have been carried out by Han et al. (11-12,16,25). In their original experiments (16) a low value of L/D(=4) and too few pressure transducers (=4) led them to incorrectly conclude that their molten polyethylene reached viscometric flow after less than one tube diameter. In their next publication (12), they showed that at least twenty tube diameters were required for the polyethylene melt to reach constancy of exit pressure. Unfortunately, this latter paper contains serious inconsistencies in their graphical data (Compare exit pressure values in Figures 5 and 6 with those of Figures 7 and 8, Reference 12). Furthermore, their attempt to investigate reported recess hole effects (26-29) suffers from two substantial deficiencies: First, the hole for the "flush" transducer (0.0625 inches) is equal to one-half of the tube diameter (0.125 inches). Such a geometry may have unknown effects on the measured radial stresses due to disturbances to the flow field. The recess hole diameter itself is 0.039 inches or about one-third the tube diameter. Secondly, and most seriously, it is not possible for the face of the "flush" transducer to be in the same plane as the fluid-tube wall interface. It must be separated by at least a tube wall thickness, actually more, because the

entire transducer face is active and must not touch a rigid surface. At the outset their basic design defeats them. The "flush" mount is in reality a recess mount like the other, differing only in the recess hole diameter and the distance between the transducer diaphragm and the fluid-tube wall interface. Under these conditions it certainly cannot be considered a valid comparison and any results obtained must be judged inconclusive with respect to the purported aim of the experiment.

In addition to measurements of the radial normal stress, $S_{rr}(R,z)$, other methods also exist for estimating the magnitude of the two normal difference functions, σ_1 and σ_2 (22-24, 30-34). These methods, however, do not enjoy a complete rigor and are based on one or more simplifying assumptions.

The <u>exit region</u> has largely been ignored in both theoretical and experimental studies. It has been postulated, however, that the velocity profile may undergo a second rearrangement in anticipation of the outlet. This should not be taken casually as the validity of the extrapolation procedure to obtain the radial stress at the tube exit, P_{RL}, rests strongly on the absence of an exit region. We have verified, using Schertzer's (22-23) consistency argument based on a dimensionless variable analysis, that <u>no</u> such exit region exists for our fluids over the range of shear investigated.

In short tubes ($L/D < 20$), extruded molten polymers may expand to 3 to 4 times the tube diameter. Jet swelling is attributed to the recovery of the residual entrance borne elastic strains and the relaxation of the shear rate dependent normal stresses. Bagley (35) and Kowalski (10) have shown that the swell ratio decays exponentially with L/D to a shear rate dependent value on the order of 1.5 to 2.0 (13,36) so that the major factor in short tubes is the entrance borne elastic stresses.

In summarizing this review section, we see that most of the aspects of capillary flow of polymeric fluids are not well understood. The literature of the past two decades contains virtually hundreds of publications dealing directly or indirectly with the formulation and testing of constitutive equations. Notwithstanding, the number of hydrodynamical problems for which an exact or even an approximate solution exists is rather small; and these problems generally belong to the realm of simple flow geometries and simple flow situations, i.e., viscometric flow. The corresponding treatments of flow in the other tube regions are either very primitive or non-existent, a fact largely due to the lack of pertinent experimental data. Thus our overriding concern was to provide a comprehensive set of reliable data bearing on the phenomena occurring in all the regions of capillary flow; a requirement most readily satisfied by axial radial stress profile and concurrent jet swell ratio measurements.

III. EXPERIMENTAL

A. Introduction

The primary goals of this experimental-research program were: (a) to investigate the effect of a recessed pressure transducer mount geometry on the measured stresses, (b) to measure the radial stress profile, $S_{rr}(R,z)$, over a wide range of shear rates, and (c) to make concurrent observations of the free stream phenomena.

B. Experimental System

A detailed description of the materials, equipment and procedure appears in the Appendix; for the reader's convenience, we will briefly review this material here.

A concentrated rubber solution and a high viscosity silicone oil were used as fluids representative of viscoelastic and viscoinelastic materials, respectively. The highly elastic rubber solution was prepared by dispersing 16.5 parts by weight Vistanex L-200* polyisobutylene ($\bar{M}_v > 5 \times 10^6$) in 83.5 parts by weight Varsol #2** mineral spirits (SpGr = 0.8076) and mixing intensively until random sampling indicated homogeneity. We were able to use Dow Corning 200 Fluid*** silicone oils (30,000 cs and 100,000 cs) as delivered. Their rheological

---

* TM - Enjay Chemical Company
** TM - Humble Oil and Refining Company
***TM - Dow Corning Corporation

properties are reported, via shear stress-shear rate and swell ratio-shear rate curves, in Figures 3 and 4. Neither of the materials experienced measureable shear degradation and viscous heating effects were negligible (temperature rise was less than 0.1^{o} Fahrenheit) over the range of shear rates examined (1 to 4000 sec^{-1}). All runs were performed at 75^{0} Fahrenheit.

The apparatus is shown schematically in Figure 5. The pneumatic circuits are of a standard design, allowing for rapid pressurization and venting (< 1/2 second) of the rheometer reservoir. Kowalski (10) has shown that if the rheometer reservoir is more than fifteen-times the tube diameter, the measured elastic and viscous properties are independent of the reservoir diameter. We used a ratio of greater than eighteen in all cases. The pressure transducers (nine Barber-Coleman Model A7556-101, 0-1500 psi) were mounted on either slits or tubes in a variety of recess configurations. An Electronics Ltd. Model 1808 Signal Conditioner and Amplifier supplied power to the pressure transducers and amplified the resultant signals by up to a factor of 1500. This gave a final sensitivity capability of better than 10 mv/psi for all the transducers at 4.00 volts excitation. Signal noise was less than 5 mv. A novel approach for the final signal measurement obviated the need for a multichannel analog recording device. All the transducer outputs were fed to a Chadwick-Helmuth Model 430-12 Data-

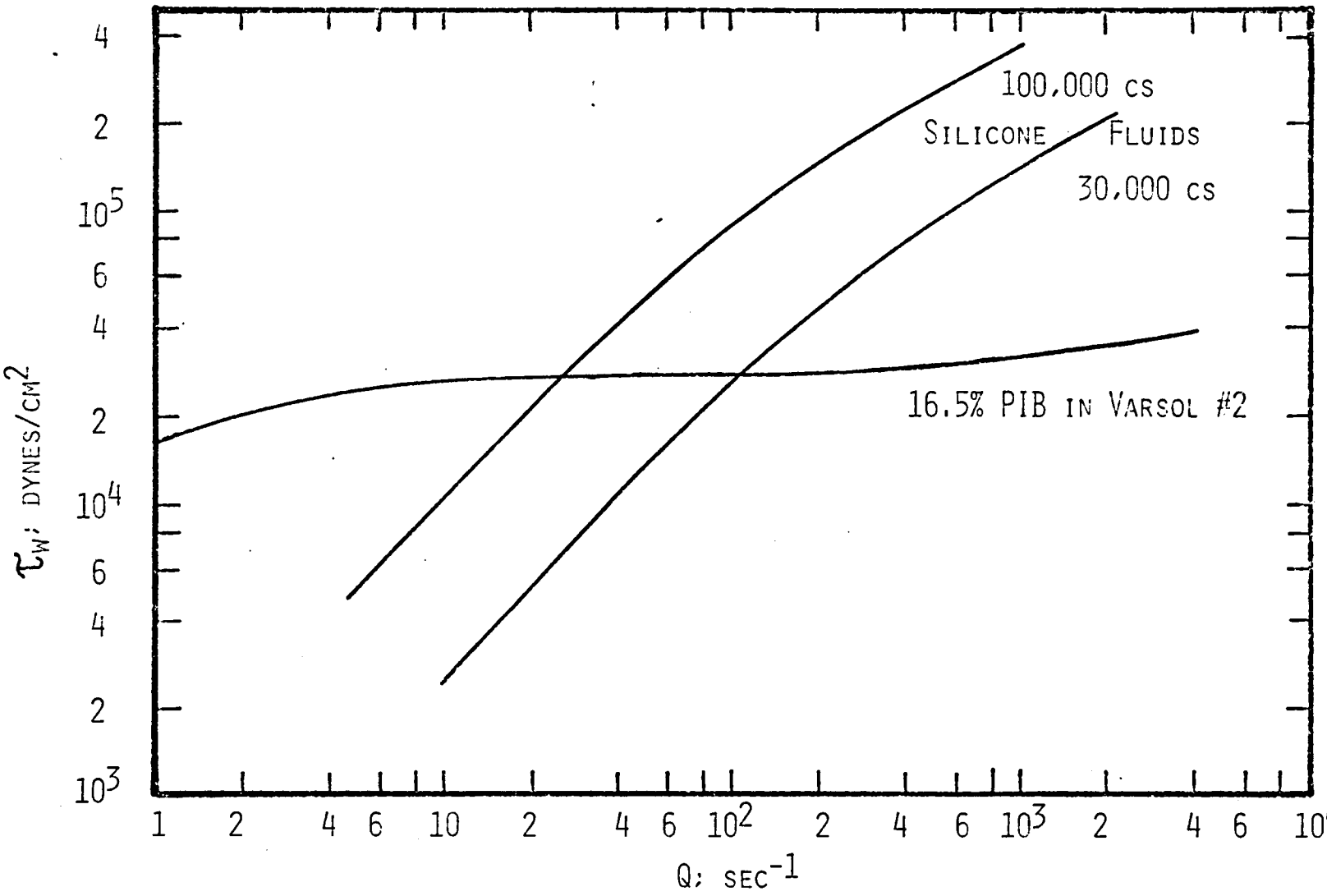

Figure 3. Shear Stress at the Wall vs. Apparent Shear Rate - 16.5% PIB in Varsol #2, Dow Corning 200 Silicone Fluids - 30,000 cs & 100,000 cs

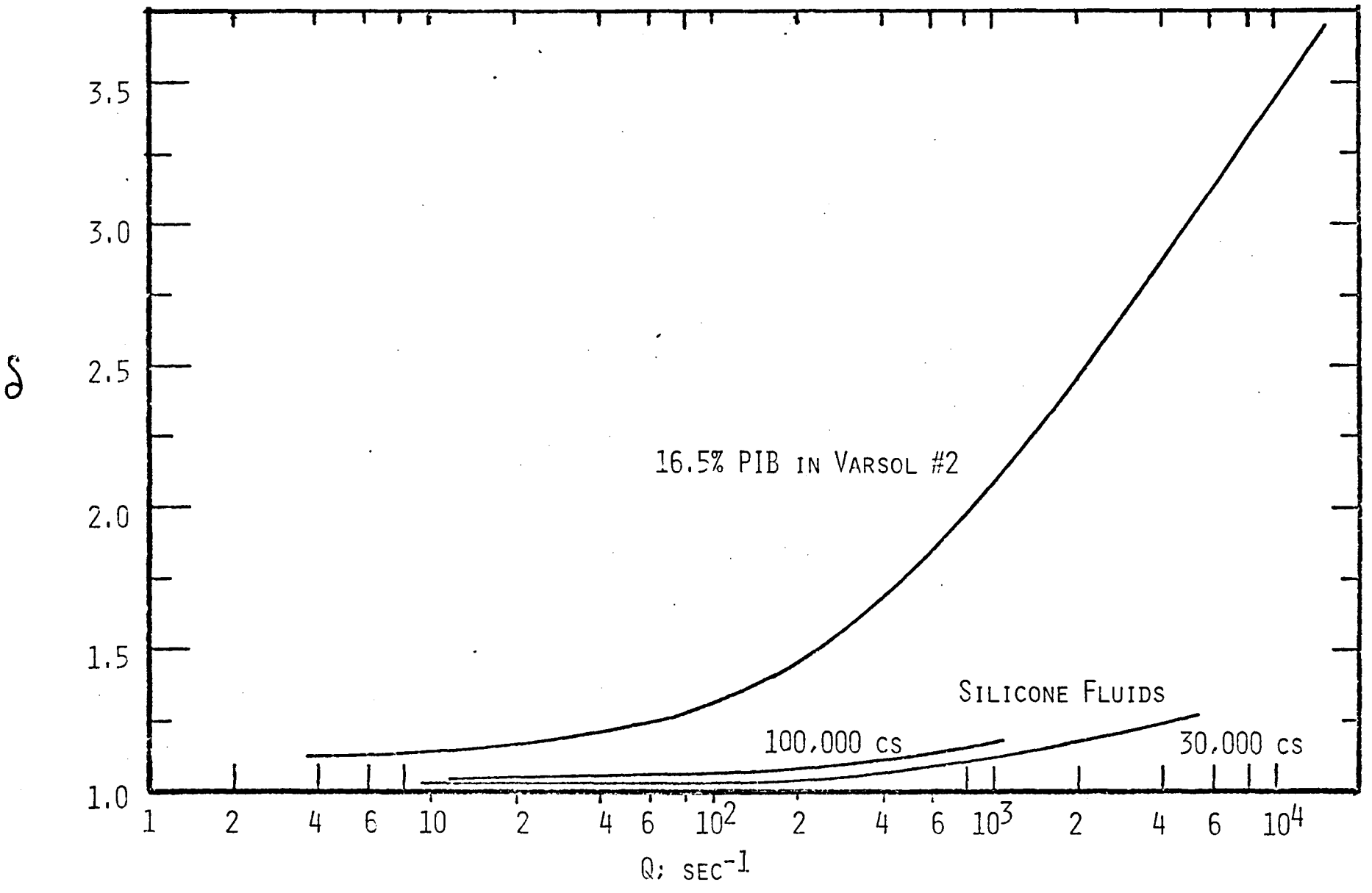

FIGURE 4. DIE SWELL RATIO FOR VISCOMETRIC FLOW VS. APPARENT SHEAR RATE - 16.5% PIB IN VARSOL #2, DOW CORNING 200 SILICONE FLUIDS - 30,000 cs & 100,000 cs

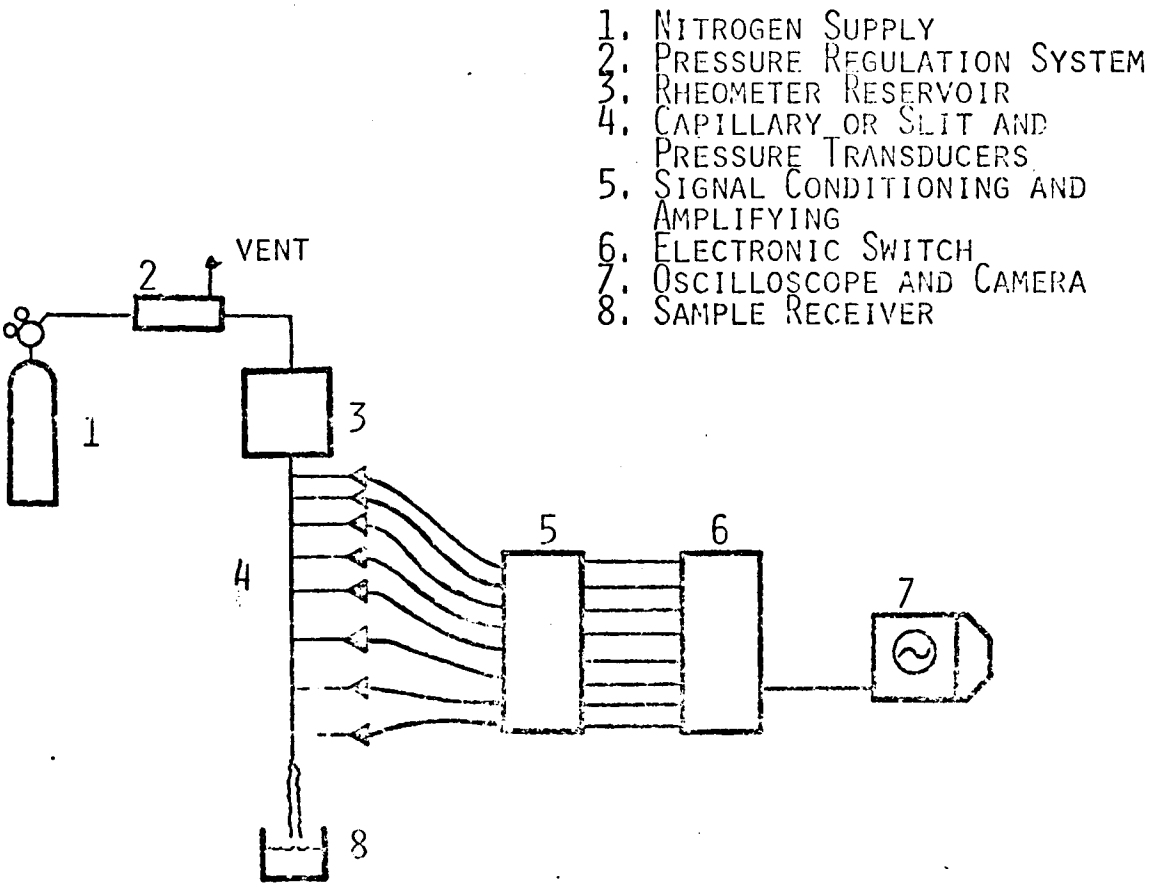

Figure 5. Schematic of Data Acquisition Equipment

switch electronic switch capable of sequentially sampling up to 12 channels at a rate of 10,000 channels/sec. The switch output was the input to an oscilloscope with Polaroid camera attachment where the transducer outputs were photographed at a scope sensitivity of 100 mv/cm. Vertical excursions from the baseline were a direct measure of the pressure. An optical comparator, measuring to the nearest 0.0001 inch, was used to secure the final pressure values. Flow curves were made with the aid of an electronic timer (0.01 second divisions) controlled by the pneumatic circuits. Care was exercised in allowing sufficient time for the runs so that pressure transients accounted for less than two per cent of the timing interval. Sample weights were determined using a Sauter balance accurate to the nearest one hundredth of a gram. The optical comparator was used to determine swell ratios, from photographs of the free jet, to better than three significant figures.

C. Recess Mount Effects

1. Introduction

In this phase we searched for possible effects of a recessed transducer mount geometry on the measured radial stress in both slit and tube configurations. An important consideration was our desire to investigate and make allowances for possible artifacts. It has been reported by Lodge et al. (26-28) that a recess mount geometry would cause an error in the measured stress equivalent to about three-times the wall shear stress. Tanner and Pipkin (29) found, for slow flow down an inclined plane, that the error was positive and equivalent to about 25 per cent of the first normal stress difference. As we pointed out, the results of Han et al. (12) are inconclusive because of their poor choice of transducer mount geometry.

2. Slit Recess Geometry

The way to study the effect of recessed transducer mount is to use two parallel plates where a true flush mounting can be achieved. To this end we constructed a slit die (Figure 6), 6.001 inches long by 3.002 inches wide, with a gap of 0.062 inches. The recess mount transducers (detail of Figure 6) were diametrically opposed to the flush mounted transducers in four pairs. Interchangeable inserts of different recess hole diameter (varied in five steps from 0.020 to 0.063 inches) were tested. The length of the recess hole was machined approximately equal to the hole diameter in all cases. The re-

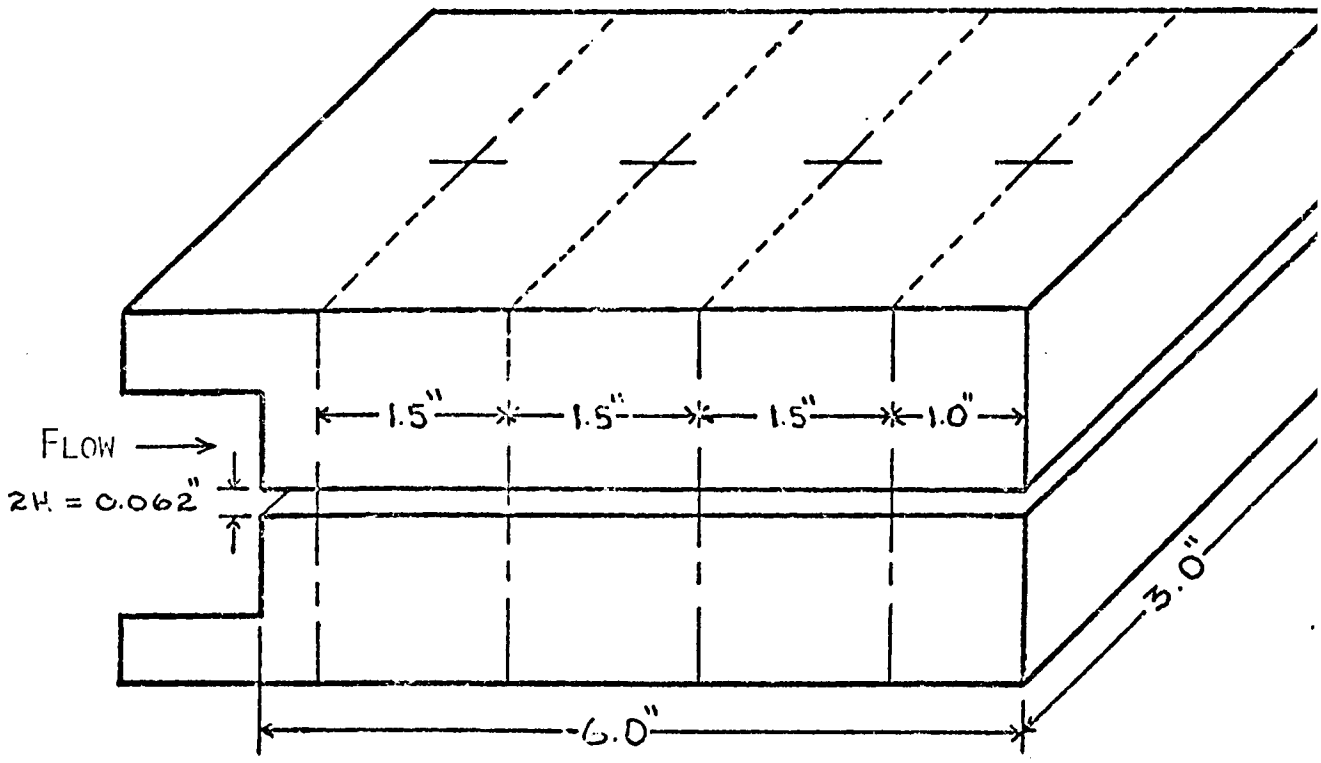

FIGURE 6A. SLIT DIE - NOMINAL DIMENSIONS AND TRANSDUCER LOCATIONS

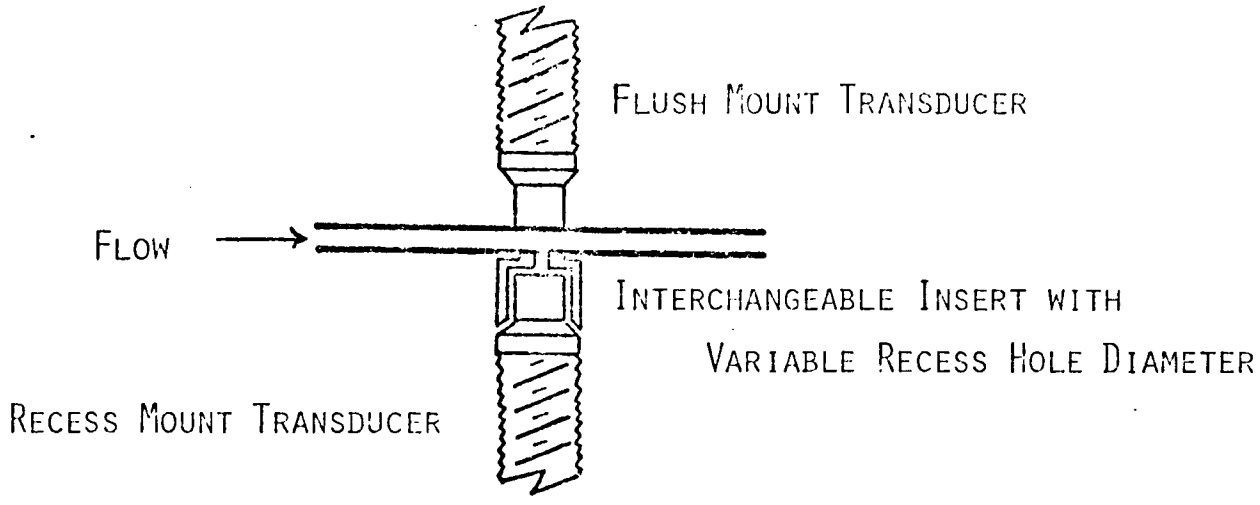

FIGURE 6B. DETAIL OF FLUSH AND RECESS OPPOSING TRANSDUCER MOUNTS

sponse time of the recess mount transducers was not significantly different from the flush mounted ones.

3. Tube Recess Geometry

The next phase of this preliminary effort dealt with the effect of recess mount geometry in tubes. At present, pressure transducers are too large compared to practical tube diameters to allow for a flush mount. One would hope that in the near future technology would develop a sub-miniature device applicable to these measurements. With this in mind, and because the geometry considerations in tubes is somewhat different from that in slits, we had to investigate one additional source of experimental error, what we call the "saddle hole effect". This is the shape of the perpendicular intersection of two right circular cylinders, the recess hole and the tube wall. As the recess hole diameter approaches the tube diameter, the surface area of the "saddle" can become substantially larger than the nominal cross-sectional area of the drill. We must consider, that comparatively large recess holes (with respect to tube diameter) might cause stress measurement errors not found for the same size hole in a slit geometry. We therefore constructed five long tubes, all of 0.312 inch inside diameter and approximately 31.5 inches long. Each tube had eight pressure transducer mounts strategically placed so as to cover all the regions of flow, and each tube differed only in the size of the recess hole drilled through the tube walls

(Figure 7). The ratio of the tube diameter to recess-hole diameter varied from about 5 to 16. To extend the range of shear rates for the viscoinelastic fluid we used a lower viscosity grade Dow Corning 200 Fluid - 30,000 cs.

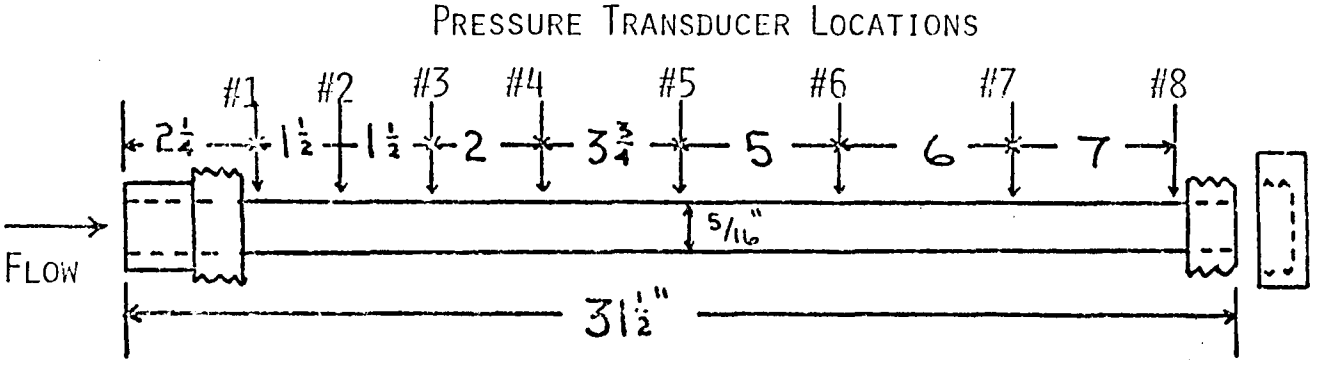

FIGURE 7A TUBE DIE - NOMINAL DIMENSIONS AND TRANSDUCER LOCATIONS

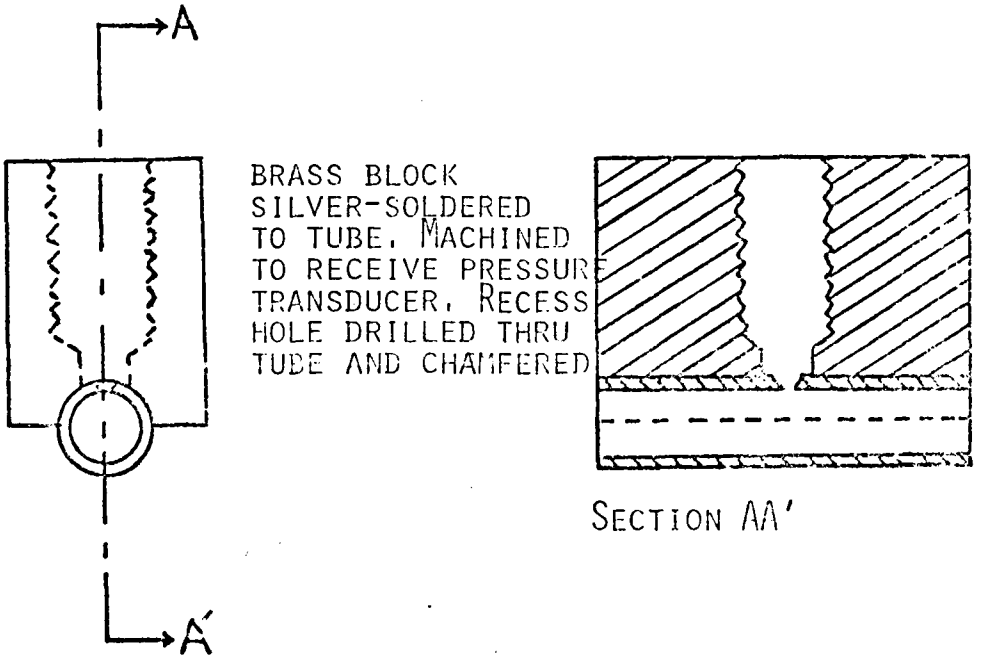

FIGURE 7B DETAIL OF RECESS TRANSDUCER MOUNT IN A TUBE GEOMETRY

D. Entrance Region Effects

A Bagley Entrance correction analysis (40) serves two purposes: (a) It provides a procedure for converting apparent shear stress, S, to the true shear stress at the wall, τ_w. This is achieved by the addition of a ficticious length of tubing, expressed as a multiple (N) of the tube diameter (D), to be added to the actual tube length (L). This procedure, which accounts for the entrance region pressure losses, is represented by the following expression:

$$\tau_w = S\frac{[\ L/D\ ]}{[L/D+N\ ]}^{*} \qquad (27)$$

(b) In addition, Philippoff and Gaskins (8) have shown that N also serves as a direct measure of a material's elasticity. The analysis, described in detail in Appendix V, was performed with a series of six tubes, all with a 0.186 inch inside diameter, and with length to diameter ratios of 2,4,8,16,64 and 100.

E. Tube Diameter Effects

Several experimenters have investigated tube diameter effects on both the viscous (41) and elastic (38,42-43) properties of polymeric materials. Their results have several important consequences regarding the calculated values for the material functions in viscometric flow. These aspects are examined in more detail in Section V. Briefly, this phase involved experiments in which

* This procedure gives values for τ_w identical to those determined by Equation 9.

the tube diameter was varied while the length to diameter was maintained constant. No regular diameter effect on the measured variables was found.

IV. RECESS MOUNT EFFECTS

A. Slit Flow

The results for the viscoinelastic fluid - Dow Corning 200 Fluid (100,000 cs) - are shown in Figures 8 and 9. The pressure profiles (Figure 8) are essentially linear, with a zero (± 1 psi) intercept (exit pressure) over the range of shear investigated (5 to 1000 sec^{-1}). The zero exit pressure is, again, like the swell ratio data of Figure 4, indicative of this material's inelastic nature. From Figure 9 one can see that for the viscoinelastic fluid there is no regular effect on the measured stress due to recess mount, over the range of hole sizes examined. Fifty per cent of the points show zero difference and an additional thirty-five per cent are evenly distributed within one psi of zero*. The slight increase in scatter at the higher shear rates is due to the increased range of the pressure transducer calibration. According to Lodge et al. (26-28) the difference should be, for example, -1.5 psi at $Q = 32\ sec^{-1}$, -3 psi at $Q = 70\ sec^{-1}$, -6 psi at $Q = 185\ sec^{-1}$ and -15 psi at $Q = 800\ sec^{-1}$. At the higher shear rates these predicted values are more than an order of magnitude greater than those measured.

---

* Because all the stress profiles for this fluid were linear there is no need to be concerned with the fact that the flush transducer records an averaged value of stress, whereas the recessed transducer records a point value of stress. Nevertheless, a method to calculate the magnitude of this error will be found in Appendix VI.

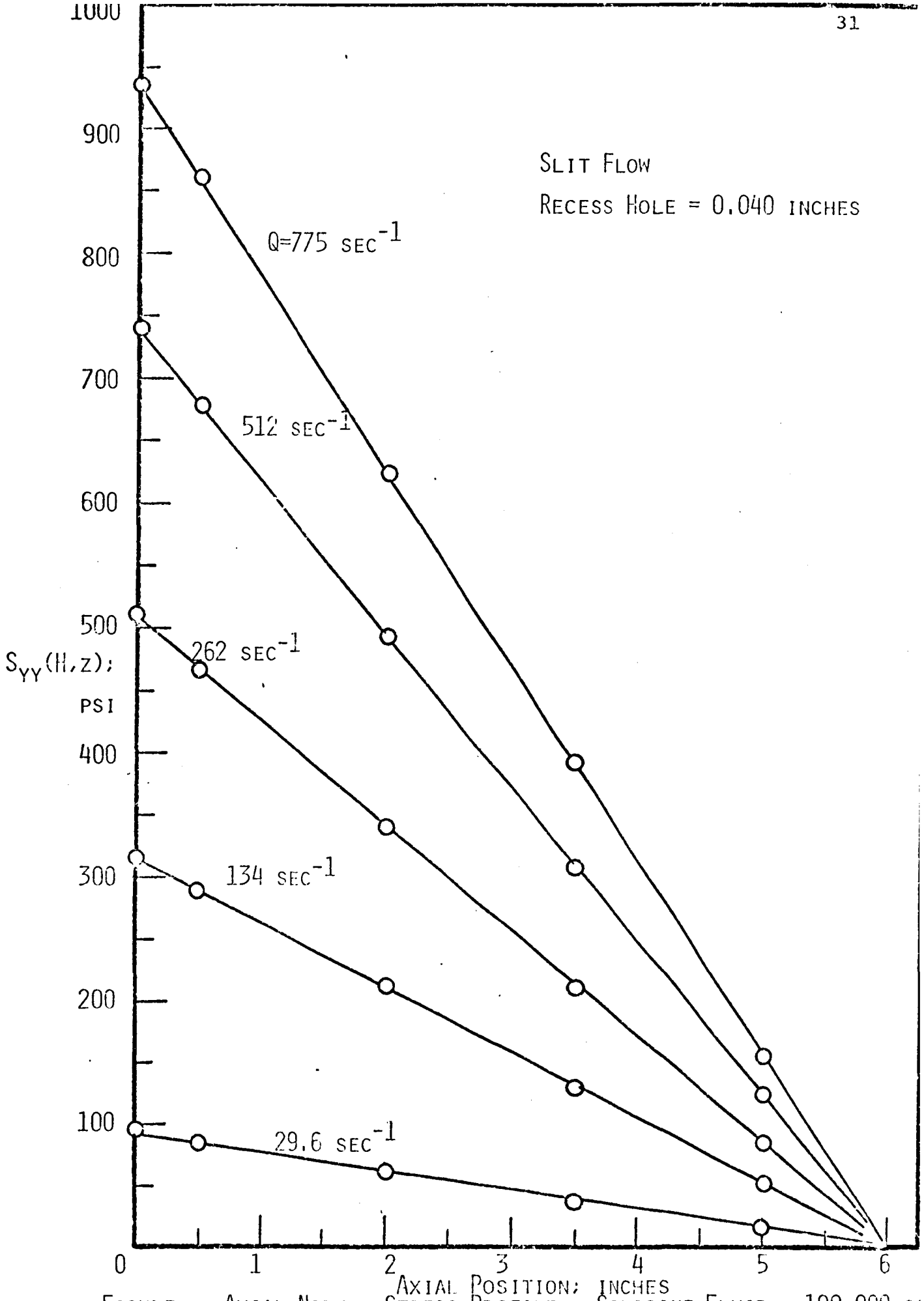

FIGURE 8 AXIAL NORMAL STRESS PROFILE - SILICONE FLUID - 100,000 cs

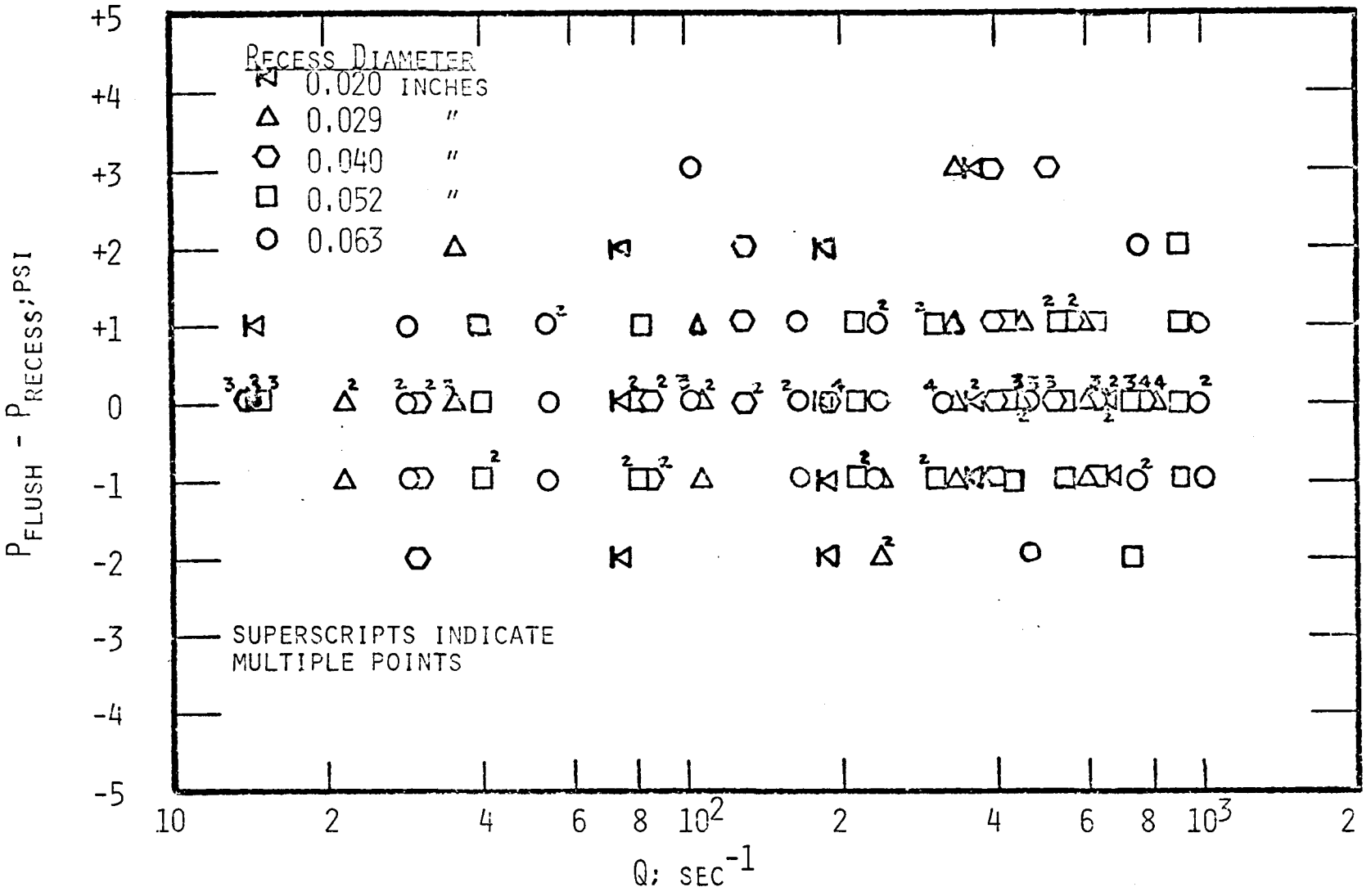

FIGURE 9 COMPARISON OF FLUSH AND RECESS MOUNTED PRESSURE TRANSDUCERS IN SLIT FLOW FOR VARIOUS RECESS HOLE DIAMETERS VS. APPARENT SHEAR RATE - SILICONE FLUID 100,000 CS

A similar examination of recess mount effects for the viscoelastic fluid - 16.5% Vistanex L-200 in Varsol #2 - is presented in Figures 10 through 12. Figures 10 and 11 display regular non-zero exit pressures at shear rates greater than 10 sec^{-1}. This is in agreement with the swell ratio data of Figure 4 which has shown the material to be highly elastic. Note also the significant excess elastic stress generated at the higher shear rates (Figure 10). The exit pressure data show less scatter than anticipated (85 per cent of the data are within a 1.5 psi scatter band) inasmuch as the execution of this phase required the transducers to be paired, resulting in an insufficient number of points for more exacting profiles.

Because of the lower shear stresses involved, the magnitude of Lodge's (26-28) hole pressure error is within the scatter band of Figure 12. Tanner and Pipkin's result (29) would predict, if we consider the first normal stress difference roughly equal to the exit pressure (see Equations 25 and 26); a regular increase to minus three psi at a shear rate of 1000 sec^{-1}. However, virtually ninety per cent of the data points are randomly within one psi of zero difference with more than one-third of the points being identically zero. Therefore, we must conclude that there is no regular recess hole diameter effect on either the exit pressure values or the flush verses recessed mount transducer values.

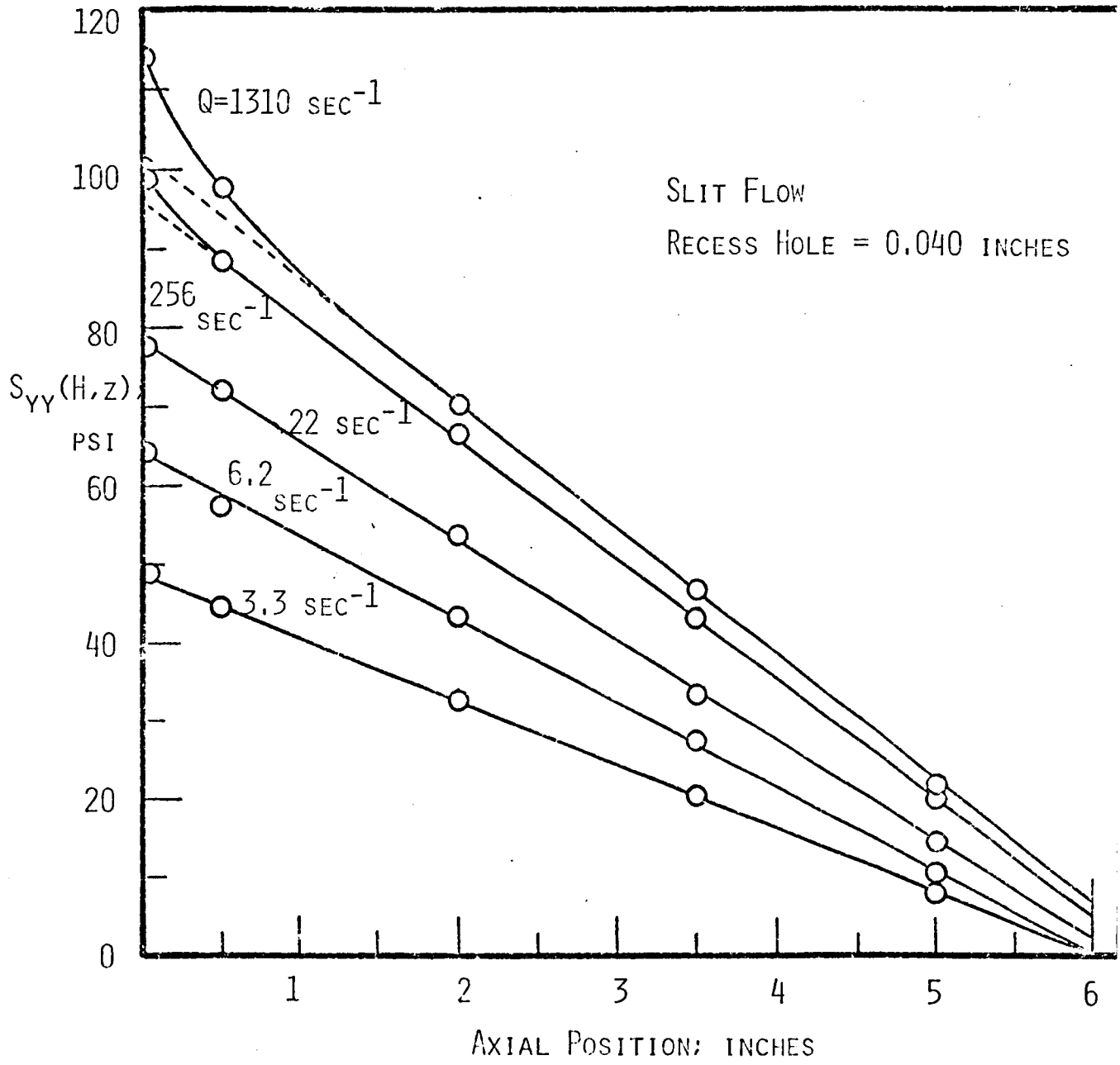

FIGURE 10 AXIAL NORMAL STRESS PROFILE - 16.5% PIB IN VARSOL #2

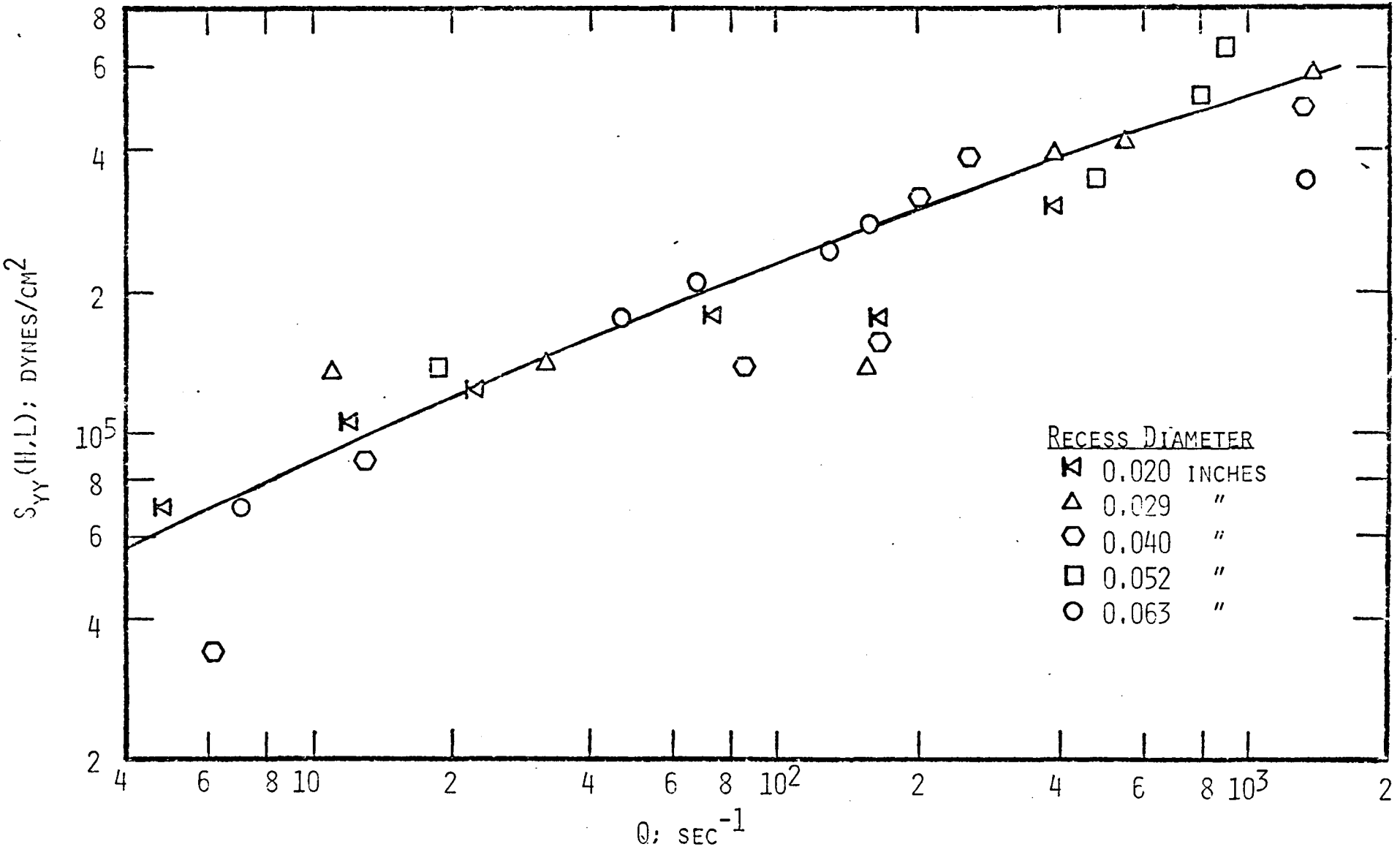

FIGURE 11 EXIT PRESSURE VS. APPARENT SHEAR RATE FOR VARIOUS RECESS HOLE DIAMETERS : SLIT FLOW - 16.5% PIB IN VARSOL #2

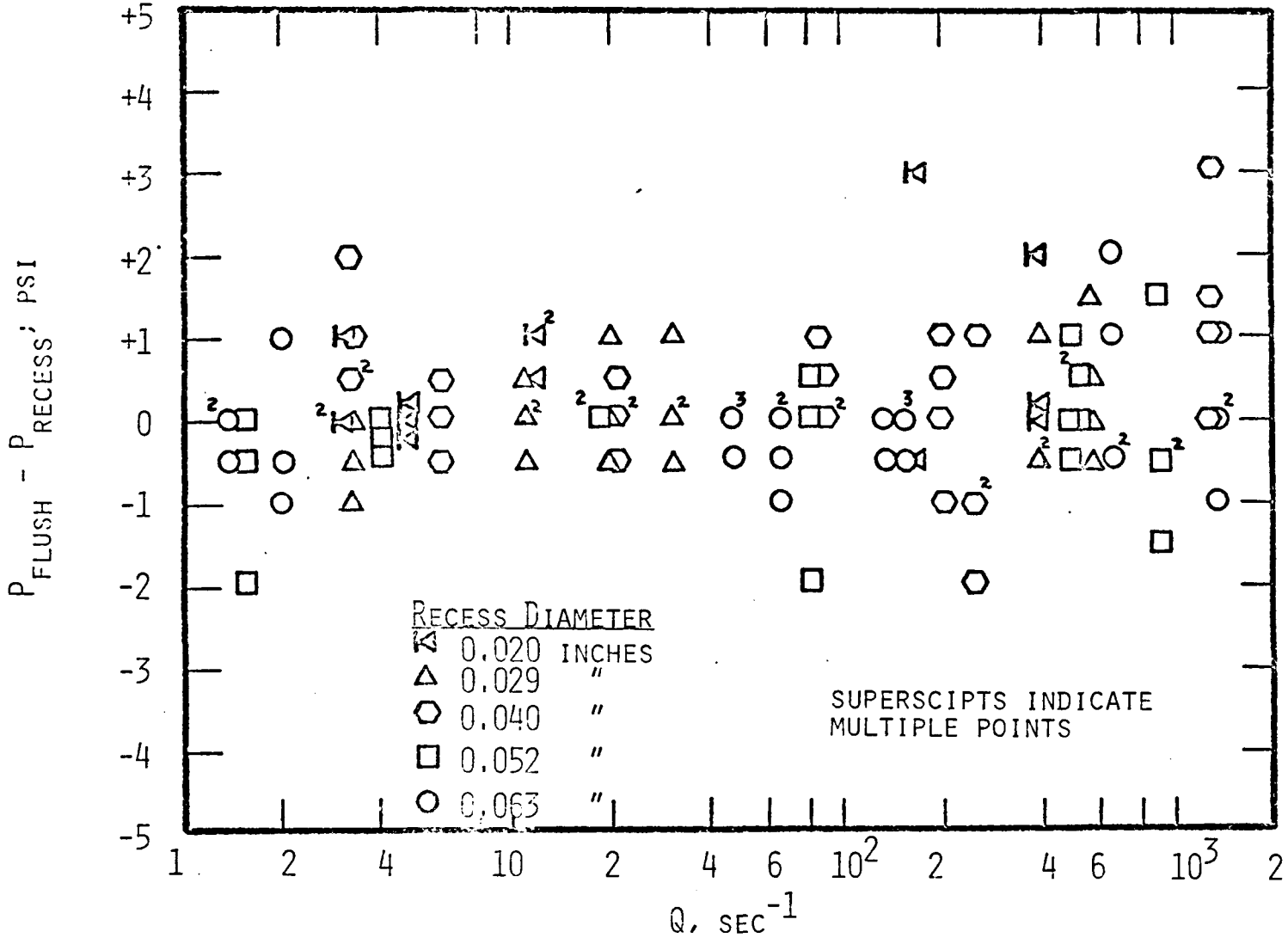

FIGURE 12 COMPARISON OF FLUSH AND RECESS MOUNTED PRESSURE TRANSDUCERS IN SLIT FLOW FOR VARIOUS RECESS HOLE DIAMETERS VS. APPARENT SHEAR RATE - 16.5% PIB IN VARSOL #2

B. Tube Flow

Typical results are shown in Figure 13 for the Dow Corning fluid, and in Figures 14 and 15 for the viscoelastic polyisobutylene solution. As in the slit die, the viscoinelastic fluid exhibits no measureable exit pressure and only a mild excess elastic stress (in comparison to the shear stress) in the relaxation region at the higher shear rates. On the other hand, one can see from Figure 14 that the rubber solution exhibits both a marked excess elastic stress and a substantial (for a polymer solution) exit pressure. In Figure 15 ninety percent of the exit pressure data fall within a one psi scatter band with no regular trend due to recess hole size. The magnitude of the tube exit pressure is the same as that found for the slit geometry (Figure 11). This is indeed indicated in the solutions to the equations of motion. Discrepancies are probably caused by the difficulty in drawing accurate profiles with the slit data due to the reduced number of profile data points.

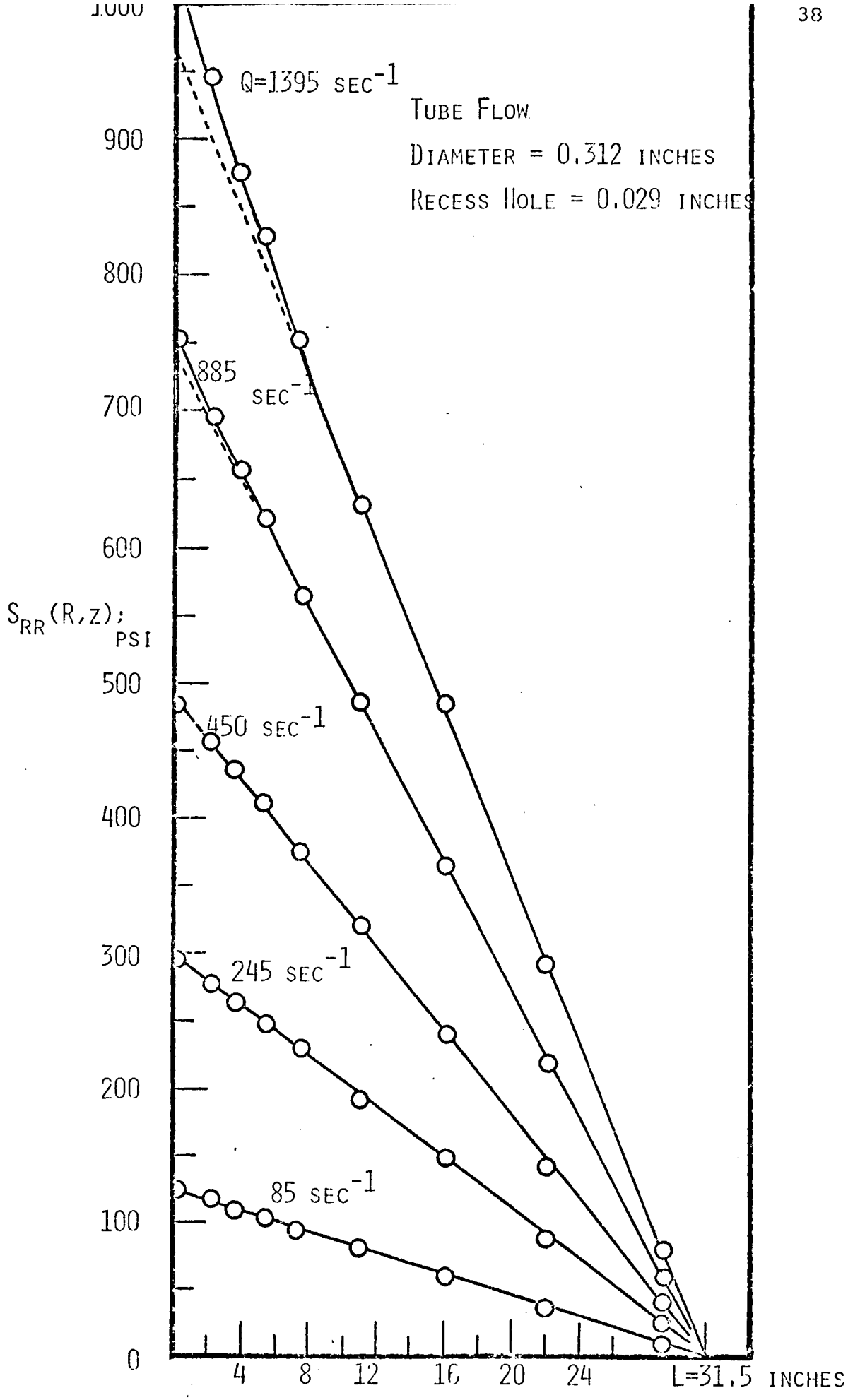

FIGURE 13. AXIAL RADIAL STRESS PROFILE - SILICONE FLUID 30,000 CS

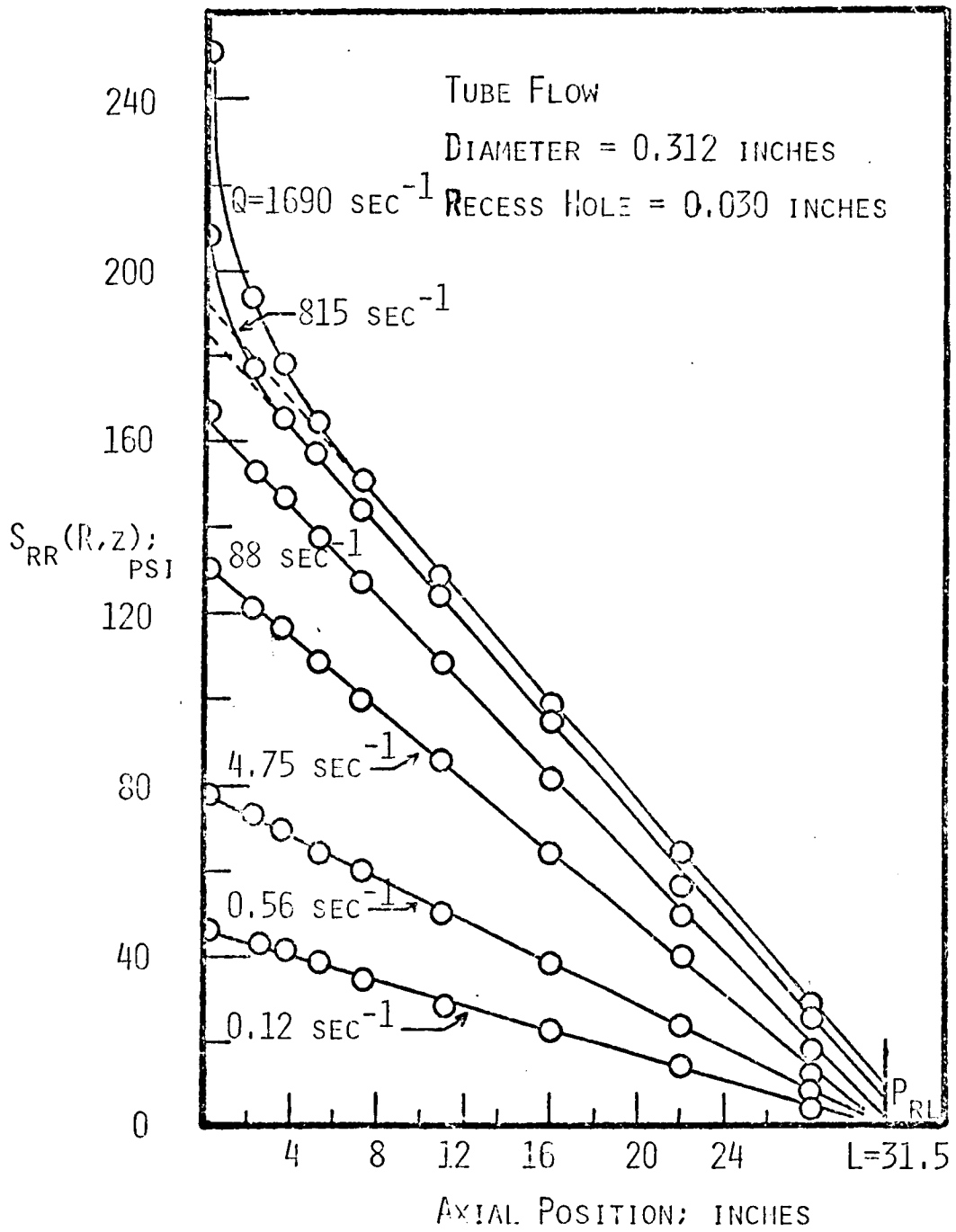

FIGURE 14. AXIAL RADIAL STRESS PROFILE - 16.5% PIB IN VARSOL #2

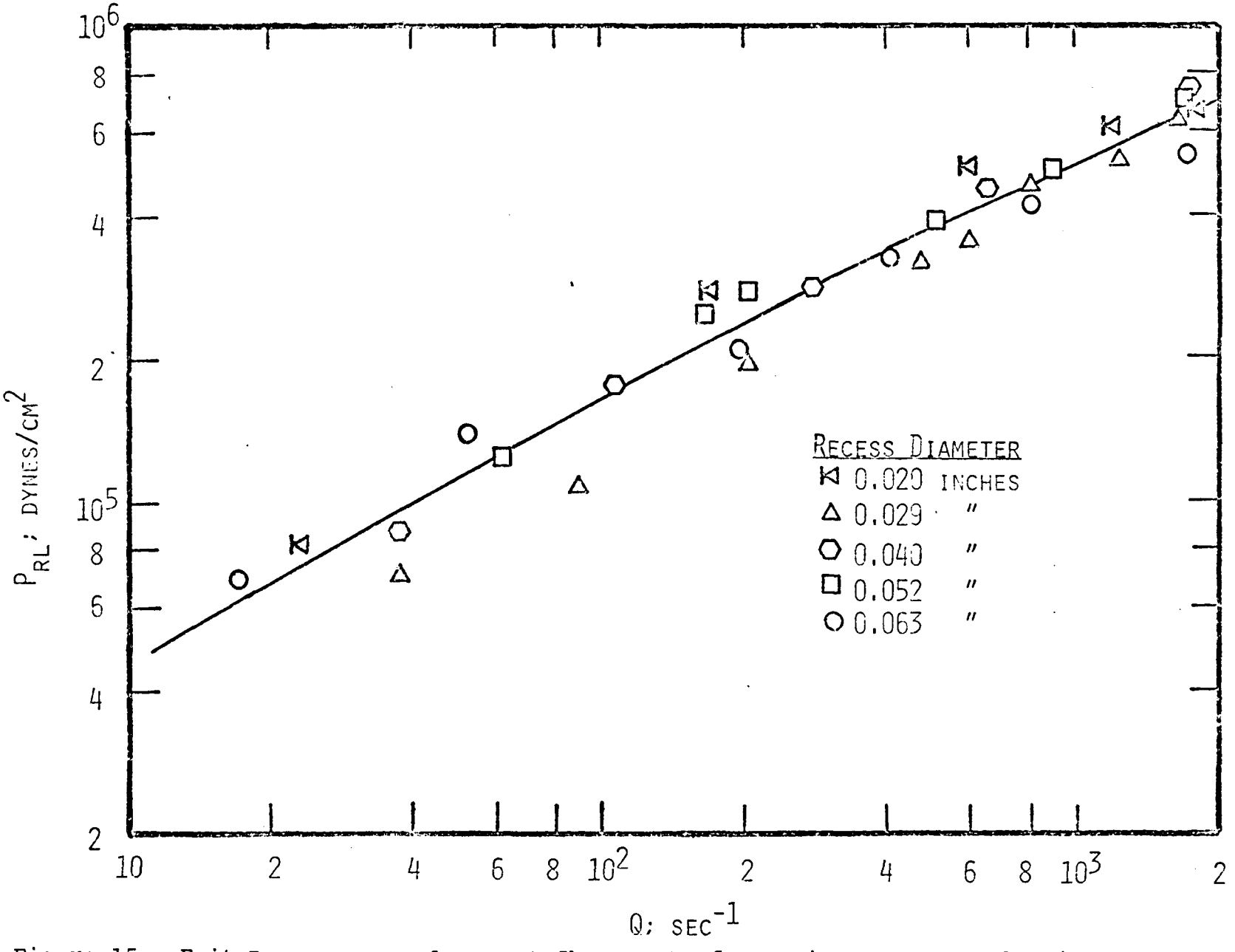

Figure 15. Exit Pressure vs. Apparent Shear Rate for Various Recess Hole Diameters : Tube Flow - Diameter = 0.312 inches - 16.5% PIB in Varsol #2

C. Conclusions

At this point we are reasonably assured that we have fully investigated the experimental artifacts that might be introduced by the necessary recess mount configurations and found them to be totally absent. In a slit flow geometry both the flush and recess mount pressure transducers gave the same values for the measured stresses independent of recess hole size from 0.020 inch to 0.0625 inches. Measurements in a tube geometry show that the measured stresses (represented by P_{RL}) are independent of the recess hole diameter over a tube diameter to recess hole diameter ratio range of from five to sixteen. Furthermore, as would be expected by considering the solutions to the equations of motion, values of the exit pressure, directly related to the first normal stress difference, are practically the same for both the slit and tube flow geometries.

V. AXIAL PRESSURE PROFILES

A. Entrance Region Effects

The basic data are presented in Figures 16 to 19. It is apparent in Figure 16 that the excess elastic stress is sizeable at high shear rates. A Bagley entrance correction analysis gives values for N ranging from 1 ($Q=1\ sec^{-1}$) to 34 ($Q=4000\ sec^{-1}$). These extraordinarily high values can be attributed solely to elastic effects since Couette losses at the low Reynold's numbers involved ($N'_{Re} < 10$) are negligible. The magnitude of this entrance correction can be used to predict the normal stress difference (8), an aspect to be considered later. The entrance correction, as empirically obtained from Figure 20, is

$$N = 0.97(Q)^{0.400} \quad ; \quad 1 \leq Q \leq 100$$
$$N = 0.76(Q)^{0.472} \quad ; \quad 100 \leq Q \leq 4000 \tag{28}$$

B. Tube Diameter Effects

Figure 18 compares the exit pressure data for the three tubes of different diameters and shows these data to fall randomly within a 0.75 psi scatter band. That is, these exit pressure measurements are independent of tube diameter,* as were the

* The manifestation of a diameter effect does not necessarily mean that an exit region exists, since fluids with a yield stress and/or fluids which slip at the wall also exhibit diameter dependent flow curves (41). Such a result would require further examination to determine its origin.

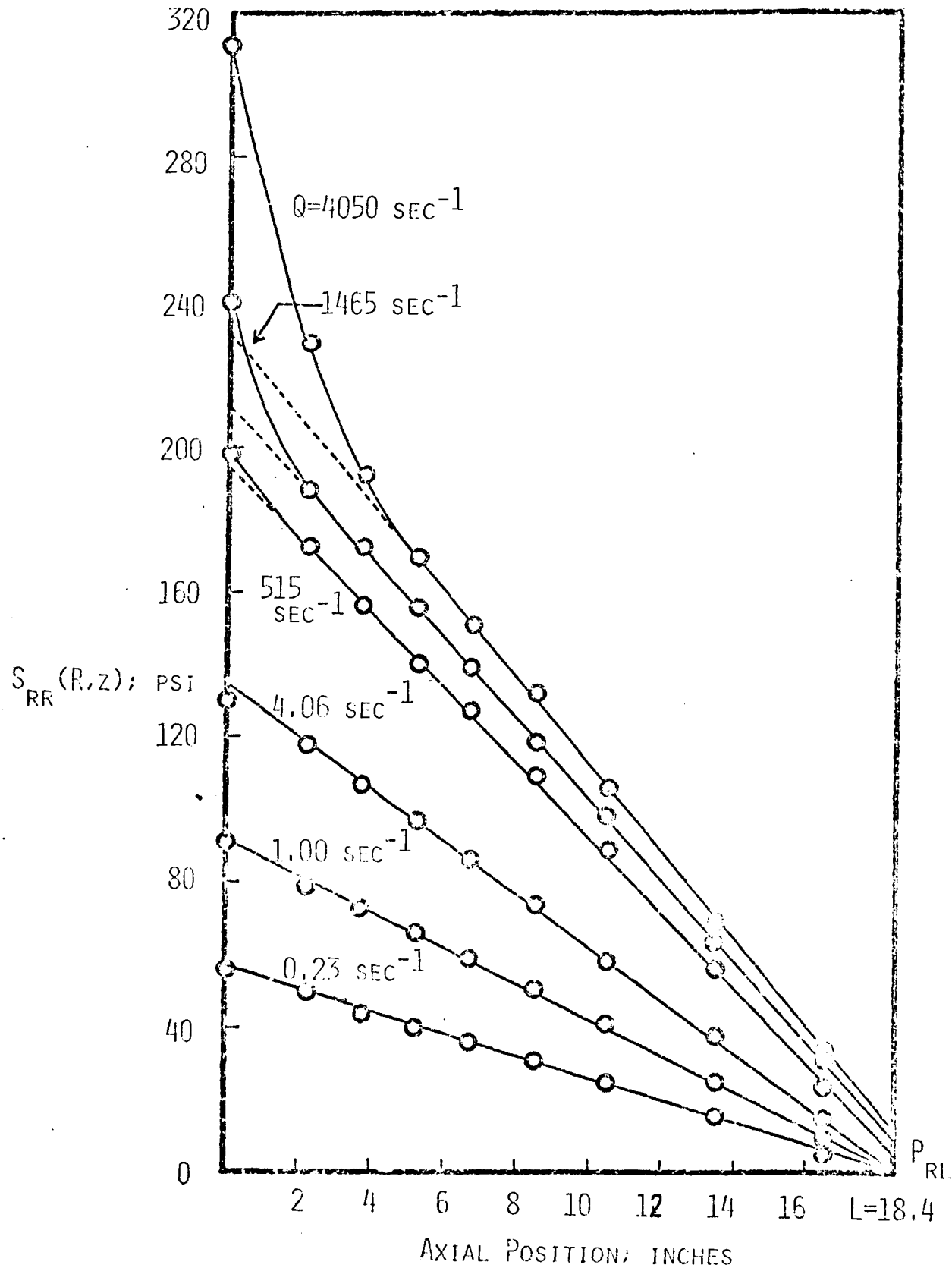

FIGURE 16 AXIAL RADIAL STRESS PROFILE - 16.5% PIB IN VARSOL #2 - TUBE DIAMETER = 0.186 INCHES

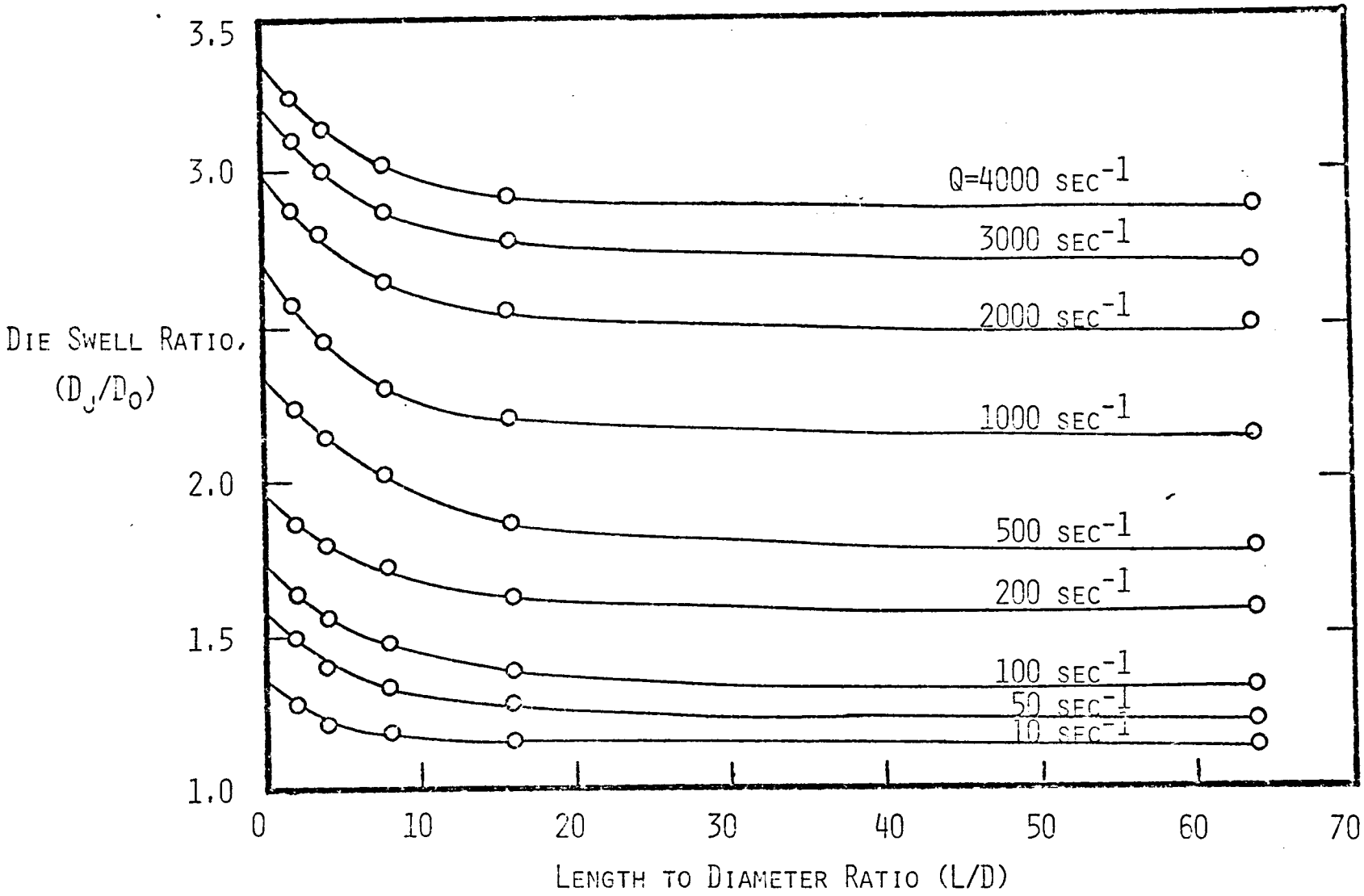

FIGURE 17 DIE SWELL RATIO VS. LENGTH TO DIAMETER RATIO - 16.5% PIB IN VARSOL #2

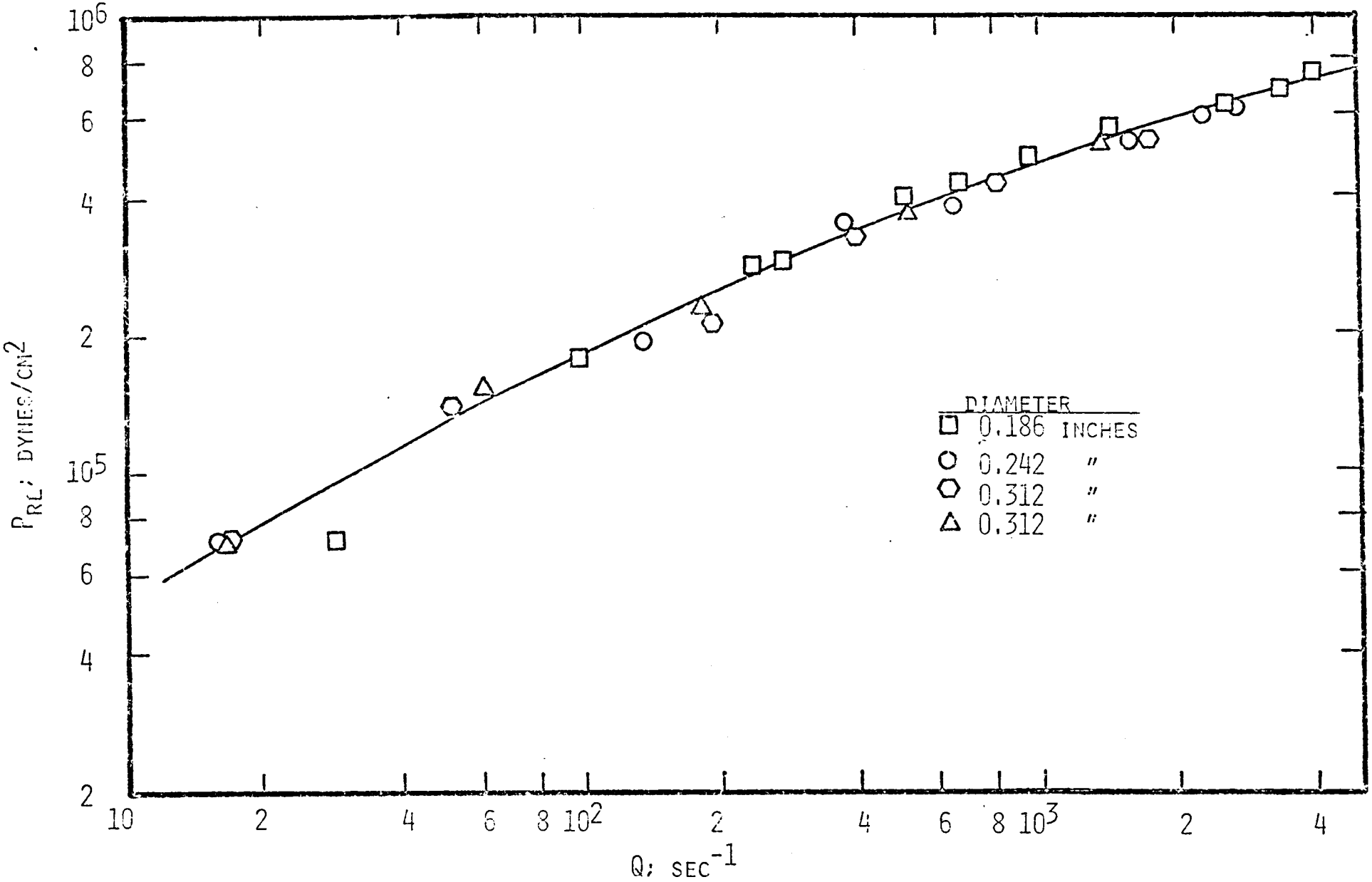

FIGURE 18 EXIT PRESSURE VS. APPARENT SHEAR RATE - 16.5% PIB IN VARSOL #2

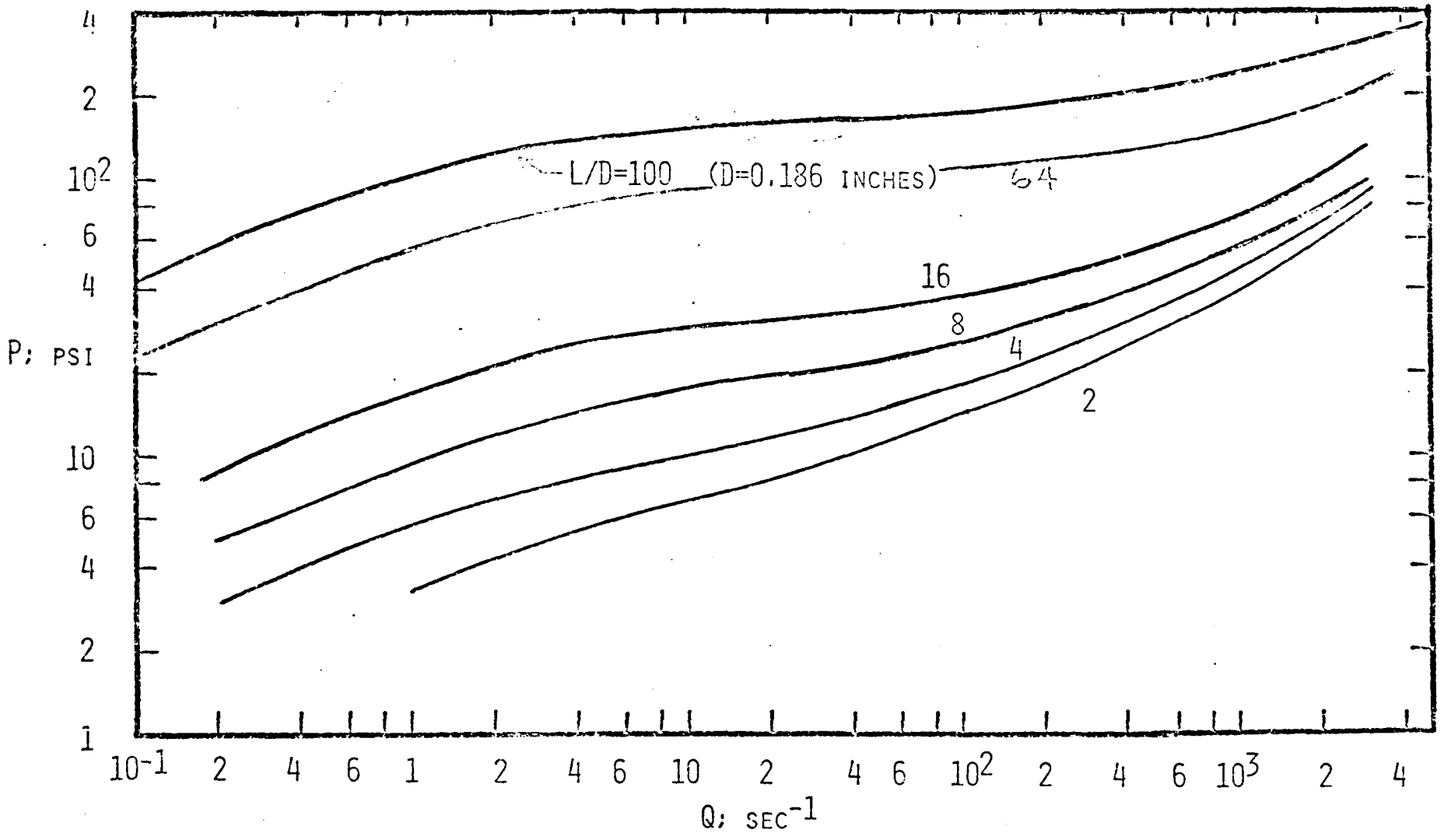

FIGURE 19 PRESSURE DROP VS. APPARENT SHEAR RATE FOR TUBES OF DIFFERENT LENGTH TO DIAMETER RATIO - 16.5% PIB IN VARSOL #2

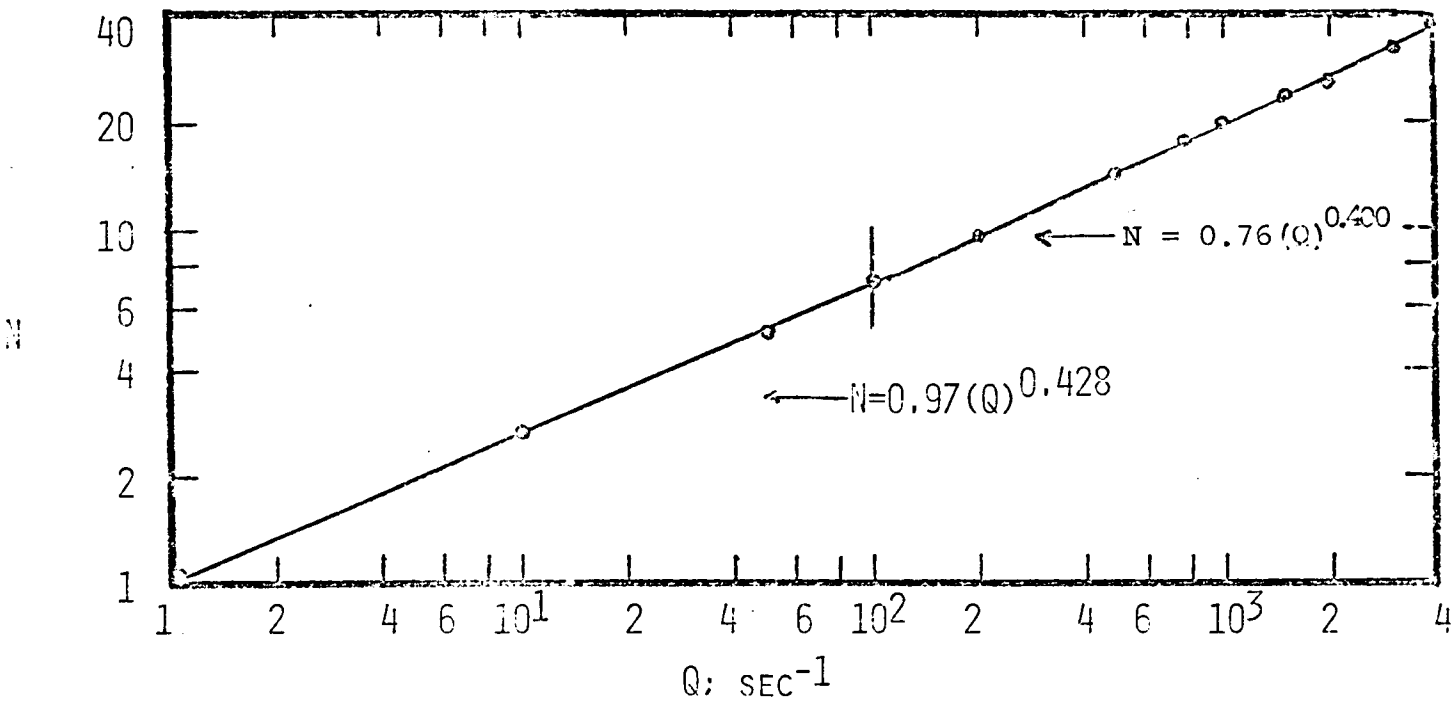

FIGURE 20 BAGLEY ENTRANCE CORRECTION IN EQUIVALENT TUBE DIAMETERS VS. APPARENT SHEAR RATE - 16.5% PIB IN VARSOL #2

flow curve measurements. Consequently, there is no exit region, and the velocity profile persists to the tube exit. We wish to underscore the significance of these findings. In order to obtain the exit pressure, it is necessary to extrapolate the stress profile. Further, evaluation of the integral term in Equation 25 requires knowledge of the velocity profile at the tube exit, commonly assumed to be the fully developed velocity profile. Therefore, the absence of an exit region justifies our procedures.

It is perhaps appropriate to note that Powell and Middleman (42) have found diameter effects in small tubes ($D < 0.08$ inches). In larger tubes (43), but still smaller than those employed here, their results were free of such anomalies. They attributed this phenomenon to elastic effects occurring during deceleration of the expanding jet. Evidently, additional studies on this critical issue are warranted.

C. Material Function Analysis

The material functions shown in Figure 21 exhibit three interesting features: (a) a nearly flat portion in the shear stress-shear rate curve, (b) both normal stress differences significantly larger than the shear stress, and most peculiarly, (c) a maximum in the second normal stress difference.

(a) Flat spots in the flow curves were also obtained by Brodnyan (44) for a concentrated polyisobutylene solution in decalin. We offer the folowing molecular argument; the solvent acts as a lubricant between the loosely-entangled polymer molecules. Once the shear stress is sufficient to disentangle the polymer chains, they are kept apart by the solvent molecules. Hence, small increases in stress above this critical level results in large changes in shear rate. The increase in the slope at the higher shear rates is probably due to the reduced time the polymer chains have to disentangle. Indeed, Lund and Pohl (45) have shown that such a flow region exists for a low molecular weight polyisobutylene without solvent. They presented arguments, similar to those here, involving the rolling and sliding of aggregates of molecules disentangled from the bulk.

The conversion of the apparent shear rate to the true shear rate at the wall via a Rabinowitsch analysis would be inaccurate because of the flat portion of the flow curve. Nonetheless, this limitation is of little consequence (46) as nothing is

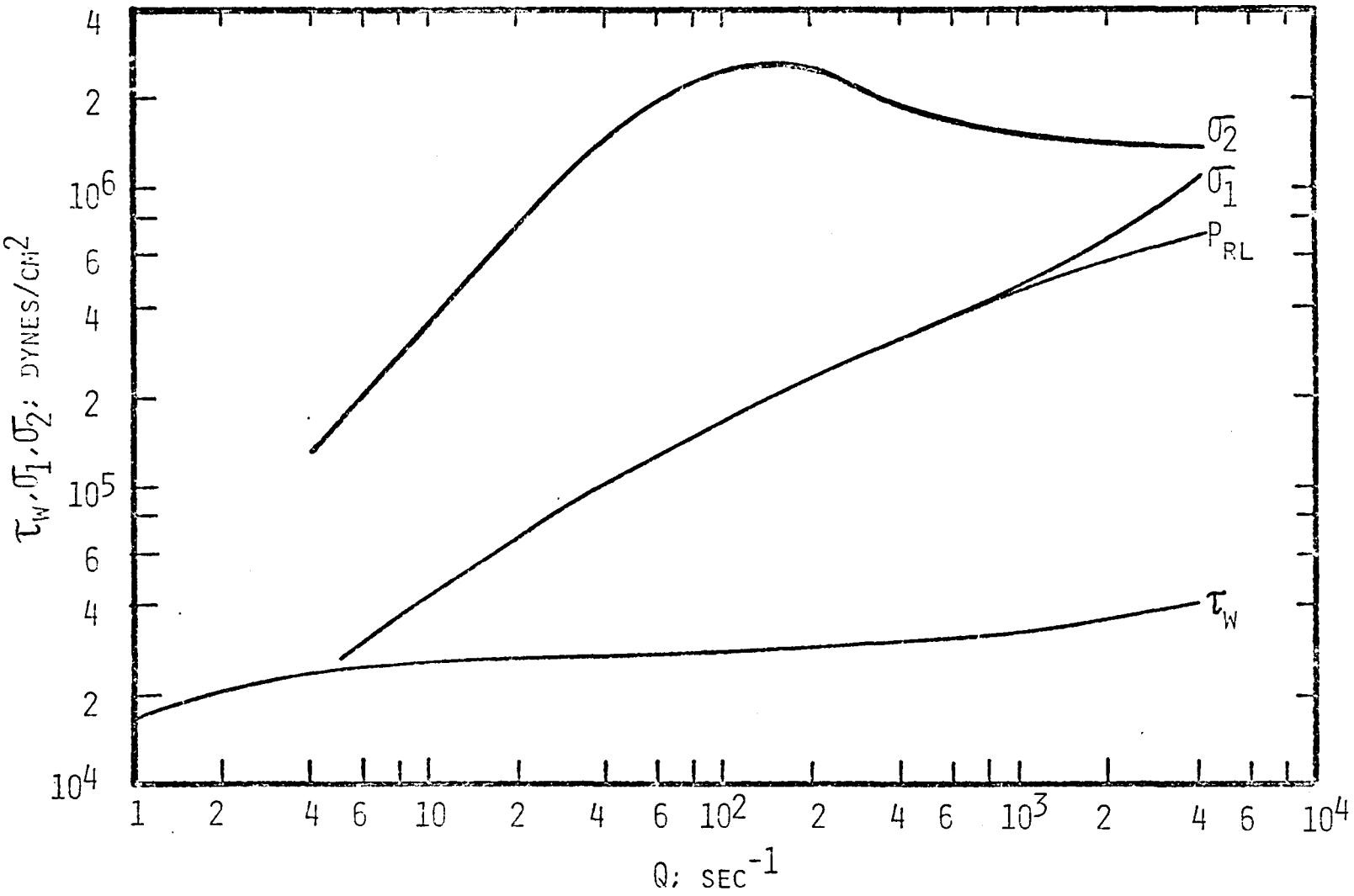

FIGURE 21 THE THREE MATERIAL FUNCTIONS: $\tau_w, \sigma_1, \sigma_2$: VS. APPARENT SHEAR RATE - 16.5% PIB IN VARSOL #2

gained by this manipulation, except for an expansion of the shear rate range. The basic relationships between the material function curves remains the same.

(b) The relative magnitudes of the three material functions presented in Figure 21 constitute timely and important findings. Many investigators persist in neglecting the second normal stress difference. They either set it, a priori, to zero (i.e., Weissenberg Hypothesis), or assume it to be very much smaller than either the first normal stress difference or the shear stress. For our fluid the second normal stress difference can be up to fifteen-times the first normal stress difference and more than sixty-times the wall shear stress. For a polyethylene melt, Han et al. (25) also found that the second normal stress difference was the largest in value. Specifically, they were in the ratio of $4(\sigma_2):2(\sigma_1):1(\tau_w)$. Their narrow shear rate range (160 to 700 sec^{-1}) perhaps prevented them from approaching the sufficiently high levels of molecular distortion which account for our relatively large normal stress differences.

As we have pointed out, the second normal stress difference has long been considered negligible with respect to the other material functions. For this reason, little theoretical material is available to predict the second normal stress difference, other than the rigorous method described earlier. On the other hand several theories exist for calculating the relative magnitudes of the first normal stress difference and the shear stress. Through the concept of recoverable shear strain, S_R $(= \sigma_1/\tau_w)$, Tanner (34), evaluating a KBKZ form of consti-

tutive equation, derived the following expression:

$$(29) \qquad S_R = 2.828[\delta^6 - 1]^{\frac{1}{2}} \ *$$

where δ is the equilibrium swell in long tubes. The experimental asymptote at low shear rates is actually 1.10 and not the value of 1.00 assumed in the theories. Therefore, for the sake of consistency, we also show the theoretical curve in Figure 22 shifted upward by 0.10 swell units. Below values of $\delta = 2.00$ ($Q=840$ sec^{-1}) agreement with the Tanner theory is quite good.

From a momentum balance around the free jet, Metzner et al. (39) derived the following expression for the first normal stress difference:

$$(30) \qquad \sigma_1 = \frac{\rho R^2 Q^2}{16 g_c n'} \left\{ [n'+1] \int_0^1 2\left[\frac{u}{V}\right]^2 \left[\frac{r}{R}\right] d\left[\frac{r}{R}\right] - \left[\frac{1}{\delta^2}\right]\left[n'+1+\frac{d\,\ell n[1/\delta^2]}{d\,\ell n[Q]}\right]\right\}$$

where n' is the slope of the tangent to the $\log[\tau_w]$-$\log[Q]$ curve evaluated at the apparent shear rate Q. In the course of this analysis the Weissenberg Hypothesis is evoked, an assumption we have shown to be inappropriate for our fluid. First normal stress differences evaluated by this method are more than an order of magnitude too small at apparent shear rates less than 1000 sec^{-1}. Even at an apparent shear rate of 4000 sec^{-1} the Weissenberg Hypothesis leads to a first normal stress difference that is one-fourth its actual value.

---

* The value of the premultiplier has been adjusted to give results consistent with our definition of recoverable shear strain.

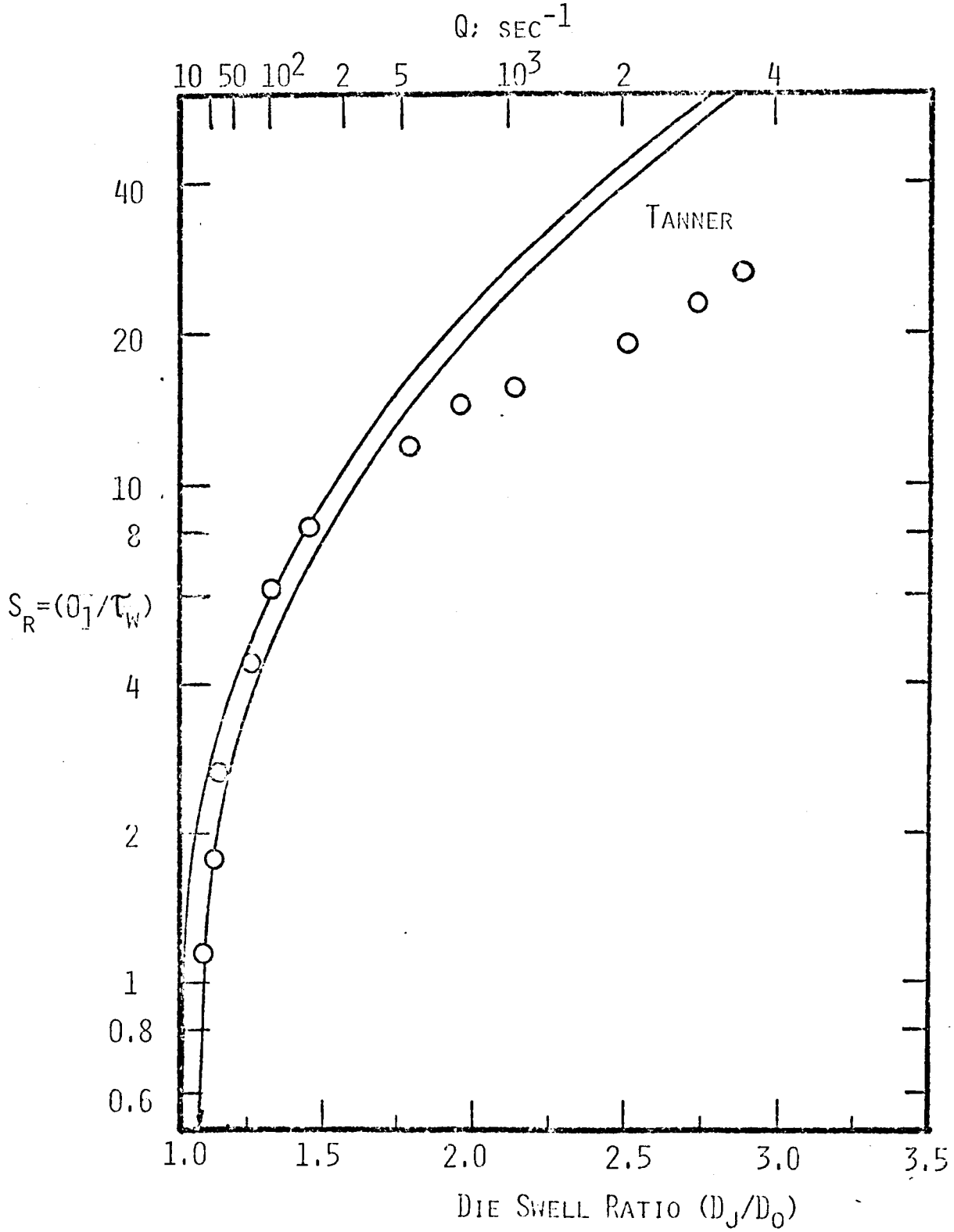

FIGURE 22 RECOVERABLE SHEAR STRAIN VS. DIE SWELL RATIO FOR VISCOMETRIC FLOW - 16.5% PIB IN VARSOL #2

A close examination of the procedure of Metzner et al. will show that the terms neglected in the momentum balance -

$$(31) \qquad p(0,L) + \int_0^R [\sigma_2/r]dr$$

are identically the exit pressure, P_{RL} (see Equation 16), a term known to be sizeable for many polymer melts. Our work has shown that the exit pressure can be sizeable for a polymer solution as well.

With the promising results for the Tanner theory in hand, we attempted to compare recoverable shear strain values at the die entrance according to the following rationale: entrance correction analysis (8) measures the amount of energy (in the form of a pressure head) lost in accelerating the highly viscoelastic fluid from the reservoir into the tube. Couette losses are small, and the lost pressure head results largely in stored elastic energy - represented by the excess elastic stress. With inelastic fluids the pressure loss is significantly smaller, and for the most part it is converted into a velocity head rather than into stored elastic energy. In Figure 23 we show recoverable shear strain values calculated by entrance correction analysis, and by using a pseudo-first normal stress difference, σ_1'. Here, σ_1' includes the excess elastic stress measured at the die entrance, in addition to the actual value of the first normal stress difference. Analytically these

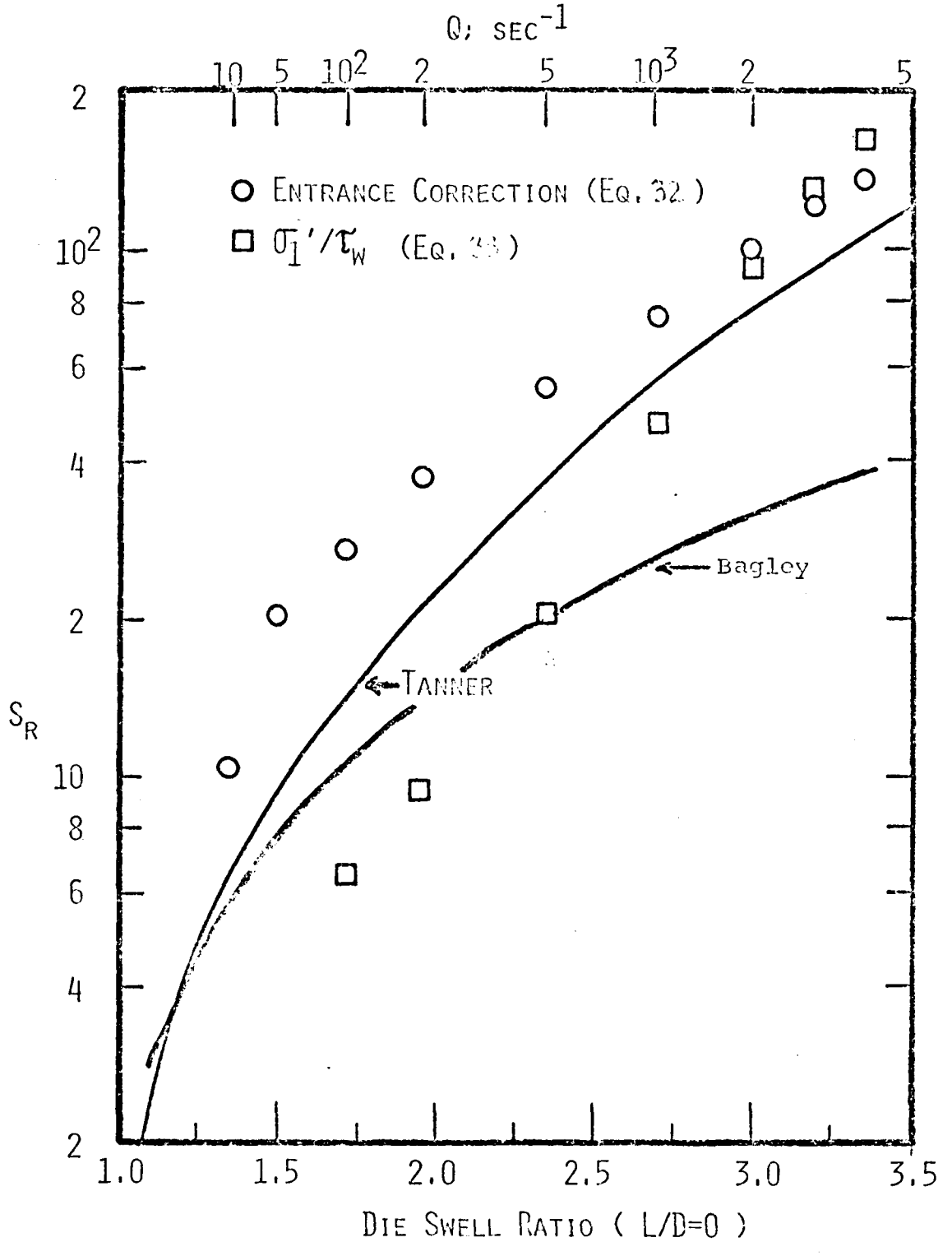

FIGURE 23 RECOVERABLE SHEAR STRAIN AT THE DIE ENTRANCE VS. DIE SWELL RATIO (ZERO LENGTH TUBE) - 16.5% PIB IN VARSOL #2

methods may be represented by:

(32) Entrance Correction $S_R = 4N$

where the value of N is given by Equation 28, and by

(33) Pseudo-First Normal Stress Difference $S_R = \sigma_1'/\tau_w$

where

(34) $\sigma_1' = [\sigma_1 + \text{excess elastic stress}|_{z=0}]$

Entry region recoverable shear strain values can also be estimated from the theory of Bagley and Duffy (33). Considering rubber-like elasticity for a two-constant Mooney material, they arrived at the expression:

(35) $\bar{S}_R = 0.707[\delta_o^4 - \delta_o^{-2}]^{\frac{1}{2}}$ *

where δ_o is the swell ratio for a zero length die. This equation gives averaged recoverable shear strain (across the die entry) values. Calculations show the averaged values to be about 15% of the wall values, and accordingly, the constant 0.707 in Equation 35, is replaced by the value 4.8 for comparison in Figure 23. The values for the Tanner theory were obtained using an extrapolated swell for a zero length die. There is substantial agreement among the methods. Thus the excess elastic stress, which we have introduced, is a reliable measure of the energy lost in the entrance region, and therefore can be regarded as an important parameter in tube flow.

* The value of the premultiplier has been adjusted to give results consistent with our definition of recoverable shear strain.

(c) To our knowledge, this is the first report in the literature on the existence of a maximum in the second normal stress difference. The graphical differentiation procedure used in calculating the second normal stress difference is reliable within ± 10%. The value of σ_2 at the maximum (Q=150 sec^{-1}) is more than 100 per cent higher than those calculated at the higher shear rates. Hence, the maximum in σ_2 is real though the exact location of the maximum is in doubt due to the inaccuracy cited. The indicated error range would place the maximum within the shear rate range of 90 to 250 sec^{-1}.

One can readily conceive of the physical circumstances that lead to this result. The normal radial stress at the tube exit - P_{RL} - arises from the distortion of the polymer molecule from its equilibrium random conformation (47). Obviously, there is a limit to this distortion, short of chain rupture. As we approach this limit, the second normal stress difference will, according to Equation 18, tend to zero. Since the second normal stress difference is also zero at zero shear rate, it stands to reason that, with $\sigma_2 > 0$ at intermediate shear rates, it must exhibit a maximum.

Based on available data for polymer melts and solutions, Bagley (1) reaches a similar conclusion. He states that as polymer melts approach recoverable shear strain values of seven units, they undergo a breakdown in Hooke's law in shear with the simoultaneous onset of melt fracture. In the case of solutions, however, this breakdown in Hooke's law in shear

coincides, not with melt fracture, but with a rapid increase in recoverable shear strain which does not level off until values of several hundred strain units are attained. Such high values would be expected if the polymer molecules were actually being uncoiled and stretched out in the flowing solution. It is just this behavior, as we have pointed out, that leads to the large values of the second normal stress difference relative to the first normal stress difference, and to a maximum in the second normal stress difference function.

D. Material Relaxation Time

Jet swell is a result of the recovery of both the residual entrance-borne elastic strains and the shear rate dependent normal stresses. We have already shown that the excess elastic stress is a direct measure of the elastic energy stored in the fluid. It seems apparent that the excess-elastic-stress decay with residence time and swell decay with residence time are manifestations of the same phenomenon, that is, stress relaxation. Consequently, the rate of decay of these variables should lead directly to values for the material relaxation time, λ. Figure 24 substantiates this assertion. Both the swell and the excess elastic stress decay exponentially with residence time, resulting in values for λ almost inversely proportional to the apparent shear rate. This is an interesting experimental observation in the sense that several recent constitutive equations also predict that a material's memory will regularly decrease with increasing levels of shear. The values determined from swell decay are slightly larger; and they cover a more extensive shear rate range because the excess elastic stress becomes unmeasureably small at shear rates less than 500 sec^{-1}. The magnitude of the relaxation times are typical of polymer solutions of this type.

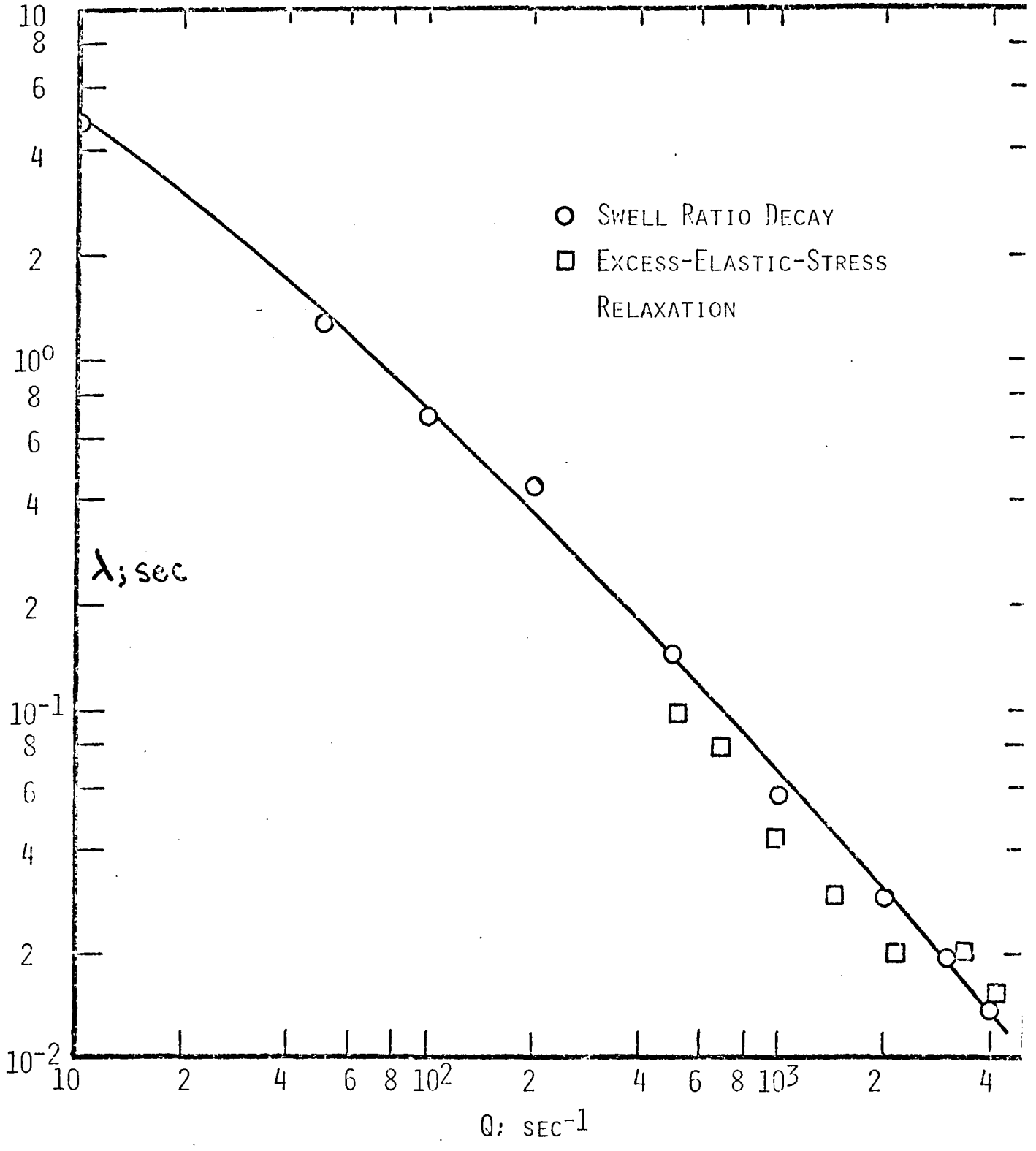

FIGURE 24 MATERIAL RELAXATION TIME VS. APPARENT SHEAR RATE-
16.5% PIB IN VARSOL #2

E. Conclusions

Axial radial stress profile measurements in tubes provide reliable values for the three material functions as well as a measure of the extent of the fluid's memory with respect to past deformations. For a viscoealstic polyisobutylene solution all three material functions were independent of tube diameter ($0.186 \leq D \leq 0.312$ inches). This finding has several important consequences. In the case of the shear stress, diameter-independence insures that: (a) the material does not possess a yield stress, (b) there is no slip at the wall, and most importantly, (c) the absence of an exit region justifies the extrapolation procedure to obtain the exit pressure, P_{RL}. Because the first normal stress difference and the second normal stress difference as well, are independent of tube diameter we can evaluate the exit pressure at the tube centerline, $p(0,L)$, as being identically zero.

The unusually flat shear stress function, the relative magnitudes of the material functions, and the maximum in the second normal stress difference can be adequately explained by molecular arguments based on a mechanism involving the uncoiling of the loosely-entangled polymer molecules with increasing shear.

Existing correlations for predicting the first normal stress difference only provide order of magnitude estimates

and are only useful over limited ranges of shear.

Excess-elastic-stress relaxation and swell decay with residence time give nearly equal values for the material relaxation times. This is indicative of their common nature - a measure of stored elastic energy.

APPENDICES

APPENDIX I. MATERIALS

A. Selection and Preparation

1. Introduction

A variety of fluids were surveyed for possible use subject to the following constraints: (a) both a viscoelastic and a viscoinelastic fluid were needed, (b) we had to use tubes with large L/D ratios (≈ 100) to insure an adequate viscometric flow region, and (c) because the transducers are physically lagre, the tube diameter could not be smaller than 0.186 inches. This resulted in overall tube lengths that exceeded thirty inches in some cases. System pressure limitations, coupled with these geometry requirements and the need to examine certain ranges of shear rate, dictated the use of fluids with a specific viscosity range.

2. Viscoinelastic

The selection of the viscoinelastic fluid was readily narrowed to two choices: (a) silicones, and (b) low molecular weight polybutylenes. Both classes are manufactured in a wide range of viscosities (directly related to their molecular weight). The adhesive quality of the polybutylenes eliminated them from further consideration because of the difficulties involved in material handling. The fluids finally selected were the 30,000 cs and the 100,000 cs viscosity grades of the silicone fluids, specifically - Dow Corning 200 Fluid^{TM}. Their viscous and elastic

properties are displayed in Figures 3 and 4 respectively. Additional properties are given in Table I-1. Neither of the visocsity grades required additional preparation prior to use, and, as long as they were kept free of extraneous matter they could be recycled without measureable change in their properties.

3. Viscoelastic

The search for a suitable viscoelastic fluid proved somewhat more difficult. Generally, polymer melts exhibit measureable elasticity, but these fluids were eliminated because of the desire to work at room temperature. Aqueous solutions of polyethylene oxide and polyacrylamide were eliminated on several counts: (a) they are readily shear degraded, (b) they exhibit property changes as a result of simple aging, and (c) they can not be made into solutions of sufficiently high viscosity to give accurate pressure profile measurements. Moderately high molecular weight polyisobutylenes, while viscous enough, were tacky and not sufficiently elastic. A concentrated solution of an extremely high molecular weight polyisobutylene ($\bar{M}_v > 5 \cdot 10^6$) in mineral spirits proved to be suitable for these studies. Specifically, a 16.5% solution of Vistanex L-200^{TM} (Enjay Chemical Company) in Varsol #2^{TM} (Humble Oil and Refining Company). Mineral spirits was the preferred solvent because of its lower vapor pressure and lower toxicity compared to other common organic solvents. Table I-1 gives additional material properties. The procedure for the preparation of homogeneous, bubble-free

Table I-1. MATERIAL PROPERTIES

Property	Dow Corning 200 Fluid		Vistanex L-200	Varsol #2	Sol'n
	30,000 cs	100,000 cs			
Natural State	Viscous Liquid	Viscous Liquid	Solid Rubber	Liquid	Viscous Liquid
SpGr	0.975	0.977	0.92	0.8076	0.826
Molecular Weight	---	---	$\bar{M}_v \simeq 5 \cdot 10^6$	125 - 145	---
Boling Point, ^oF	---	---		306 - 379	---
Surface Tension, dynes/cm	21.5	---	---	---	---

solutions follows: Briefly, the polyisobutylene is supplied in a compressed block of rubber crumb. The block was reduced to the original crumb-size particles (0.5-1.0 inch), and then cut into smaller, 1/4 inch pieces. A four gallon master-batch of solution was prepared by placing the required amount of crumb in a five gallon container,adding the mineral spirits, and then rolling on a ball-mill for 48 hours to initiate the solvation process. Six successive treatments of alternating intensive mixing for 1 hour (in a heavy-duty drill press with a large impeller) with a 23 hour solvation period in a 40° C oven were sufficient to homogenize the solution as indicated by random sampling. Bubbles were found to completely rise within 48 hours of the last mixing period.

APPENDIX II. EQUIPMENT

A. Introduction

A general description of the experimental setup was given in Section III. Here, we present a detailed description of the individual components, accompanied by diagrams, and manufacturers' specifications where appropriate.

B. Pneumatic and Timing Circuits

1. Introduction

A schematic of the pneumatic circuit is shown in Figure II-1. This section of the system consists of three basic components: (a) nitrogen pressure regulation (low range/0-100 psi, medium range/0-600 psi, high range/0-1500 psi), (b) electric solenoids for controlling rheometer pressurization and venting, and (c) the timing circuit.

2. Nitrogen Pressure Regulation

Each regulation circuit for the different pressure ranges contained a Hoke-Phoenix two-stage pressure regulator, Model # 521, equipped with a Marsh Instrument Company pressure gauge of the following type:

a. Low range - Master Test type 100, 0-100 psi, 1 psi subdivisions

b. Medium range - Safe Case Master Test type 200-c, 0-600 psi, 2 psi subdivisions

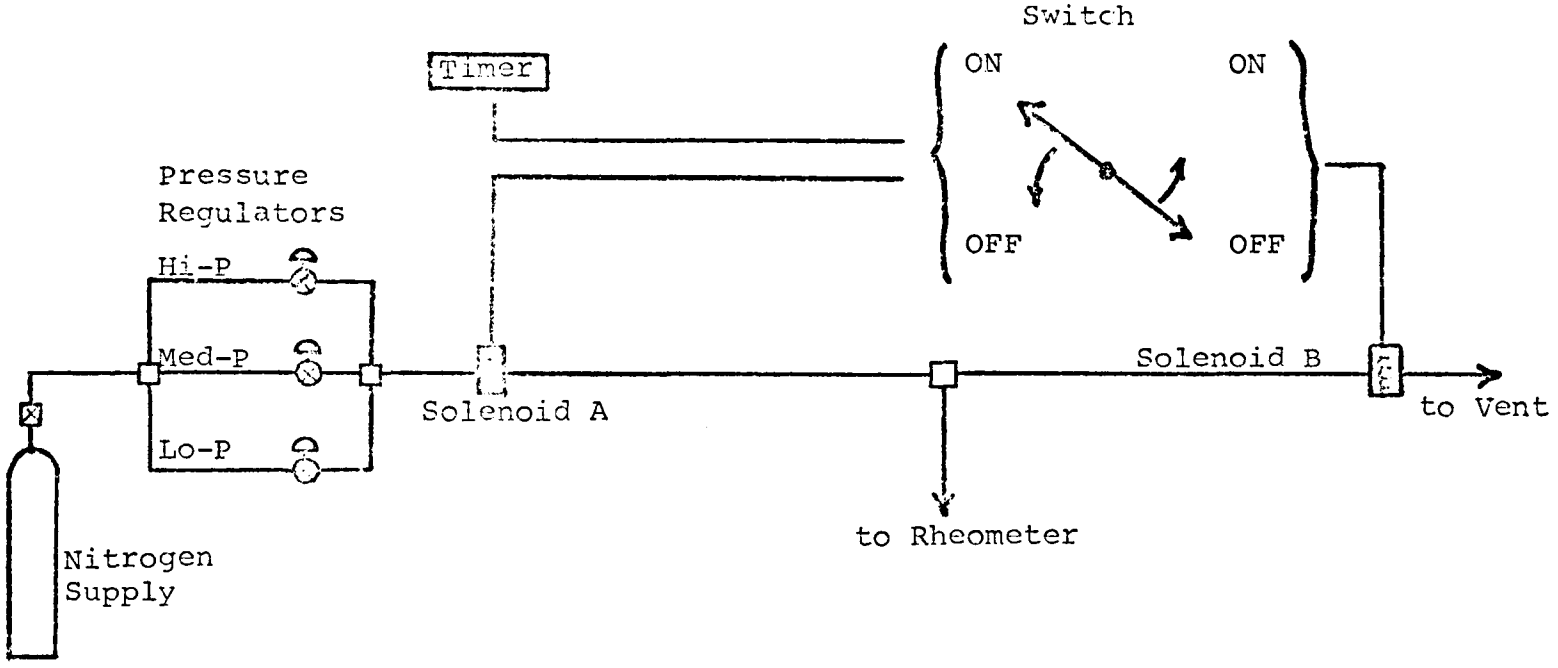

Figure II-1. Pressure Regulation and Timing Circuits

c. High range - Safe Case Master Test type 200, 0-1500 psi, 10 psi subdivisions

The pressure gauges were calibrated with a primary standard - Ashcroft Dead Weight Gauge Tester Model #1300 - and found to be within the manufacturers' error specification (less than 0.25% of full scale) over the useful gauge pressure range.

3. Electric Solenoids

The solenoid valves - Automatic Switch Company Model #826296 - are closed in the deenergized state and open when energized. A pair of these solenoids work together in the following fashion. In the at rest state, solenoid A is de-energized and solenoid B is energized, that is the nitrogen supply is shut off from the rheometer, and the rheometer itself is vented to the atmosphere. When the switch is thrown on, solenoid A opens and solenoid B closes, simoultaneously. The nitrogen supply is admitted to the rheometer while the vent is closed. The pressure rises rapidly (< 1/2 second) in the reservoir, and the material flows from the reservoir through the attached die. Turning the switch off, deenergizes, or closes, solenoid A, and at the same time energizes, or opens, solenoid B. This effects the simoultaneous closing of the nitrogen supply and opening of the rheometer vent, depressurizing the rheometer.

4. Timing Circuit

The same switch that controls the pair of solenoids, for

the pressure regulation circuit, also controls the electric timer - Standard Electric Time Company Model S-1/option 7 - so that the timer automatically records the actual time of pressurization. Flow runs were of sufficient duration to keep pressure transients below 2% of the total run time.

C. Rheometer

1. Introduction

The basic design of the rheometer is geometrically simple. It consists of a cylindrical shell with provisions for: (a) filling with a variety of polymeric fluids whose consistency may be extremely viscous, or even gum like, (b) pressurizing and venting, and (c) attaching dies of various flow geometries. Important considerations were: (a) pressure requirements - up to 2000 psig, (b) compatibility between materials of construction and the test fluids, and (c) general flexibility of purpose.

2. Design

According to Kowalski (10), if the reservoir to tube diameter is maintained at a ratio of ≥ 15, then the rheometer reservoir behaves as an infinite reservoir. We could have simply chosen a reservoir diameter sufficiently larger than our largest tube, but to increase the utility of the instrument, we chose to construct a series of nestled shells. Each shell diameter was 15 times a standard size tube diameter (see Table II-1), and was machined from cold-rolled, low-carbon, round, mechanical seamless steel tubing, type 1018. Stainless steel was unnecessary because the test fluids were not corrosive, and organic solvents (as opposed to water) were used. In addition, stainless steel is difficult to machine. The shell

Table II-1. **RHEOMETER DIMENSIONS**

Shell		Standard Tubes	0-ring Location 3/16" Viton 0-ring on a --- inch circle
O.D.; inches	I.D.; inches	I.D.; inches	
7.500	5.600	0.370	5.935
5.590	4.665	0.312	5.185
4.655	3.720	0.248	4.185
3.710	2.790	0.186	3.310
2.780	1.920	0.128	2.435*
1.910	0.975	0.065	1.498*

* 1/8" O-ring

wall thicknesses were sized according to standard thick-walled cylinder pressure-design equations. All the shells were 8.00 inches long, and each contained an o-ring groove and viton o-ring at both ends to maintain the pressure seal (see Table II-1). The largest cylinder was tapped for a series of 3/8-16 Allen head bolts. There were 15 bolts on the circle, and thread depth was at least 1.5 inches. The top and bottom plates for the rheometer were machined from 1.4 inch thick, 8.0 inch diameter, hot-rolled, leaded, low-carbon steel plates, type C1117. The top plate was fitted with an adaptor for connection to the pressurization circuit, and was then bolted to the largest shell with the 3/8 inch bolts. The bolts were tightened to the recommended torque to effect a pressure tight seal. The bottom plate was further machined to accept interchangeable fittings, depending on whether or not a slit or tube die was being used. This plate was also bolted to the largest diameter shell. In general, if any of the smaller reservoir diameters would be required, all the larger size shells were used. This procedure insures that the reservoir is centered over the die. As it happens, we did not investigate the effect of reservoir to tube diameter ratio (nor did we plan to), so only the largest shell was used. The ratio of the reservoir diameter to tube diameter was greater than 18 in all cases. As the design is rather straightforward, only the bottom plate and mounting adaptors will be shown in more detail in Figures II-2 a-b.

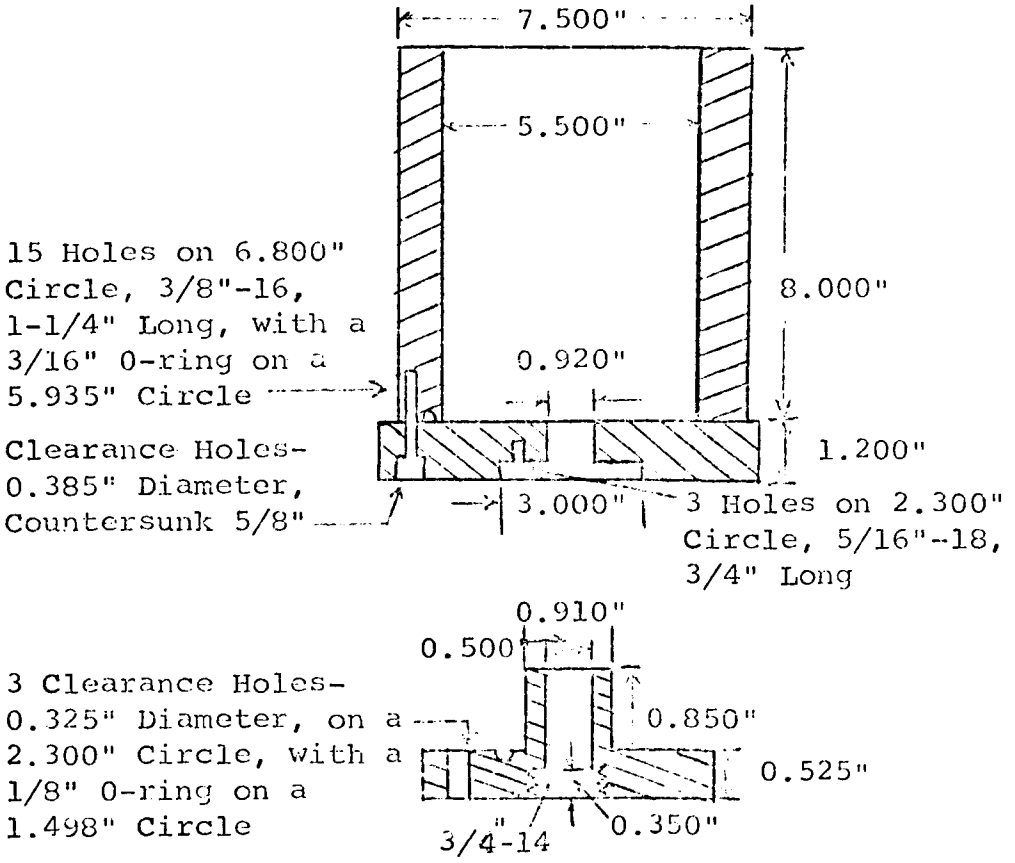

Figure II-2a. Rheometer Base and Shell (1/4 Size) and Universal Die Mount (1/2 Size)

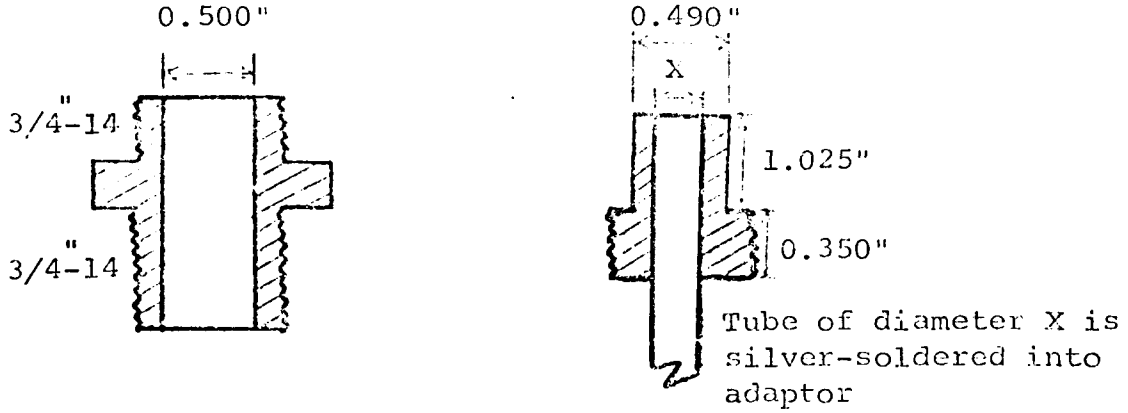

Figure II-2b. Adaptors for Slit and Tube Mounting - Full Size

D. Dies

1. Introduction

Each phase of the research program required a die(s) particular to that phase. For example, the study of the effect of a recess mount on the measured stresses necessitated a slit flow geometry to that a true flush mount could be realized. The following sections describe the individual dies (set of dies) necessary for the individual phases.

2. Slit Die for Recess Mount Effect Study

Aluminum plate, type 2024-T3, was chosen as the material of construction, mainly for its ease in machining. However, die weight, and compatibility with the test fluids, were also considered. The details of construction are shown in Figures II-3a-b. The slit length is 6.001 inches, the slit width is 3.002 inches and the slit gap is 0.062 inches. To simplify construction, the gap was machined from only one face. The two faces were fastened together with a series of 3/16-18 Allen head bolts. A steel washer was used under the bolt head to protect the aluminum. The transducers were mounted in four diametrically opposed pairs. Each pair consisted of a flush mount and a recess mount transducer. The mounting details are shown in Figure II-3b. The interchangeable inserts with the different recess hole diameter were machined from aluminum rod, type 2024-T3. An end plate, to seal the die exit, was

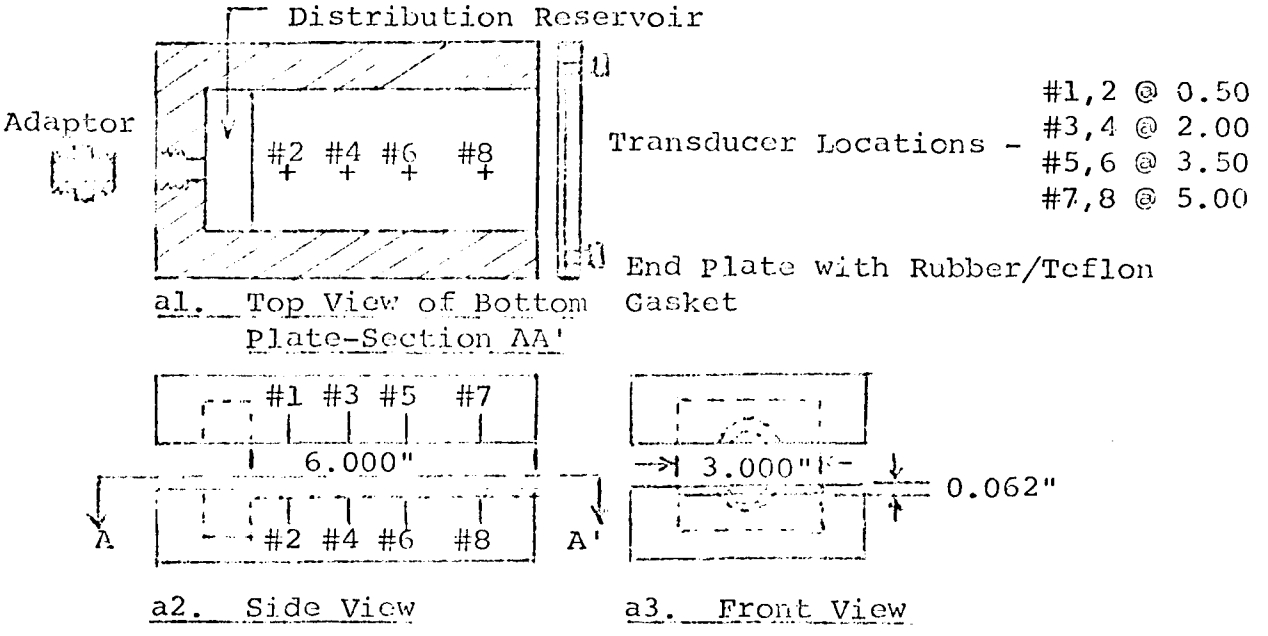

Figure II-3a. Slit Die - Nominal Dimensions and Transducer Locations

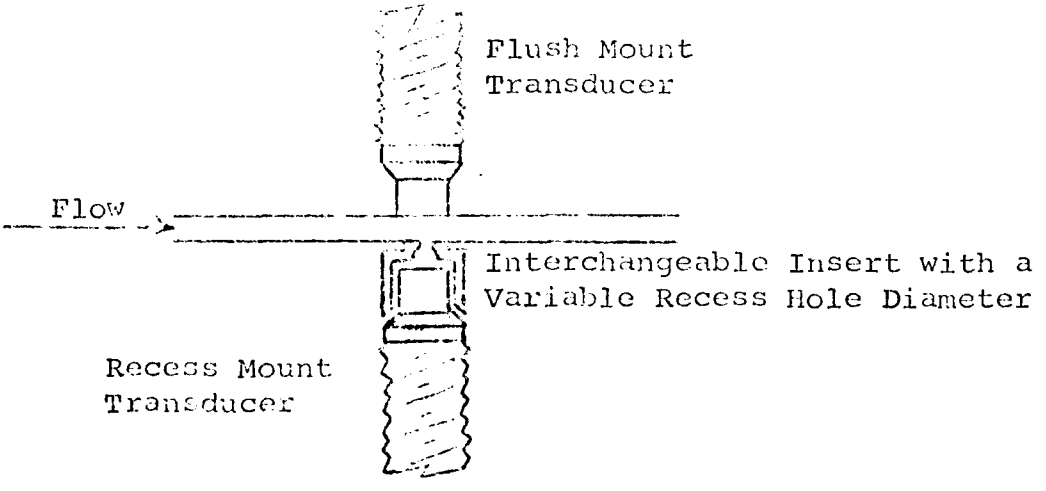

Figure II-3b. Detail of Slit Transducer Mounting

used to static test and calibrate the pressure transducers, in situ. A two-part gasket was used, consisting of a Teflon facing over a standard rubber gasket backing.

3. Tube Dies for Recess Mount Effect Study

The intersection of the recess hole with the tube wall gives a saddle-shaped hole profile. As the recess hole diameter approaches the tube diameter, considerably more surface than the nominal cross-sectional area of the drill is removed from the tube wall. This might have an effect on the measured stresses not found in the slit flow recess geometry. Five tubes were constructed from seamless, type S304 stainless steel tubings, identical in all respects except for the size of the recess hole, which was varied in five steps, from 0.020 inches to 0.063 inches. The transducer mounts here were somewhat more complicated than those used in the slit die, especially in that they contained a bleed hole to remove entrapped air, and therefore improve the response time of the recess transducers. Mount details are shown in Figures II-4a-b. The bleed holed were sealed with a set screw-lead shot combination. Each tube was 31.500 inches long with an inside diameter of 0.312 inches, and had eight transducer mounts located 2.250, 3.750, 5.250, 7.250, 11.000, 16.000, 22.000 and 29.000 inches from the tube entrance. The tube was attached directly to the rheometer through the use of an adaptor previously described in

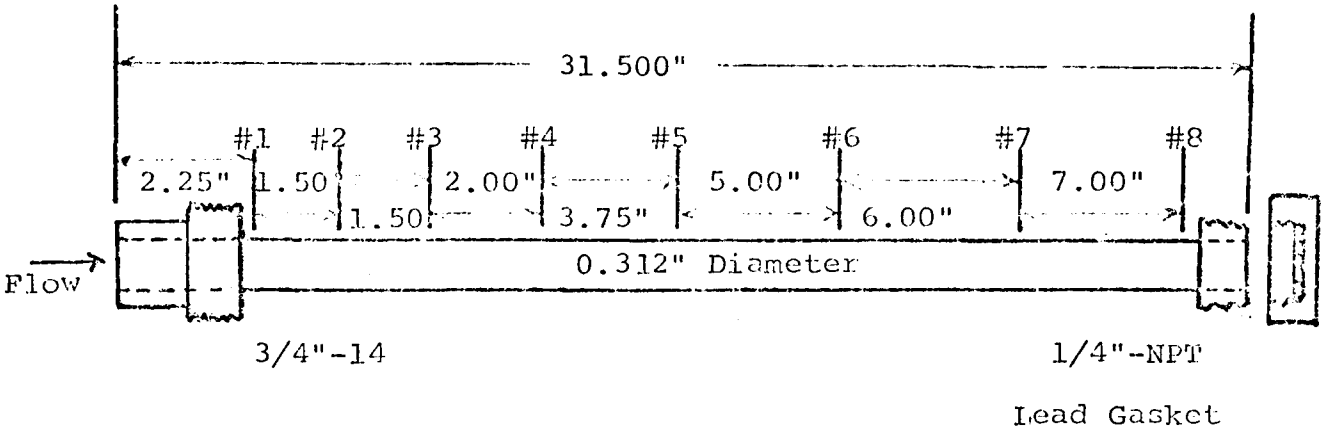

Figure II-4a. Transducer Locations and Nominal Dimensions

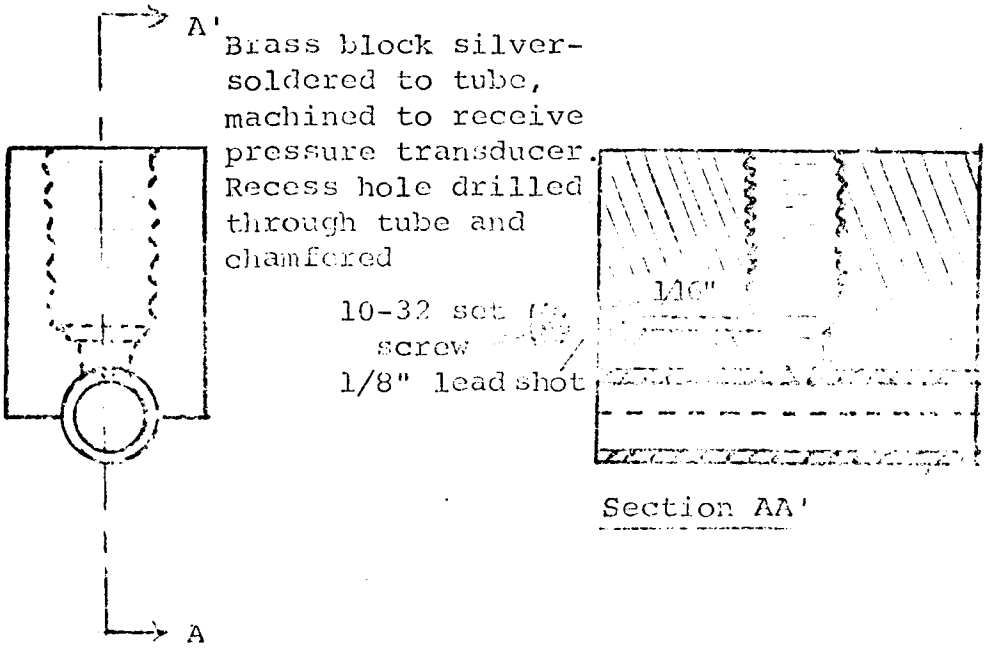

Figure II-4b. Detail of Recess Transducer Mount in a Tube

Figure II-2b. A 1/4"-NPT, male fitting was silver-soldered to the tube exit. A lead gasketed cap screwed over this fitting enabled static testing and transducer calibration *in situ*.

4. Tube Dies for Tube Diameter Effects

In addition to the 0.312 inch inside diameter-0.052 inch recess hole diameter tube described in the previous section, two more tubes were constructed from seamless, type S304 stainless steel tubing: 0.186 tube diameter-0.029 recess hole diameter and 0.242 inch tube diameter-0.040 inch recess hole diameter combinations. The same type of transducer mount was used except that smaller size ball mill grooves were used, in order to accommodate the smaller diameter tubes. In the 0.186 inch tube the mounts were located 2.250, 3.750, 5.250, 6.750, 8.500, 10.500, 13.500 and 16.500 inches from the entrance. In the 0.242 inch tube the mounts were located 2.250, 3.750, 5.250, 7.000, 9.500, 13.000, 17.000 and 22.000 inches from the entrance. These tubes were also fitted with exit fittings to allow static testing and calibration.

5. Tube Dies for Swell Ratio Decay and Entrance Correction Studies

For the swell ratio decay study, a series of tubes was constructed, from 0.186 inch diameter stainless steel tubing, with length to diameter ratios of 2, 4, 8, 16 and 64. For the en-

trance correction study, one additional tube was used; this was the 0.186 inch diameter, 31.500 inch long tube used in the tube diameter effect study.

E. Signal Conditioning and Amplification

This section of the apparatus is composed of three basic parts: (a) strain gauge pressure transducers, (b) signal conditioning circuits - excitation and balance controls, and (c) amplifying circuits - offset and gain controls. Originally, a feasibility study was performed to ascertain the approximate magnitudes of the recess hole pressure errors, and of elastic effects through a measure of the exit pressure. For this purpose, we designed a complete strain gauge conditioning and amplification system for six pressure transducers. There was not a sufficient amount of channel separation ($\approx$40 dB), but a first order correction to the measured pressures indicated that the research would be justified with more sensitive equipment. Rather than elaborate on the original design (Appendix III-1), we instead describe the finalized version of the equipment (Figure II-5). The main improvement was the replacement of the original circuits, with an Electronics Ltd. Model 1808, 8 channel, strain gauge conditioner and amplifier. Some important features of this instrument are: (a) individual, variable bridge excitation; 0-10 VDC, (b) individual bridge balance circuits, (c) individual, variable gain controls; 20-1500X, and (d) channel separation of greater than 100 dB.

The pressure transducers are Barber-Colman Models A-7556-100 and A-7556-101, 0-1500 psig range. The newer model (-101)

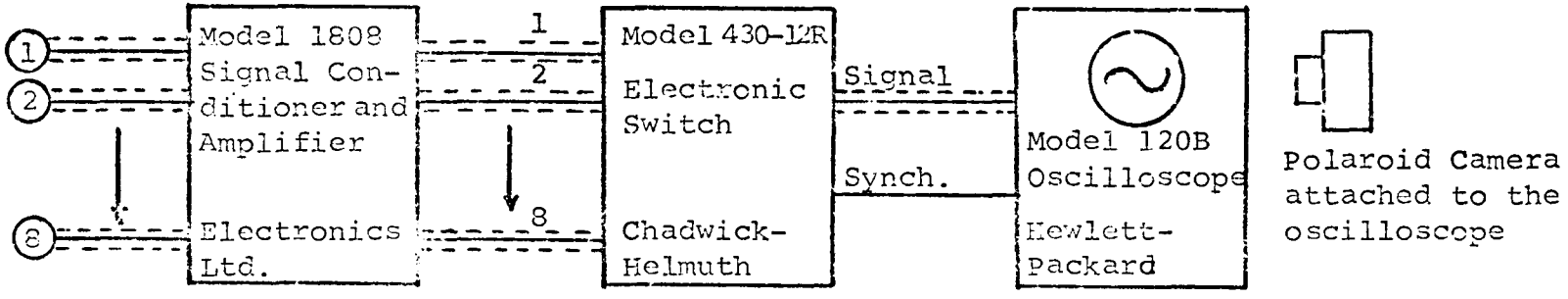

Figure II-5. Signal Conditioning and Amplification Equipment Layout

had detachable electrical leads which made them far more desirable than the older model (-100). The prescribed (by the manufacturer) electrical calibration procedure, utilizing a shunt resistor supplied by the manufacturer, gave poor results. The method eventually adopted involved a static load calibration after the transducers had been mounted in the various test geometries, and it gave fairly reproducible results.

The specific manufacturer's specifications and the circuit diagrams for the transducers and strain gauge conditioning and amplifying equipment will be found in Appendix III-2.

F. Signal Sampling, Display and Measurement

A multichannel oscillographic recorder is the preferred method of data handling. However, lack of funds prevented its purchase. An alternate procedure was developed which was just as accurate, though more cumbersome. An electronic switch (Chadwick-Helmuth Model 430R-12) using the eight amplifier outputs as the signal input, sequentially sampled each channel at a rate of 1000 channels per second, and displayed the signals on an oscilloscope, thus giving an essentially continuous record of all the transducer outputs (see Appendix III-3). A synchronization circuit triggers the scope trace every time the first transducer channel is selected. A Polaroid transparency (type 146L) is taken of the oscilloscope trace. As long as the exposure time is long enough for all the channels to have been selected ($>$ 0.01 second), a complete record of the eight channel outputs will be obtained. The picture is in the form of a positive transparency; an optical comparator was used to measure the outputs (vertical excursion from the baseline) to the nearest 0.0001 inch. Calibration of the tranducers involved capping the slit die (or tube), static loading at various pressures, taking pictures of the transducer outputs and fitting the data with a quadratic equation by the method of least-mean-squares. In some cases, hand drawn calibration curves proved just as reliable as the computer calculated curves.

APPENDIX III. MANUFACTURERS' SPECIFICATIONS, EQUIPMENT DATA SHEETS AND CIRCUIT DIAGRAMS

APPENDIX III-1. ORIGINAL SIGNAL CONDITIONING AND AMPLIFIER CIRCUITS

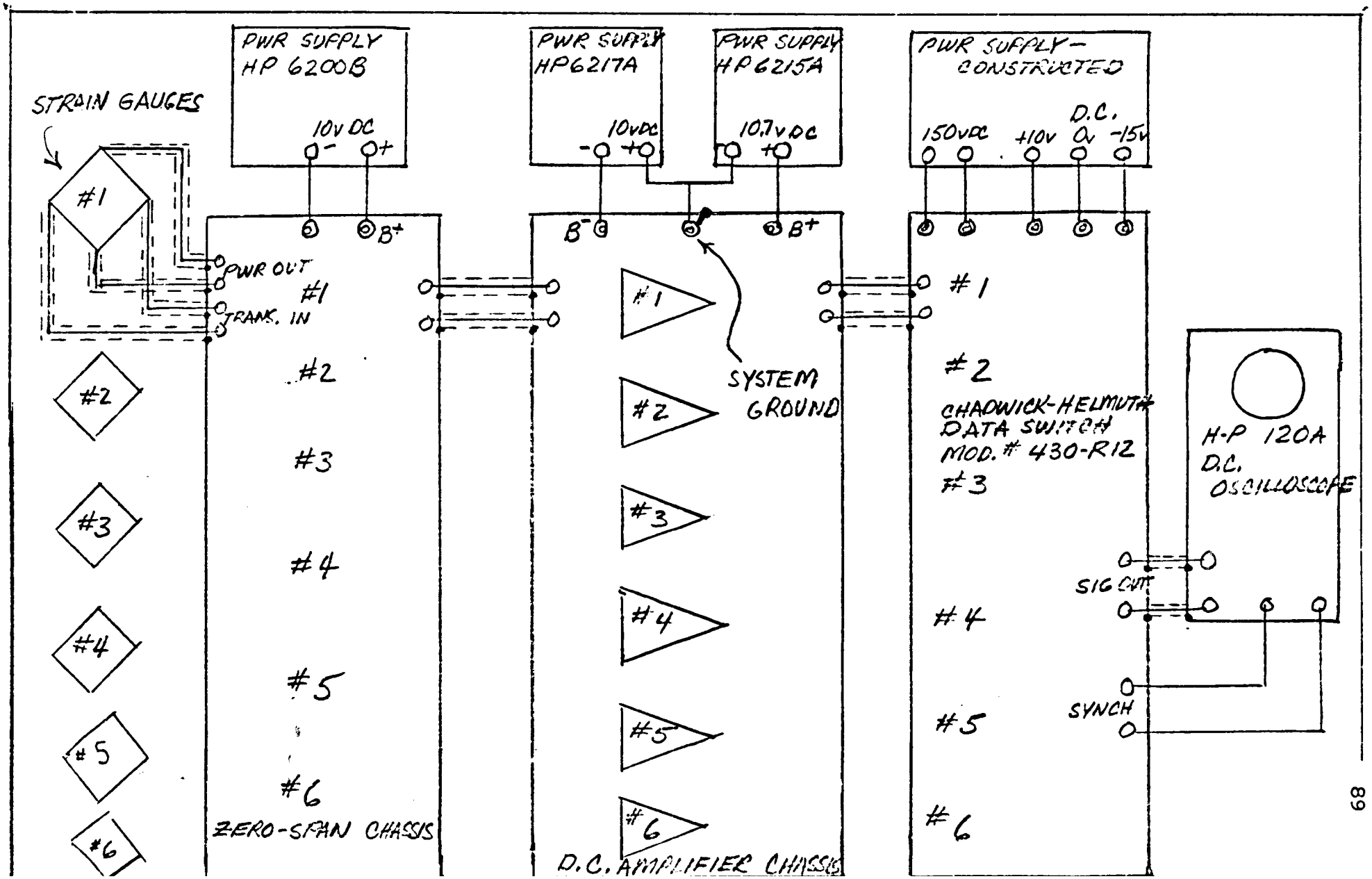
PWR SUPPLY HP 6200B
10v DC
PWR SUPPLY HP6217A
10vDC
PWR SUPPLY HP6215A
10.7v DC
PWR SUPPLY — CONSTRUCTED
150vDC
+10v
D.C. 0v
-15v
STRAIN GAUGES
#1
#2
#3
#4
#5
#6
PWR OUT
TRANS. IN
B+
B-
SYSTEM GROUND
ZERO-SPAN CHASSIS
D.C. AMPLIFIER CHASSIS
CHADWICK-HELMUTH DATA SWITCH MOD. # 430-R12
H-P 120A D.C. OSCILLOSCOPE
SIG OUT
SYNCH

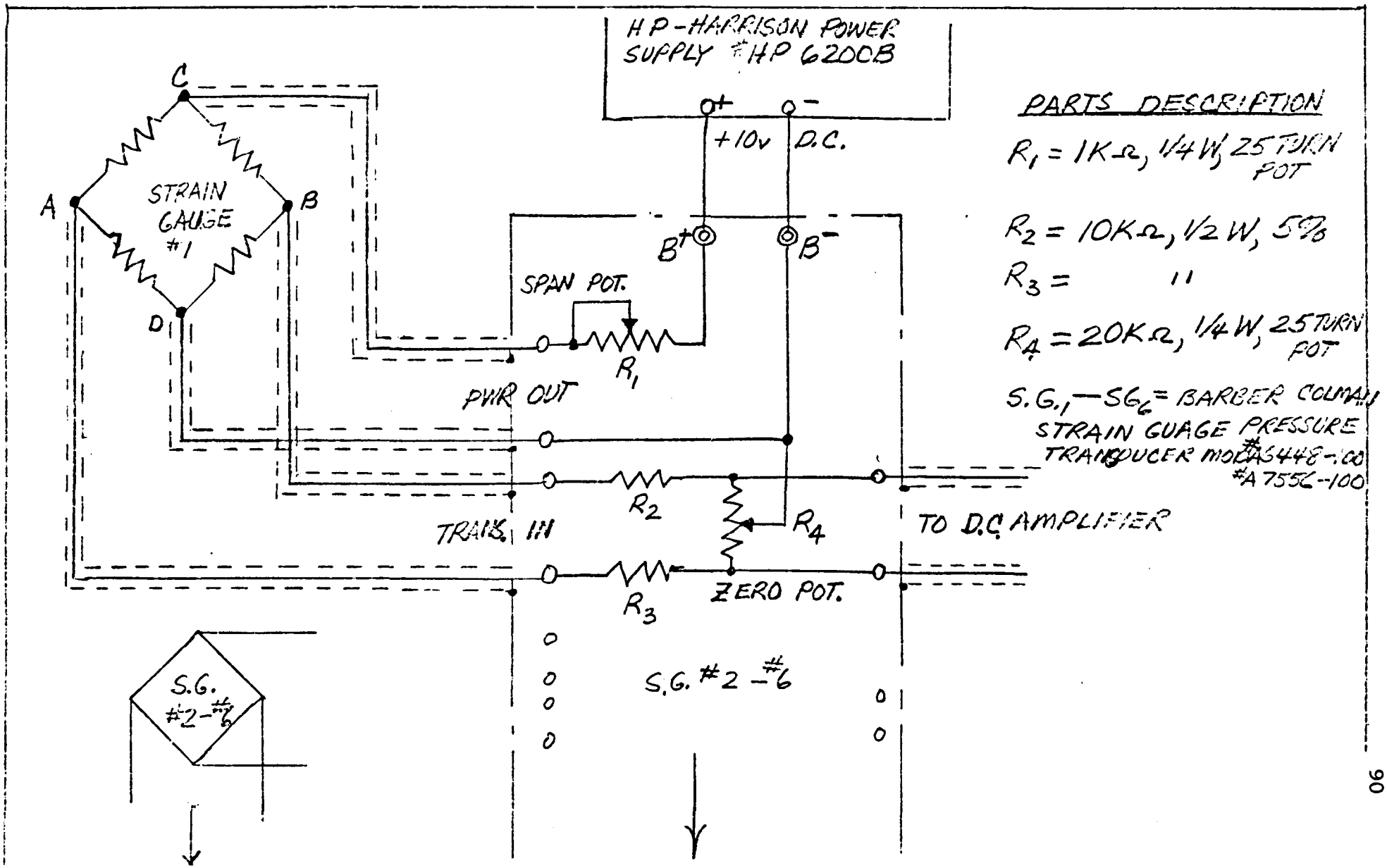

PARTS DESCRIPTION

R_1 = 1KΩ, 1/4 W, 25 TURN POT

R_2 = 10KΩ, 1/2 W, 5%

R_3 = "

R_4 = 20KΩ, 1/4 W, 25 TURN POT

S.G.1 — S.G.6 = BARBER COLMAN STRAIN GUAGE PRESSURE TRANSDUCER MODEL #AS448-100 #A 755C-100

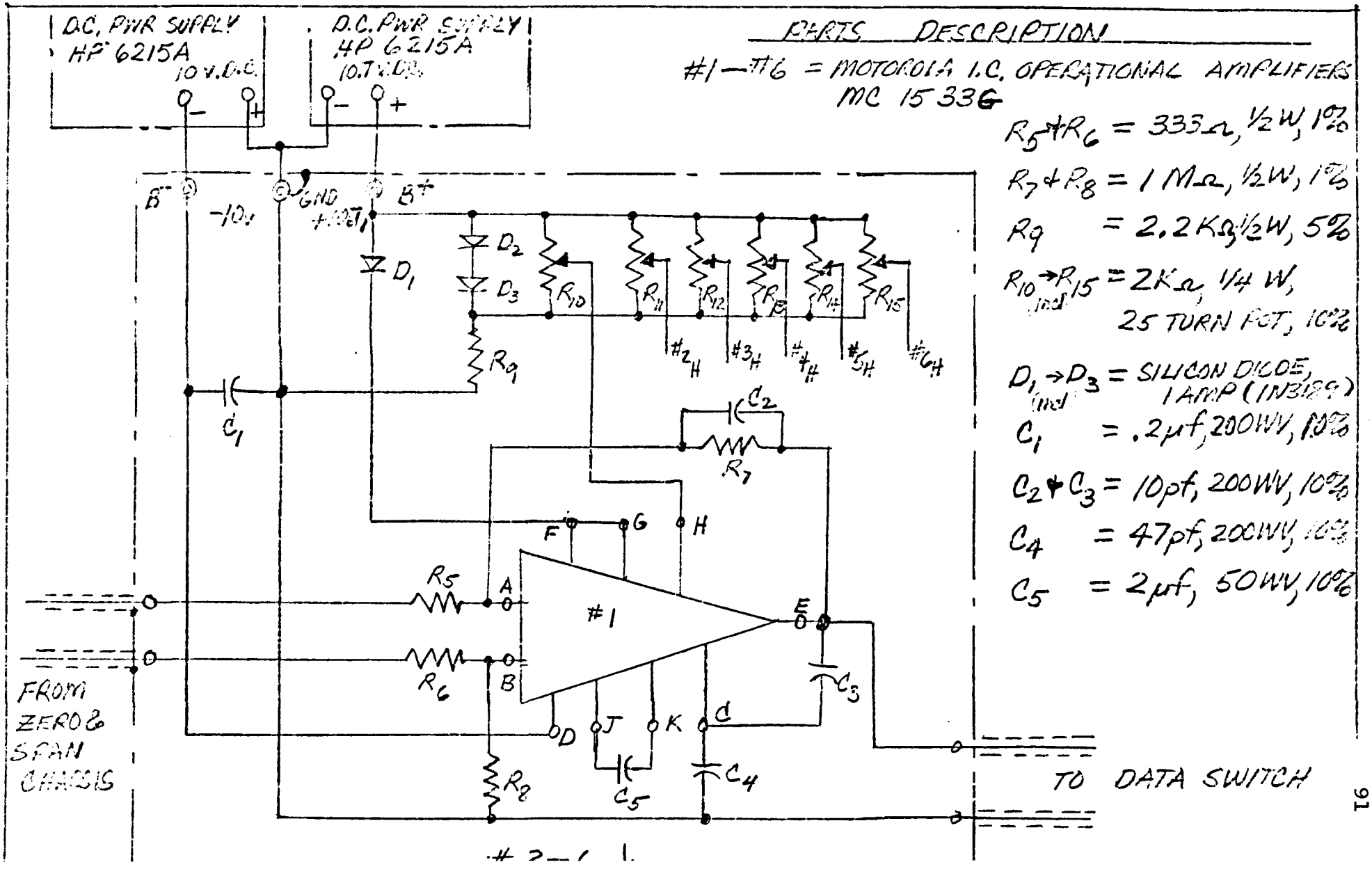

PARTS DESCRIPTION

#1—#6 = MOTOROLA I.C. OPERATIONAL AMPLIFIERS MC 1533G

$R_5 + R_6$ = 333Ω, ½W, 1%

$R_7 + R_8$ = 1 MΩ, ½W, 1%

R_9 = 2.2 KΩ, ½W, 5%

$R_{10 \text{ incl}} \rightarrow R_{15}$ = 2KΩ, ¼ W, 25 TURN POT, 10%

$D_{1 \text{ incl}} \rightarrow D_3$ = SILICON DIODE, 1 AMP (IN1183)

C_1 = .2μf, 200WV, 10%

$C_2 + C_3$ = 10pf, 200WV, 10%

C_4 = 47pf, 200WV, 10%

C_5 = 2μf, 50WV, 10%

APPENDIX III-2. FINALIZED PRESSURE TRANSDUCER SIGNAL CONDITIONING AND AMPLIFICATION CIRCUITS

SENSING ELEMENTS

PRESSURE TRANSDUCERS FOR PLASTIC APPLICATIONS

- **High Temperature Application**
- **Cooling not required**
- **Extended Pressure Ranges**

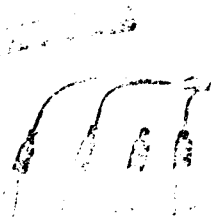

- **Rugged, Reliable Performance**
- **Thermocouple Combination and Connector Options**

Barber-Colman Pressure Transducers have been developed specifically for the plastics industry, for use with extruders and blow molding machines. The design incorporates a proven four active arm bridge type bonded strain gauge sensing element to which a fixed d-c potential is supplied. When the pressure changes, the four arms of the strain gauge change resistance causing an unbalance in the circuit. The magnitude of the resultant change is indicated by the instrument used.

Unlike other units, these improved transducers do not require forced water cooling. Installation is greatly simplified; there is no possibility of damage to the sensitive transducer because of loss of cooling media. Constructed of stainless steel (including the diaphragm) these units have proven exceptionally reliable. No special installation precautions are necessary. Their rugged design will stand up to 240 inch pounds of torque.

Performance characteristics are outstanding. Hysteresis and non-linearity is less than 1% of full scale. Zero drift is a minimum. The unit will operate at stem temperatures as high as 700°F.

Models are available with 6" or 12" stem lengths and 1/2-20 or 5/8-18 mounting threads. Pressure ranges are up to 20,000 psi. A specification record furnished permits field calibration of the indicator to the transducer using the simple shunt resistor method.

Special Order Variations:

When temperature measurement is required, an iron-constantan thermocouple can be incorporated in the body of the transducer, making a combination unit. Models are also available using a male with female connector attached directly to the transducer, in place of the cable as shown in the photograph. (The cable is then ordered separately.)

SPECIFICATIONS

Pressure Measuring Element – Bonded Strain Gauge.

Configuration – Four active-arm Wheatstone Bridge.

Excitation Voltage – 10 volts d-c or a-c maximum.

Nominal Resistance – 350 ohms.

Linearity – .5% of full scale.

Hysteresis – .5% of full scale.

Sensitivity – 3.5 ± .5 millivolts per volt (*open circuit*).

Frequency Response — 2000 cps

Thermo Zero Shift – 1.0% FS/100°F.

Thermal Sensitivity Shift – .2% FS/100°F.

Stem Temperature – 700°F maximum.

Mounting Torque – 240 inch-pounds maximum.

Stem Length – 6" or 12" by selection.

Stem and Thd. Dia. – 1/2 or 5/8 by selection.

Material — Type 416 Stainless Steel.

Thermocouple Calibration – Type J Iron – Constantan (combination units only).

NOTE: *A certificate of specifications accompanies each transducer.*

ORDERING NUMBERS

PRESSURE TRANSDUCERS FOR PLASTIC EXTRUDERS

Model	P.S.I Range	Stem Length	Thread Size
A-7555-100	0- 1,500	6"	1/2-20
A-6448-100	0- 3,000	6"	1/2-20
A-6449-100	0- 5,000	6"	1/2-20
A-6450-100	0-10,000	6"	1/2-20
A-7338-100	0-15,000	6"	1/2-20
A-7552-100	0-20,000	6"	1/2-20
A-7605-100	0- 1,500	12"	5/8-18
A-7154-100	0- 3,000	12"	5/8-18
A-6966-100	0- 5,000	12"	5/8-18
A-6687-100	0-10,000	12"	5/8-18
A-7006-100	0-15,000	12"	5/8-18
A-7007-100	0- 1,500	12"	1/2-20
A-7153-100	0- 3,000	12"	1/2-20
A-7003-100	0- 5,000	12"	1/2-20
A-7001-100	0-10,000	12"	1/2-20
A-7005-100	0-15,000	12"	1/2-20

Combination thermocouple - pressure models, and models with attached connectors also available. See Price List.

TRANSDUCER WIRING

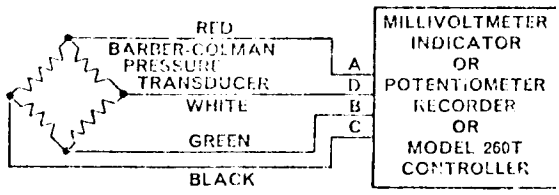

DIMENSIONS

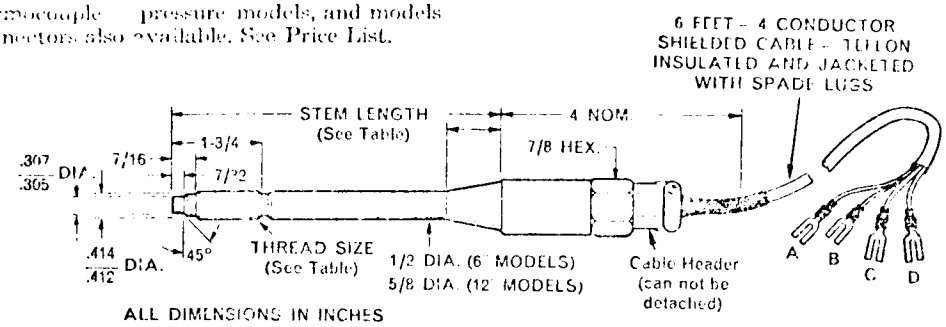

ALL DIMENSIONS IN INCHES

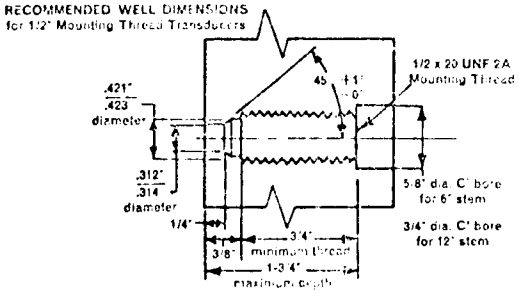

NOTE: All diameters shown must be concentric to within .002 T.I.R.

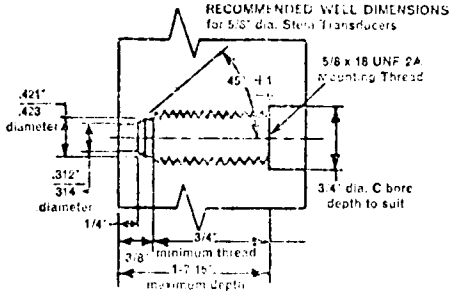

NOTE: All diameters shown must be concentric to within .002 T.I.R.

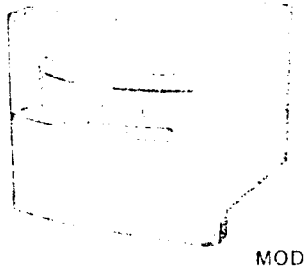

MODEL 287A

The Model 287A is a compact (6 7/8" wide x 6 1/4" high) indicator which incorporates a measuring system and d c power supply into a single integral unit. A solid state power supply chassis is used and contains two adjustments—zero and span.

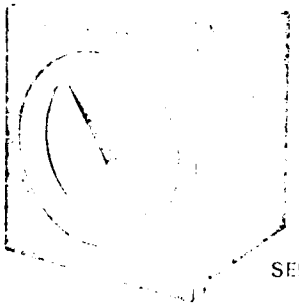

SERIES 2000

Round or strip chart recorders and indicators are used where it is desirable to record and indicate a single pressure such as an extruder die or optimum melt.

INSTRUMENTS FOR USE WITH BARBER-COLMAN PRESSURE TRANSDUCERS

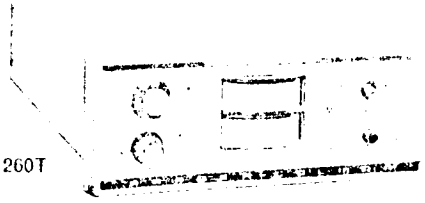

MODEL 260T

The Model 260T is a dual mode pressure controller with automatic reset. It is used for the control of commercial variable speed screw drives or eddy current clutches. Speed is automatically increased or decreased to maintain a selected pressure.

Please Note:

Pages 95-98, Modular Signal Conditioning, copyright 1970 by Electronics L.T.D., not microfilmed at request of author. Available for consultation at the City University of New York Library.

University Microfilms

INPUT MODULE

Set each of the input controls as follows:

CAL:	3	GAIN:	Full CCW
GAIN x 10:	20	BALANCE:	Any Position
COMP:	OFF	S:	Full CCW
MODE:	Z	Z:	Any position

METER MODULE

MODE:	EXC	CHANNEL SELECTOR:	1
RANGE:	10 V	POWER:	ON

BRIDGE INPUT OPERATION: The following sequence should be followed when checking out a new input installation, beginning with channel 1.

1. Select appropriate COMP setting. OFF.
2. Determine what value of excitation voltage is desired and adjust span control (S) until desired excitation voltage is read on the 10V meter scale. Nominally 4.00 Volts.
3. Place meter module MODE switch in the BAL position.
4. Select desired GAIN x 10 setting. Set so that all channels have the same output during flow runs.
5. Adjust zero (Z) control for zero meter reading. (This adjustment is factory set and should not require additional adjustment.)
6. Place MODE switch in the operate (OPR) position.
7. Adjust BALance control to obtain a meter reading of zero.
8. Place MODE switch in the zero (Z) position.
9. Select 1V meter RANGE.

10. Re-adjust zero (Z) control if necessary, to obtain a meter reading of zero.
11. Place MODE switch in the operate (OPR) position.
12. Re-adjust balance control for a meter reading of zero.
13. Return meter RANGE switch to 10V position.

FULL BRIDGE-FOUR ARM ACTIVE

7 WIRE W/SHIELD

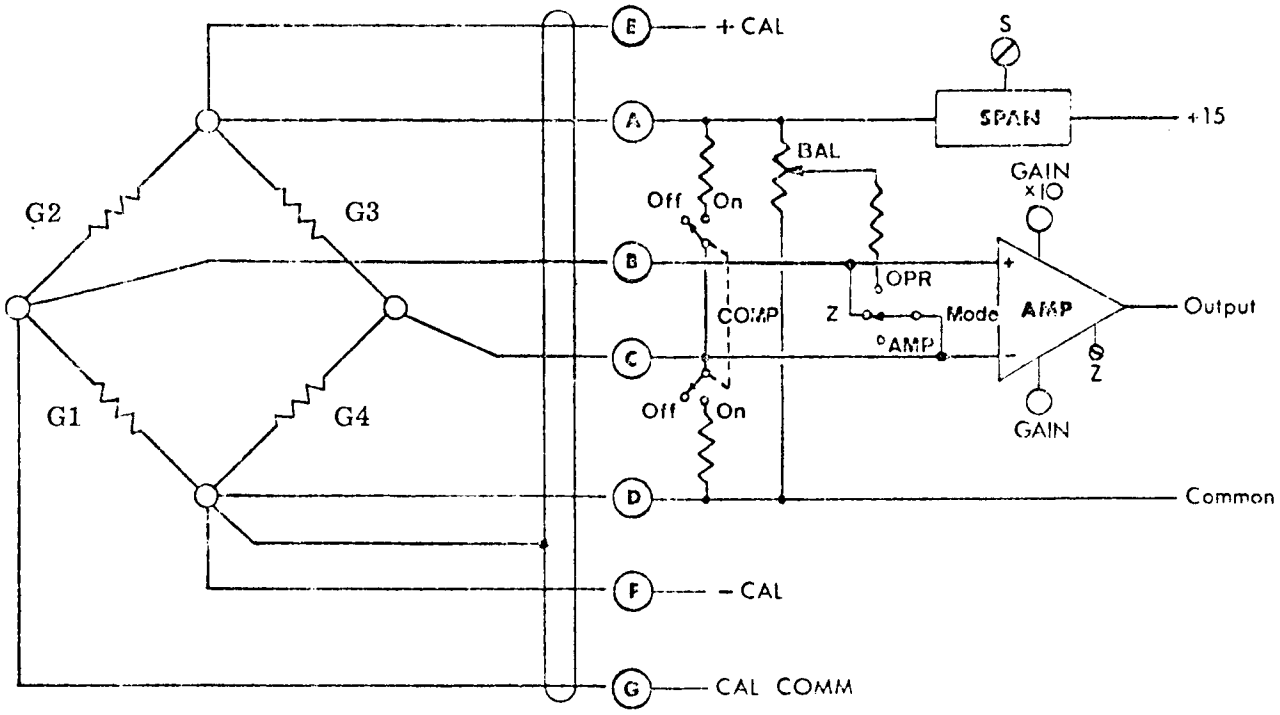

G1=G2=G3=G4=100 ohms or greater

CAL: Plus or minus

COMP: Off

MODE: OPR

TYPICAL APPLICATIONS INCLUDE:
Load cells, wire or foil strain gages, pressure transducers, torque transducers, accelerometers, angular position transducers, vibration transducers, force sensors, resistance thermometers, flow transducers, resistance photocells and others.

J1-D

INPUT

- + EXCITATION
- + AMP INPUT
- - AMP INPUT
- EXCITATION COMMON
- + CAL
- - CAL
- CAL COMMON

P1-P8

MS-3106A-16S-1P

MATING CONNECTOR, WIRE VIEW

J9

POWER

- +15VDC HOT
- +15VDC COMMON
- GROUND

P9

MS-3106A-14S-6S

MATING CONNECTOR, WIRE VIEW

J10

REMOTE

- + REMOTE MASTER CAL
- - REMOTE MASTER CAL
- COMMON
- SWITCHED OUTPUT
- OUTPUT COMMON
- SWITCHED EXCITATION
- EXCITATION COMMON

P10

MS-3106A-10SL-4S

MATING CONNECTOR, WIRE VIEW

J11
& J12

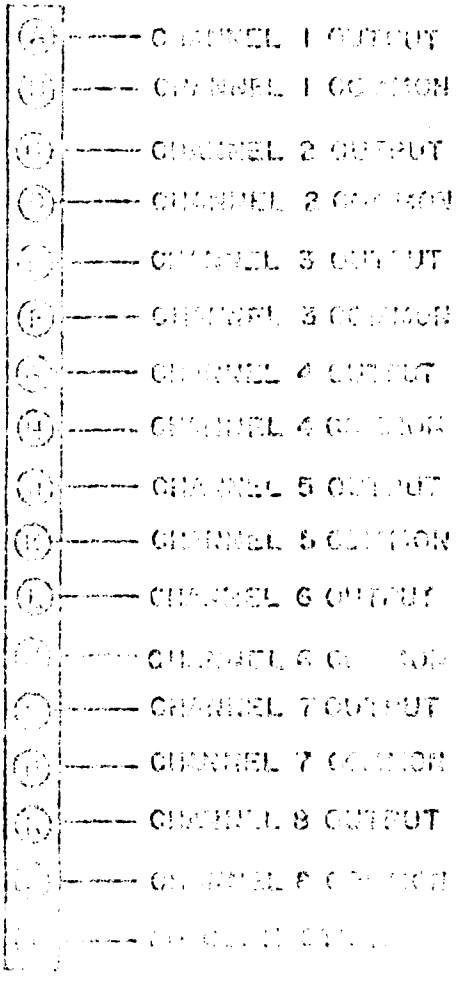

P11 & P12
MS-3106-20-27P

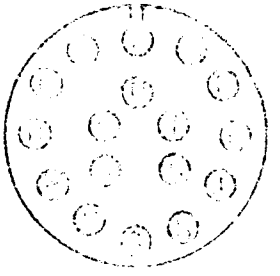

MATING CONNECTOR,
WIRING VIEW

OUTPUT
CONNECTORS SHOULD BE WIRED IN THE FOLLOWING MANNER:

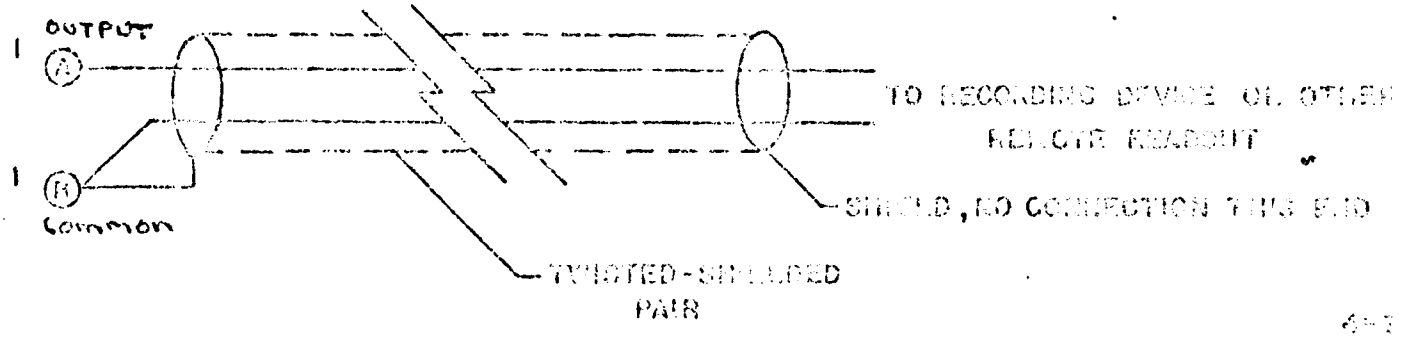

APPENDIX III-3, ELECTRONIC SWITCH

430

DATASWITCH, MODELS 430R-6, 430R-12, 430R-18, 430R-24

"Quick look" at phase, distortion, and amplitude becomes increasingly important in vibration tests as larger numbers of accelerometers are used. The viewing window of an optical oscillograph, with a VMS system controlling the galvos, does give some measure of "quick look". However, a brighter display, clearly separated traces, is superior. A bright distinct display permits instant recognition of gross phase shifts or large resonant buildups at any instrumented point of a complex structure. In "mode shape" testing such a display is very helpful to direct the trial and error changes in shaker location, phasing, and drive that are necessary for perfect excitation of every high order mode.

The DATASWITCH displays 6, 12, 18, or 24 channels of VMS data on any DC coupled single beam oscilloscope. Each channel is presented as a slow-motion spot, with vertical excursion proportional to signal amplitude, and no horizontal motion. With the "Phase Position" control at the SLIP-SYNC, all spots can be frozen at any point in their slow-motion cycle. Freezing at maximum amplitude gives a display of the mode shape, easy to observe and photograph. Figure 1 is a POLAROID time exposure of a 1 cps slow-motion display of 11 accelerometers on a cantilever beam with a very high "Q" first mode resonance. Figure 2 is a POLAROID picture of the same test under same conditions, with the spots frozen at 90° in the wave, showing the mode shape and the perfect in-phase condition existing. (For a pure mode all signals must be either in phase or 180° out of phase). In some cases these POLAROID pictures may supplant oscillograph recording. In any case when slow-motion is "On" VMS oscillograph recording can be simultaneous with DATASWITCH oscilloscope display.

Amplitude is easy to scale from the bar created by the moving spot on a long persistence scope, or by freezing at both extremes of spot motion. Phase differences between traces can be read from the "Phase Position" control on the SLIP-SYNC. For instance, freeze channel 1 at zero crossing and read the "Phase Position" dial. Rotate it to freeze channel 2 at zero crossing, and read it again. The difference between the two readings is the phase shift between channel 1 and channel 2

Distortion can be recognized by jerky movement or local reversals in the spot travel, with slow-motion "On".

The DATASWITCH is a free running (non-synchronized) electronic switch. A suffix to the model number (430R-6, 430R-12, 430R-18, or 430R-24) defines the number of input channels. It sequentially switches input channels to a single output at a 1,000 cps rate, each input being presented for about 1 millisecond, except the last channel. The last input is presented for about 4 milliseconds, allowing for its display and retrace of the oscilloscope. A sync command is available to trigger the oscilloscope sweep at the instant the DATASWITCH returns to channel 1. Sweep time controls of the oscilloscope should be set approximately at 6, 12, 18, or 24 milliseconds. Models 430R-6, 430R-12, 430R-18, can operate individually, or in cascade up to a total of 36 channels.

SPECIFICATIONS

Sampling Modes:	free-running - 1 kc rate synchronized -- 0 to 10 kc
Switching Time:	8 microseconds "Off" between channels.
Hold Time:	free running -- 1 millisecond on each channel but the last. 4 milliseconds on last channel, giving CRO time to retrace. synchronized -- period of sync commands, less 8 microsecond Switching Time.
Input impedance:	1000 ohms (needs low impedance source, and must be DC coupled)
Max. Input signal levels:	5 volts peak (note that VMS is typically set with 5 volts peak as full scale)
Noise:	less than 50 mv during Hold Time
Gain in signal channels:	Approx. 0.95
Source Impedance at output:	10 K ohms
Required "Sync In" signal for synchronized operation:	Positive pulses 15 v minimum, rise time 2 micro sec max. Source Impedance 500 ohms or less.
"Sync Out" signal to initiate sweep on CRO:	Plus 25 volts peak pulse from 10 K Impedance, simultaneous with switching to channel #1.

Model Numbers & Prices:			
	6 Channel	#430R-6	$ 410.00
	12 "	430R-12	$ 620.00
	18 "	430R-18	$ 830.00
	24 "	430R-24	$ 1040.00
Size and weight:	19" wide, 3-1/2" high, 10" deep; 13#		
Power Supply:	Requires +10 vdc, -15 vdc, +150 vdc. These voltages are all furnished to the 430R-N by the Model 412R POWER SUPPLY.		

WFC/JCH 10-15-63

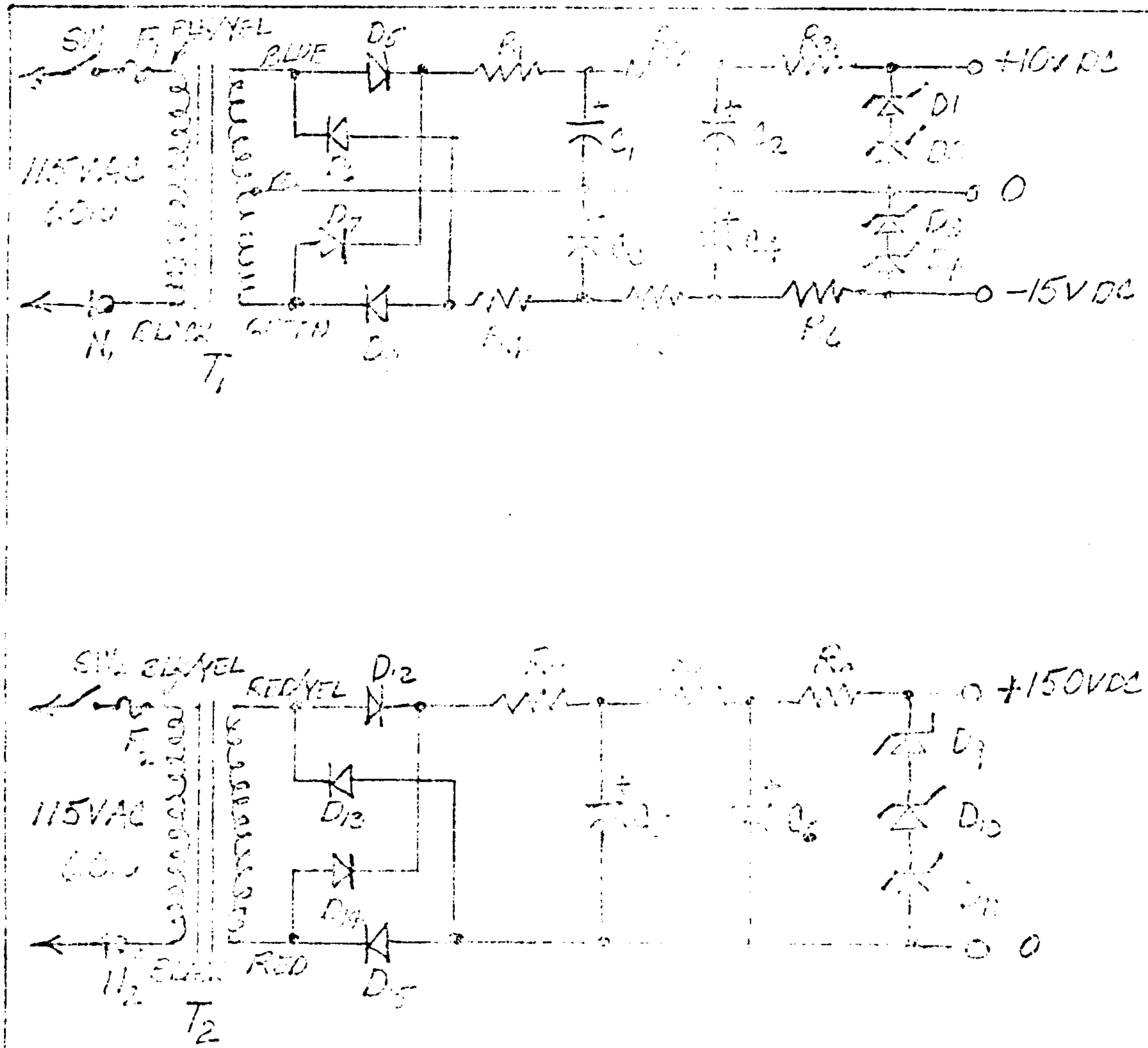

PARTS — DESCRIPTION

$R_1 = 2.7\Omega, 1W$ $C_1 = C_3 = 100\mu fd @ 50v$

$R_2 = 22\Omega$, [illegible] $C_2 = C_4 = 250\mu fd$ [illegible]

$R_3 =$ [illegible] $2W$ $D_1 =$ IR , [illegible]

$R_4 = 4.7\Omega, 1W$ $D_2 =$ [illegible]

$R_5 = 22\Omega$, [illegible] $D_3 =$ [illegible]

$R_6 =$ [illegible] $D_4 =$ [illegible]

$T_1 =$ TRIAD F-91X $N_1 =$ NE51

$SW_1 =$ [illegible]

$F_1 =$ $D_5 = D_6 = D_7 \ldots = GE, IN$[illegible]

$R_7 =$ [illegible] $5W$ *$D_9 \ldots = IR, IN$[illegible]

$R_8 = 500\Omega, 20W$ $D_{12} = D_{13} \ldots = D_{15} =$

$R_9 = 750\Omega, 20W$ $= GE, IN547$

$C_5 = 100\mu fd$, [illegible]

$C_6 = 250\mu fd$ [illegible]

$T_2 =$ TRIAD F-[illegible]

$SW_2 =$ SINGLE [illegible]

$F_2 =$

* [illegible]

APPENDIX IV. OPERATIONAL PROCEDURE

PROCEDURE

1. Fill the rheometer with the test fluid.
2. Seal the rheometer by tightening every other bolt, in sequence, to the same torque, incrementing the torque by 100 in-lbs until the final torque (450 in-lbs) is reached.
3.* Mount die on the rheometer using the correct adaptor.
4. Mount pressure transducers in the slit by screwing into place until they seat on the 45^{o} shoulder. Back off two full turns. Place most sensitive transducer at the exit and the sensitive at the entrance, etc. Some tubes have bleed holes which need a small lead shot and set screw to seal. Insert set screw lightly; do not seal yet.
5. Connect the transducers to the signal conditioner and amplifier. The amplifier leads have already been connected to the electronic switch, which is in turn connected to the oscilloscope.
6. See Appendix III-2 for the detailed procedure for setting up the amplifier. It takes at least one hour for the electronic system to stabilize. Once established, it will remain so for at least twelve hours.

---

* It is sometimes more convenient to reverse the order of steps 3 and 4.

cont.

7. Turn on the oscilloscope. Turn on the power supply for the Dataswitch; turn on the Dataswitch. Set the scope "vertical" sensitivity to 100 mv/cm, "trigger source" to external , "horizontal" display time to 2 msec/cm, both selector switches to AC, and the "sweep magnifier" to 1X. Camera setting is usually 1. sec exposure time at f5.6-8. These values for the camera depend on scope intensity, and are chosen as a matter of convenience so that the scope intensity is comfortable to view by eye, and so that the transparency of the outputs is of a consistent quality.
8. It is important not to move the "horizontal position" once the system is calibrated. Slight curvature of the scope tube causes a slightly non-linear trace. This causes errors in the measured outputs if the output is shifted after calibration.
9. Turn on the "main" switch for the pressurization and timing circuits.
10. Turn on the"timer", "auxilliary timer" and "solenoid main" switches (to the right); turn off "recorder", "vacuum" and "bleed" switches (to the left).
11. Connect pressure line to the rheometer and adjust pressurization circuit for the desired range (Appendix IIB).

cont.

12. Before opening the nitrogen supply be sure all regulator valves are closed; open nitrogen supply.
13. Set a low pressure on the regulator, sufficient to cause slow flow of the test fluid. The purpose of this stage is to purge air from the die and recess mounts.
14. Turn run switch on; when the material begins to flow from the die exit turn the switch off.
15. Once a pressure has been set on the regulator, the only way to run a subsequent test at a lower pressure is to completely bleed the supply and regulator line using the "bleed" switch on the control panel.
16. Cap the die with the end plate.
17. Increase the pressure on the regulator. Turn run switch on; material will begin to flow through the recess hole, forcing out entrapped air until the test fluid will begin to ooze out around the transducer stem (and bleed hole). As each mount is purged, tighten the transducers (hand tight is usually sufficient) and the bleed hole set screws.
18. Care must be taken not to over tighten the transducers (they will rupture internally), or the set screws (this will force the lead shot all the way into the bleed hole, plugging it, requiring that it be drilled clean after the runs).

cont.

19. Sometimes the transducers will not form an effective seal on the mounting shoulder; Teflon tape around the threads may be necessary. Be sure that the tape does not interfere with the bleeding process. Another effective method of sealing is to use O-rings placed over the transducer neck, against the shoulder. This method, though, creates a larger recess reservoir and sometimes increases the transducer response time.

20. After all the transducers have been tightened, a quick method for determining bleed effectiveness is to pressurize the system while at the same time watching the response of all the transducers on the scope. Slow response times will be readily noticed. Sometimes no response is noted. This is generally due to the transducer diaphragm touching a solid surface, jamming the pressure sensing mechanism. Back off the transducer slowly; if at some point there is a rapid change in the output, this was the cause.

21. The system is mechanically ready. The last adjustment necessary before actual measurement is the individual channel balance and gain. Letting the material flow slowly, adjust all the gains so that all the outputs are the same. Be sure that at the higher pressures the outputs will not be off scale. Further, the optical comparator becomes very inconvenient to use if the outputs cover more than 2.0 inch.

cont.

22. Recap the die. To static calibrate, select a variety of pressures spanning the entire range. Take a picture (Polaroid Type 146L Transparency) of the baseline, turn run switch on, allow for steady state response and take picture of the final outputs. The camera film holder can be adjusted vertically so that several pictures can be obtained on the same frame.

23. After a sufficient number of static test points have been measured, flow runs can be made. Uncap the die, weigh receiver, set pressure, zero timer, turn run switch on, allow for sufficient response time, turn run switch off, weigh receiver to determine the amount of fluid extruded during the automatically timed interval. Repeat the process at various run pressures.

24. When too much material has been emptied from the reservoir, the response time of the pressure regulation system becomes too large, and the reservoir must be refilled, either reusing the just collected material or a fresh charge. Rather than pouring the material through the small opening on top; it is generally more convenient to remove the top plate of the rheometer, fill and then reclose.

25. A tripod mounted Polaroid camera (model #910) with a close-up lens attachment (kit #540) is used for swell measurements. A 3000 ASA positive film (Polaroid type 47)

cont.

and a backlit diffusing screen coupled with the automatic exposure system of the camera were used to give sharp jet profiles (Figure IV-1) which were analyzed on the optical comparator. The tube outside diameter served as an internal measurement reference. Magnification was on the order of 1X.

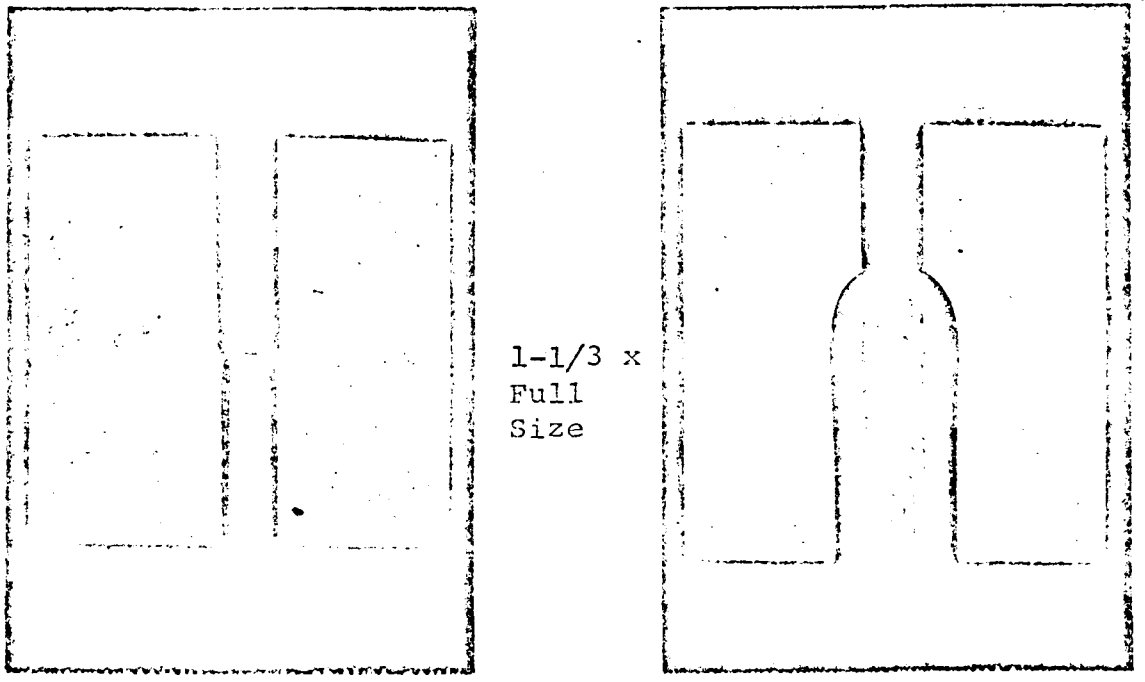

Silicone Fluid (30,000 cs)

Tube Diameter = 0.186"

L/D = 16

Q = 3060 sec^{-1}

Swell Ratio = 1.19

Polyisobutylene Solution

Tube Diameter = 0.186"

L/D = 16

Q = 2960 sec^{-1}

Swell Ratio = 2.76

Figure IV-1. Comparison of Swell under Similar Flow Conditions

APPENDIX V. BAGLEY ENTRANCE CORRECTION ANALYSIS

E. B. Bagley (40) was the first to undertake the study of losses in driving pressure in the entrance region. He postulated that the axial pressure dropped suddenly in the entrance region and then assumed a linear form (Figure V1).

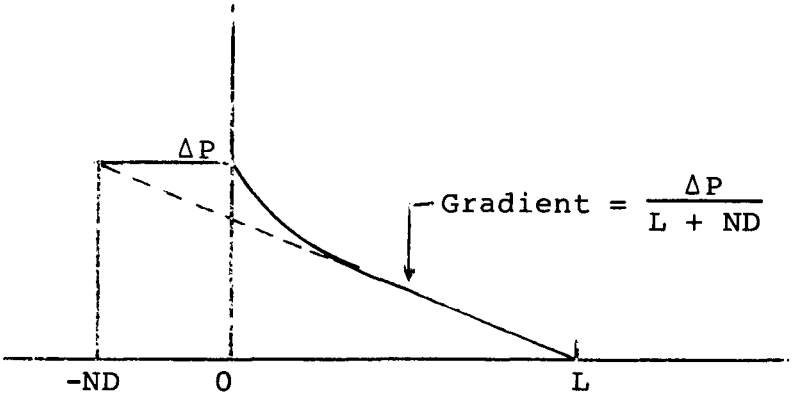

Figure V1. Schematic Bagley Entrance Correction Analysis

Bagley proposed the addition of a ficticious tube length, ND, to the actual length such that the driving pressure gradient becomes [ΔP/(L+ND)]. The true shear stress at the wall for the viscometric flow region can now be written as

$$\tau_w = \frac{D(\Delta P)}{4(L+ND)}$$

Rearranging and solving for (L/D) yields the equation of a straight line and a means of obtaining N.

$$\frac{L}{D} = \frac{\Delta P}{4\tau_w} - N$$

Since τ_w is a unique function of Q, $\varphi(Q)$, we can write

$$\frac{L}{D} = \frac{\Delta P}{4\varphi(Q)} - N$$

A series of ΔP verses Q flow curves for a series of L/D ratio tubes can be plotted with [L/D] verses [ΔP] for constant [Q]. The intercept of the resulting line with $\Delta P=0$ should yield N.

This procedure is illustrated by Figures V2 through V4.

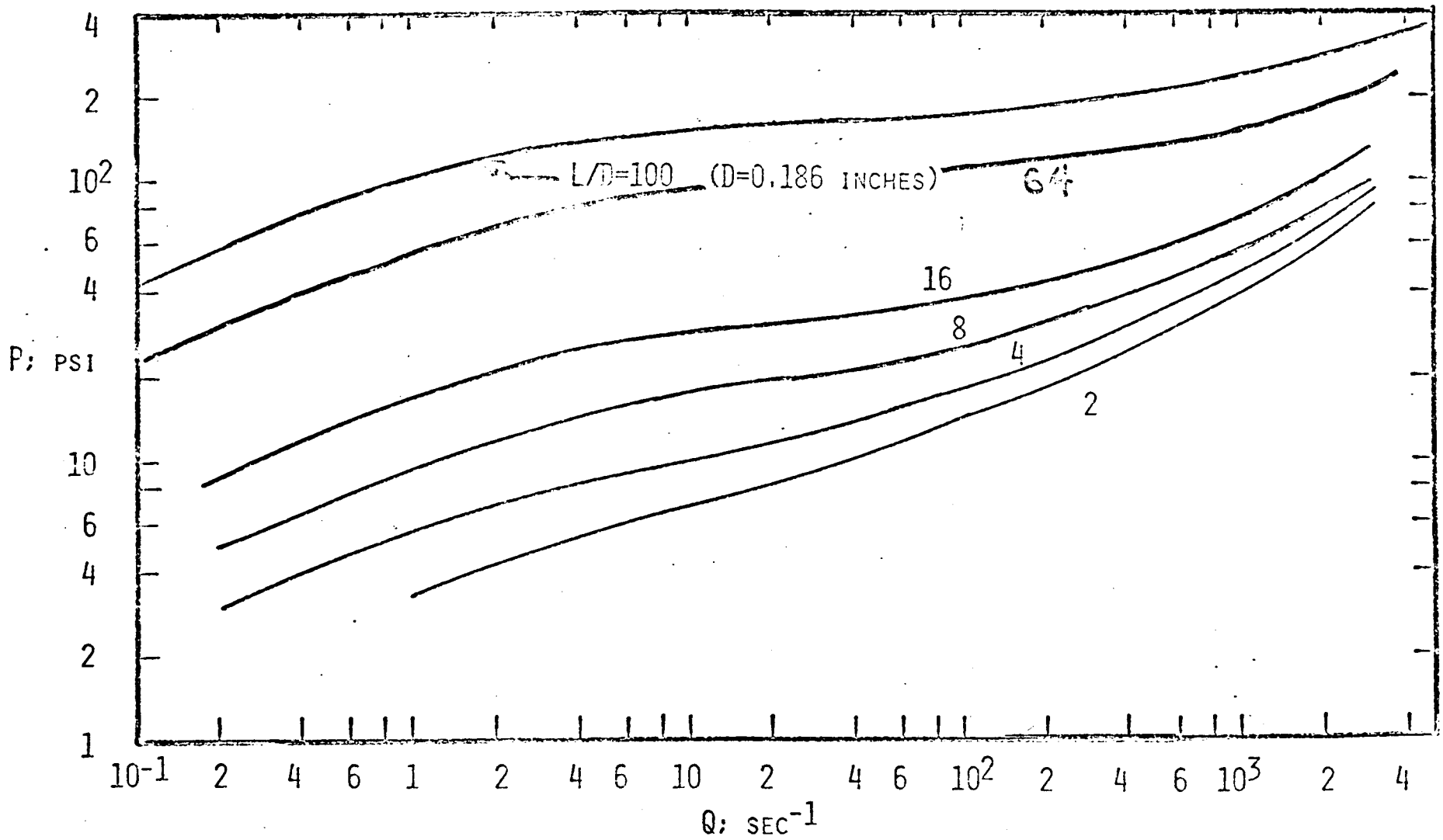

FIGURE V-2 PRESSURE DROP VS. APPARENT SHEAR RATE FOR TUBES OF DIFFERENT LENGTH TO DIAMETER RATIO - 16.5% PIB IN VARSOL #2

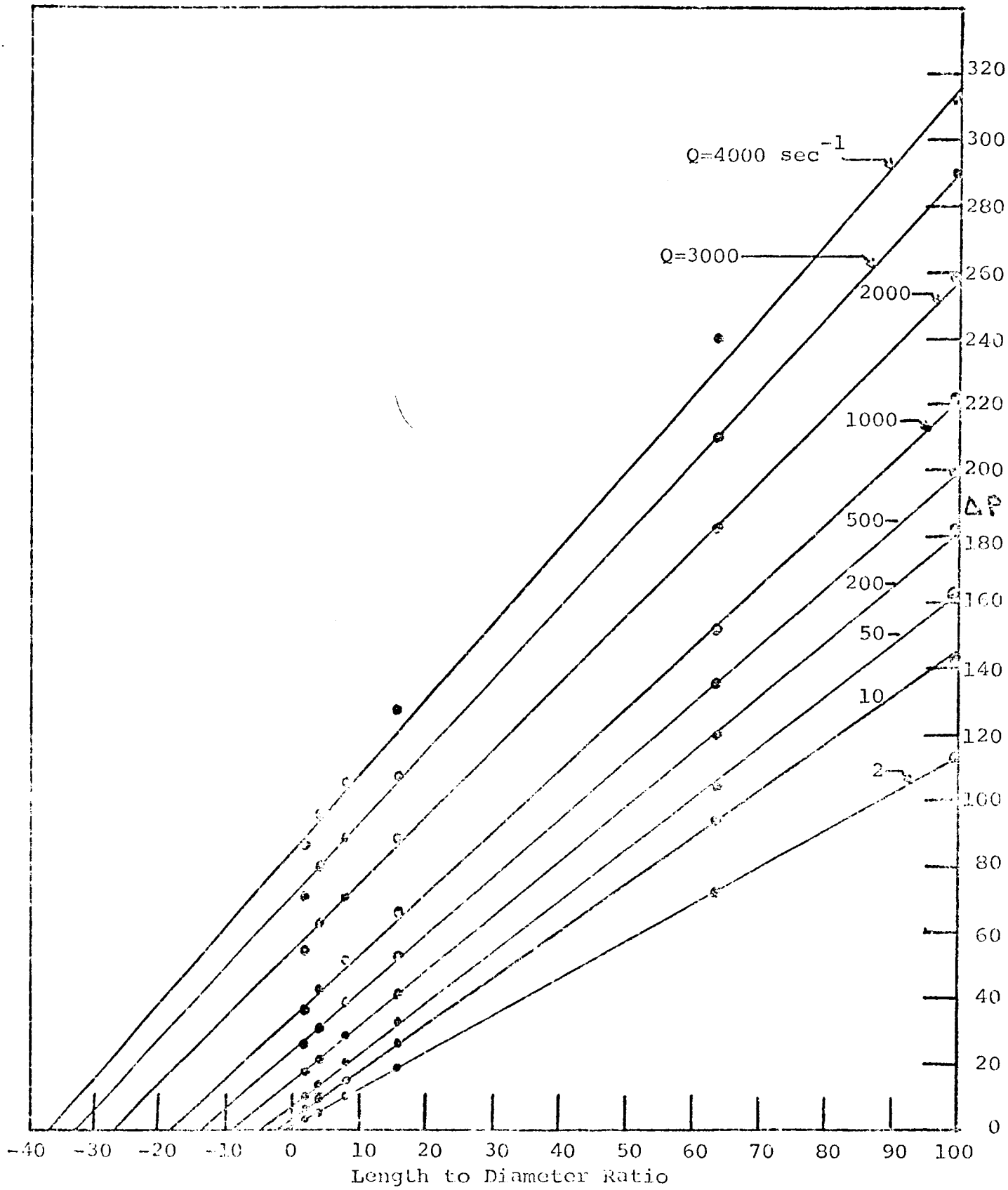

Figure V-3. Pressure Drop vs. Length to Diameter Ratio with Apparent Shear Rate as a Parameter - Polyisobutylene Solution

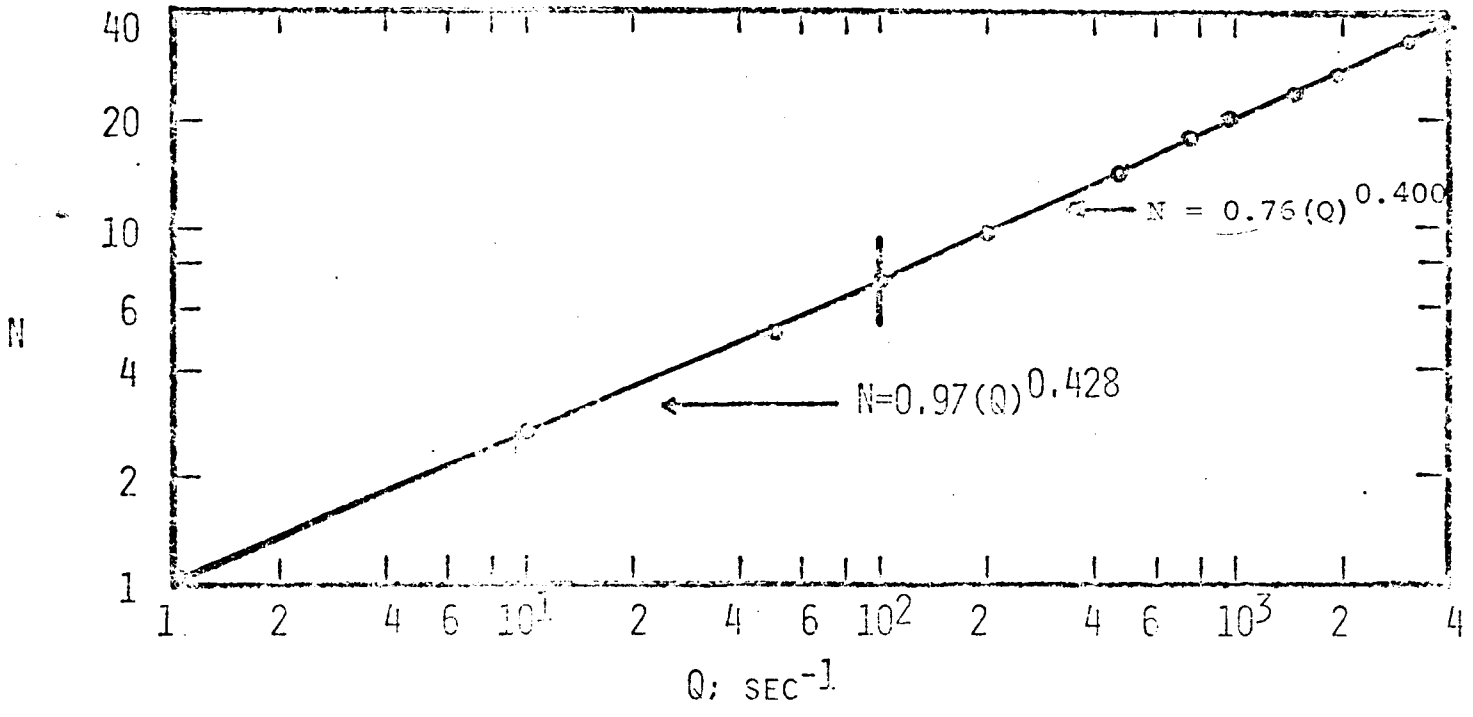

FIGURE V-4 BAGLEY ENTRANCE CORRECTION IN EQUIVALENT TUBE DIAMETERS VS. APPARENT SHEAR RATE - 16.5% PIB IN VARSOL #2

APPENDIX VI. PRESSURE ERROR DUE TO A PRESSURE GRADIENT ACROSS THE TRANSDUCER DIAPHRAGM

Given an arbitrary pressure profile, P(z), we seek to find the error introduced by the fact that the flush mounted pressure transducer records a pressure averaged over the diaphragm area, rather than the point value of the pressure at the geometric midpoint (as is the case with the recessed transducer).

Assuming that the transducer diaphragm responds symmetrically about the geometric center*, we can represent the flush mount transducer pressure value by the expression:

$$\bar{P} = \frac{\int_0^D P(z)\,dA}{\int_0^D dA} \qquad \text{(VI-1)}$$

Consequently, the error, ξ, would be evaluated as

$$\xi = \bar{P} - P_{D/2} \qquad \text{(VI-2)}$$

From the figure below, we see that the differential area, dA, is simply the chord length, h(z), integrated over the axial distance, D (diaphragm diameter).

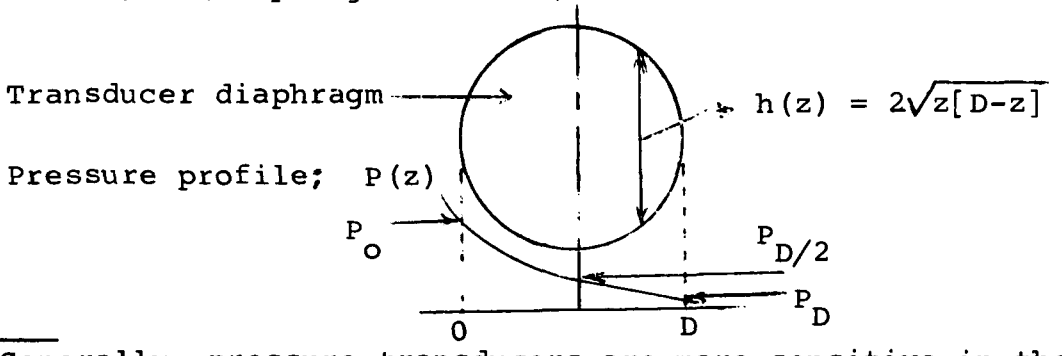

* Generally, pressure transducers are more sensitive in the center and therefore this assumption would cause the error values (ξ) calculated by this procedure to be larger than they really are.

Thus Equation VI-1 becomes

$$\bar{P} = \frac{\int_0^D [P(z)][2\sqrt{z[D-z]}]dz}{\int_0^D [2\sqrt{z[D-z]}]dz}$$

As a first approximation, the function P(z) may be obtained from the actual values recorded by the flush mounted pressure transducers. Although these recorded values are in error by the amount ξ, the perturbation to ξ introduced by this procedure is far smaller than ξ itself under our pressure profile conditions.

If the profile is linear (e.g., $P(z) = P_o - [P_o - P_D][z/D]$), as is almost all of the data for the viscoinelastic fluid, the evaluated ξ, as expected, is identically zero. On the other hand, if the profile is non-linear, a quadratic relation is gererally sufficient (e.g., $P(z) = P_o - [P_o - P_D][z/D] - C[zD - z^2]$ *), then ξ is calculated to be $\xi = CD^2/16$.

By this method, for the viscoelastic fluid, values for ξ were much smaller than the random scatter exhibited in the flush verses recess transducer value comparisons in Figure 12. As we previously mentioned, since the profiles for the inelastic silicone fluids were linear, the values of the calculated ξ are zero.

---

* The magnitude of the non-linearity in the pressure profile is directly related to the value for the constant C. The larger the value of C, the larger the non-linear effect.

APPENDIX VII. TABULATED DATA

Table 1A. Tabulated Data for Figure 3 - Silicone Fluid (30,000 cs)

Recess Hole Diameter; inches									
0.020		0.029		0.040		0.052		0.063	
$\tau_w \cdot 10^{-4}$ dynes/cm^2	Q sec^{-1}	$\tau_w \cdot 10^{-4}$ dynes/cm^2	Q sec^{-1}	$\tau_w \cdot 10^{-4}$ dynes/cm^2	Q sec^{-1}	$\tau_w \cdot 10^{-4}$ dynes/cm^2	Q sec^{-1}	$\tau_w \cdot 10^{-4}$ dynes/cm^2	Q sec^{-1}
.359	15.2	.428	17.8	.428	16.3	.376	12.9	.512	18.4
.513	20.4	.684	26.2	.854	31.6	1.01	40.0	1.20	43.0
1.64	63.0	1.52	58.5	2.72	102.	1.36	52.4	2.17	82.1
2.27	92.1	3.13	138.	5.70	271.	1.73	67.6	3.90	163.
5.23	244.	3.91	177.	7.95	414.	2.65	108.	8.55	466.
6.88	343.	4.34	198.	12.3	836.	3.26	137.	11.1	702.
9.37	529.	8.28	451.	14.3	1005	4.86	228.	12.7	854.
13.6	930.	10.3	646.	15.1	1080	6.45	323.	16.3	1270
15.3	1110	13.5	960.	17.5	1380	11.3	739.	17.3	1410
15.9	1170	16.2	1280						

cont.

Table 1B. Tabulated Data for Figure 3 - Silicone Fluid (100,000 cs)

Recess Hole Diameter; inches									
0.020		0.029		0.040		0.052		0.063	
$\tau_w \cdot 10^{-4}$ dynes/cm^2	Q sec^{-1}	$\tau_w \cdot 10^{-4}$ dynes/cm^2	Q sec^{-1}	$\tau_w \cdot 10^{-4}$ dynes/cm^2	Q sec^{-1}	$\tau_w \cdot 10^{-4}$ dynes/cm^2	Q sec^{-1}	$\tau_w \cdot 10^{-4}$ dynes/cm^2	Q sec^{-1}
.780	7.28	.427	4.11	.392	4.13	1.53	15.0	.534	5.22
1.78	14.6	.780	6.61	1.50	14.7	4.27	40.5	3.10	28.7
4.09	40.5	2.35	21.4	3.38	29.6	5.66	60.8	4.49	44.6
6.66	74.5	4.09	35.7	8.01	86.8	7.44	82.6	5.16	54.1
10.8	128.	9.72	108.	11.2	134.	11.2	147.	8.37	102.
13.9	188.	12.0	114.	14.5	190.	15.1	214.	12.2	162.
21.2	361.	17.1	234.	18.2	262.	19.1	309.	15.7	232.
26.2	525.	20.0	330.	22.4	396.	23.5	431.	19.9	321.
29.2	651.	25.0	463.	26.3	512.	26.2	528.	21.2	398.
		28.3	591.	27.3	557.	28.8	620.	24.0	476.
		33.6	810.	33.3	775.	31.3	739.	27.2	625.
						35.5	933.	36.1	1010

cont.

Table 1C. Tabulated Data for Figure 3 - Polyisobutylene Solution

The tabulated data given below is in terms of apparent shear stress, S. These values can be converted to the true shear stress at the wall, τ_w, via the expression

$$\tau_w = S\frac{(101.)}{(101.+N)}$$

where N, the Bagley entrance correction is given by the equations

$$N = 0.97(Q)^{0.400} \qquad 1 \leq Q \leq 100$$

$$N = 0.76(Q)^{0.472} \qquad 100 \leq Q \leq 4000$$

Recess Hole Diameter; inches									
0.020		0.029		0.040		0.052		0.063	
$S \cdot 10^{-4}$ dynes/cm^2	Q sec^{-1}	$S \cdot 10^{-4}$ dynes/cm^2	Q sec^{-1}	$S \cdot 10^{-4}$ dynes/cm^2	Q sec^{-1}	$S \cdot 10^{-4}$ dynes/cm^2	Q sec^{-1}	$S \cdot 10^{-4}$ dynes/cm^2	Q sec^{-1}
1.63	1.17	1.73	1.42	1.79	1.75	1.59	1.04	.834	.140
1.95	2.34	2.12	3.22	2.15	3.90	1.67	1.27	1.31	.530
2.65	31.0	2.41	10.9	2.50	16.2	2.07	2.95	2.10	3.21
2.70	40.2	2.50	14.8	2.70	37.3	2.31	6.24	2.22	5.40
2.94	101.	2.65	30.4	2.92	108.	2.58	21.0	2.39	11.0
3.21	296.	2.85	87.0	3.04	164.	2.77	52.2	2.53	18.4
3.29	361.	3.32	379.	3.11	202.	3.10	177.	2.66	35.6
3.39	537.	3.55	813.	3.38	544.	3.14	230.	2.79	61.8
3.47	602.	3.89	1260	3.49	653.	3.45	545.	2.91	86.1
3.90	1220	4.28	1690	3.58	800.	4.01	1400	3.20	248.
4.35	1830					4.37	1850	3.67	914.

Table 2. Tabulated Data for Figure 4 - Silicone Fluids (30,000 cs and 100,000 cs) and Polyisobutylene Solution

Silicone Fluids				Polyisobutylene Solution	
30,000 cs		100,000 cs			
δ	Q^{-1}_{sec}	δ	Q^{-1}_{sec}	δ	Q^{-1}_{sec}
1.000	21.7	1.019	19.0	1.150	5.10
1.025	42.4	1.037	39.1	1.131	7.00
1.012	62.1	1.056	74.8	1.178	29.9
1.045	81.1	1.071	101.	1.322	92.3
1.038	104.	1.076	130.	1.433	219.
1.019	129.	1.086	183.	1.735	440.
1.038	156.	1.088	195.	1.970	800.
1.077	211.	1.095	270.	2.129	1080
1.071	289.			2.436	1730
1.084	349.			2.698	2810
1.077	518.			2.940	4940
1.071	589.			3.440	10900
1.103	600.				
1.077	740.				
1.116	926.				
1.149	1350				
1.149	1540				
1.188	2180				
1.188	3060				
1.253	4340				

Table 3. Tabulated Pressure Transducer Data for Figures 8 and 9 - Silicone Fluid (100,000 cs)

Recess Hole Diam; inches	Q sec^{-1}	Pressure; psi								
		Position	0.000	0.500		2.000		3.500		5.000	
		Mount	---	Flush	Recess	Flush	Recess	Flush	Recess	Flush	Recess
0.020	14.6		50.	42.	41.	31.	31.	18.	18.	--	7.
	40.5		115.	108.	108.	79.	78.	47.	48.	18.	18.
	74.5		187.	175.	175.	126.	128.	78.	76.	32.	32.
	128.		302.	276.	277.	203.	203.	128.	125.	53.	52.
	188.		389.	355.	357.	262.	262.	164.	162.	65.	66.
	361.		596.	538.	538.	390.	387.	243.	243.	95.	96.
	525.		737.	674.	674.	--	--	305.	305.	124.	124.
	651.		819.	674.	674.	--	--	337.	337.	135.	135.
0.029	6.61		22.	15.	;5	10.	11.	7.	7.	--	--
	21.4		66.	58.	58.	41.	42.	26.	26.	--	10.
	35.7		115.	100.	98.	72.	72.	45.	45.	19.	19.
	108.		273.	245.	245.	180.	180.	112.	113.	45.	44.
	144.		338.	301.	302.	220.	220.	137.	137.	55.	55.
	330.		562.	515.	516.	373.	370.	228.	228.	86.	87.
	463.		701.	650.	650.	466.	465.	290.	290.	118.	118.
	591.		795.	730.	730.	530.	529.	329.	330.	134.	134.
	810.		945.	865.	865.	625.	625.	393.	393.	160.	160.
0.040	29.6		95.	83.	84.	59.	61.	37.	37.	15.	15.
	86.8		225.	207.	207.	152.	153.	95.	95.	37.	38.
	134.		315.	290.	288.	212.	212.	132.	131.	52.	52.
	190.		407.	373.	373.	273.	273.	170.	170.	68.	68.
	262.		510.	467.	465.	341.	340.	213.	212.	87.	86.
	396.		628.	578.	578.	423.	420.	261.	260.	100.	101.
	512.		740.	678.	678.	495.	492.	307.	307.	122.	122.
	557.		768.	705.	704.	513.	512.	322.	319.	128.	127.
	775.		935.	861.	861.	624.	624.	392.	392.	107.	107.

cont

Table 3 (cont.). Tabulated Pressure Transducer Data for Figures 8 and 9 - Silicone Fluid (100,000 cs)

Recess Hole Diam; inches	Q sec^{-1}	Pressure; psi									
		Position	0.000	0.500		2.000		3.500		5.000	
		Mount	---	Flush	Recess	Flush	Recess	Flush	Recess	Flush	Recess
0.052	15.0		43.	38.	38.	29.	29.	18.	18.	--	--
	40.5		120.	105.	105.	74.	75.	44.	45.	19.	18.
	82.6		209.	--	190.	138.	139.	85.	84.	33.	33.
	147.		315.	289.	290.	213.	212.	130.	130.	53.	53.
	214.		424.	383.	383.	284.	283.	173.	174.	73.	74.
	309.		536.	487.	488.	359.	360.	224.	223.	89.	88.
	431.		661.	608.	608.	437.	438.	277.	276.	110.	110.
	528.		737.	679.	679.	490.	489.	311.	310.	123.	124.
	620.		809.	742.	742.	539.	540.	342.	342.	142.	141.
	739.		879.	804.	804.	581.	583.	368.	368.	147.	147.
	933.		997.	913.	912.	659.	660.	417.	415.	166.	166.
0.063	5.22		15.	14.	14.	9.	9.	6.	6.	--	--
	28.7		85.	74.	75.	56.	56.	34.	33.	14.	14.
	54.1		145.	137.	138.	97.	97.	60.	59.	20.	19.
	102.		235.	215.	215.	158.	158.	99.	97.	39.	39.
	162.		342.	313.	313.	227.	227.	143.	142.	57.	58.
	232.		441.	400.	399.	292.	293.	182.	181.	71.	71.
	321.		558.	503.	503.	365.	365.	227.	227.	89.	89.
	398.		595.	545.	545.	394.	393.	241.	241.	91.	92.
	476.		673.	615.	615.	445.	445.	273.	275.	112.	112.
	625.		765.	702.	702.	508.	508.	312.	312.	122.	123.
	738.		842.	774.	775.	557.	556.	344.	345.	139.	139.
	1010		1015.	930.	930.	665.	665.	413.	414.	170.	169.

Table 4. Tabulated Pressure Transducer Data for Figures 10, 11, and 12 - Polyisobutylene Solution

Recess Hole Diam; inches	Q sec^{-1}	Pressure; psi										
		Position	0.000	0.500		2.000		3.500		5.000		P_L*
		Mount	---	Flush	Recess	Flush	Recess	Flush	Recess	Flush	Recess	
0.020	4.80		56.	53.3	53.5	39.0	39.0	25.0	24.8	--	12.5	1.00
	11.9		68.	63.0	62.0	45.3	44.8	29.5	28.5	--	15.0	1.50
	22.4		76.	69.0	68.0	51.0	50.0	32.8	32.8	--	--	1.75
	72.5		85.	78.0	77.0	58.0	56.5	37.0	36.8	--	19.0	2.50
	390.		91.	84.0	84.0	62.0	60.0	40.3	40.0	--	19.0	4.25
0.029	3.30		50.	47.5	48.0	32.5	32.5	21.0	22.0	--	--	--
	11.0		70.	65.5	65.5	48.5	48.5	31.5	31.0	14.0	14.5	2.00
	20.1		75.	66.5	67.0	50.0	49.5	33.0	32.0	14.0	14.0	2.25
	31.8		76.	68.5	69.0	51.0	51.0	34.0	33.0	14.0	14.0	2.00
	154.		85.	77.0	80.0	58.0	57.5	38.0	36.5	16.5	17.0	2.75
	392.		91.	83.0	83.0	63.0	62.0	40.5	37.5	19.0	19.5	5.50
	564.		93.	83.5	84.0	63.0	63.0	42.0	40.5	20.0	20.5	6.60
	1400		115.	96.0	96.0	71.0	71.5	48.0	48.0	24.0	24.5	8.50
0.040	6.16		63.	57.0	57.0	42.0	43.0	27.5	27.0	--	11.0	0.50
	13.0		78.	71.0	71.0	52.0	54.0	33.5	33.0	14.0	14.5	1.50
	30.1		83.	76.0	76.0	57.0	57.5	36.5	37.0	16.5	16.5	2.50
	85.0		89.	81.0	82.5	62.5	62.0	40.0	40.0	18.0	18.0	2.00
	166.		90.	83.0	83.0	64.5	63.5	40.5	40.0	18.0	18.0	2.25
	201.		97.	86.0	86.0	65.5	65.0	43.5	42.5	19.0	20.0	4.50
	256.		98.	88.0	89.0	67.0	66.0	44.0	46.0	20.0	21.0	5.50
	1310		118.	97.0	97.0	70.5	69.0	47.0	44.0	23.0	22.0	7.00

cont.

* P_L is obtained by the linear extrapolation of the profile to the slit exit.

Table 4 (cont.). Tabulated Pressure Transducer Data for Figures 10, 11, and 12 - Polyisobutylene Sol'n

Recess Hole Diam; inches	Q sec^{-1}	Pressure; psi										P_L^*
		Position	0.000	0.500		2.000		3.500		5.000		
		Mount	---	Flush	Recess	Flush	Recess	Flush	Recess	Flush	Recess	
0.052	1.54		39.	35.0	35.0	28.0	27.5	18.0	20.0	--	13.0	--
	4.04		53.	49.0	49.0	37.3	37.5	26.0	26.5	--	18.0	--
	18.4		74.	66.0	66.0	49.5	49.5	32.0	32.0	--	--	2.00
	80.0		82.	78.0	78.0	59.0	59.0	39.5	39.0	--	19.0	3.00
	312.		92.	84.0	84.0	64.5	63.4	46.0	46.5	--	19.0	5.00
	489.		100.	88.0	87.5	67.5	67.5	48.0	48.5	20.0	20.0	5.00
	798.		106.	90.0	90.0	71.0	70.5	49.0	48.5	22.0	21.5	7.50
	899.		109.	91.5	92.0	73.5	72.0	50.0	50.5	24.0	25.5	9.50
0.063	1.35		28.	26.0	26.0	20.5	20.5	14.0	14.5	--	8.0	--
	2.00		39.	36.0	35.0	29.0	29.5	19.0	20.0	--	11.5	--
	7.00		56.	54.0	52.5	41.0	42.0	27.5	27.5	14.0	14.0	1.00
	46.0		75.	67.5	68.0	52.0	52.0	35.0	35.0	17.5	17.5	2.50
	66.8		78.	70.0	70.0	53.5	54.5	36.5	36.5	17.5	18.0	3.00
	134.		87.	79.0	79.0	59.0	59.5	40.0	40.0	19.5	19.5	3.50
	157.		89.	81.5	81.5	61.5	61.5	41.5	41.0	19.5	20.0	4.00
	654.		101.	88.0	87.0	67.0	67.5	45.5	43.5	21.0	21.5	7.50
	1320		112.	90.0	91.0	67.5	67.5	46.0	45.0	22.0	22.0	8.50

* P_L is obtained by the linear extrapolation of the profile to the slit exit.

Table 5. Tabulated Pressure Transducer Data for Figure 13 - Silicone Fluid (30,000 cs)

Recess Hole Diam.; inches	Q sec^{-1}	Axial Position	Pressure; psi								
			0.00	2.25	3.75	5.25	7.25	11.00	16.00	22.00	29.00
0.020	150.		204.	187.	178.	166.	156.	129.	98.	63.	16.
	341.		403.	369.	348.	328.	300.	255.	195.	120.	31.
	707.		662.	606.	570.	540.	492.	417.	319.	195.	49.
	1170		930.	834.	787.	739.	679.	571.	433.	264.	68.
0.029	32.7		49.	52.	52.	45.	43.	36.	27.	16.	4.
	85.0		125.	117.	108.	101.	93.	80.	58.	35.	9.
	243.		295.	276.	261.	247.	229.	190.	146.	85.	22.
	450.		484.	457.	435.	411.	373.	318.	238.	141.	37.
	645.		626.	581.	547.	517.	476.	401.	302.	181.	48.
	883.		750.	694.	657.	621.	567.	484.	363.	217.	57.
	1175		953.	882.	831.	781.	717.	612.	461.	274.	73.
	1395		1013.	945.	874.	826.	750.	629.	483.	288.	77.
0.040	102.		159.	143.	138.	130.	122.	102.	78.	44.	12.
	333.		399.	358.	339.	319.	297.	249.	190.	113.	29.
	702.		658.	606.	574.	539.	495.	418.	316.	190.	51.
	1135		882.	799.	752.	709.	650.	550.	412.	250.	66.
0.052	67.5		101.	90.	81.	76.	69.	61.	46.	27.	7.
	227.		285.	250.	237.	221.	211.	175.	131.	79.	21.
	586.		564.	516.	495.	462.	425.	361.	272.	164.	43.
	1300		955.	864.	813.	766.	703.	603.	447.	272.	71.

cont.

Table 5 (cont.). Tabulated Pressure Data for Figure 13 - Silicone Fluid (30,000 cs)

Recess Hole Diam.; inches	Q sec^{-1}	Axial Position	Pressure; psi								
			0.00	2.25	3.75	5.25	7.25	11.00	16.00	22.00	29.00
0.063	36.2		58.	52.	50.	48.	41.	36.	25.	19.	5.
	68.4		127.	116.	105.	102.	93.	79.	59.	36.	10.
	162.		228.	219.	204.	195.	179.	152.	117.	69.	19.
	490.		538.	484.	457.	435.	401.	342.	258.	158.	43.
	603.		585.	532.	501.	480.	441.	369.	283.	172.	46.
	1270		950.	865.	--	770.	704.	594.	449.	374.	73.

Table 6. Tabulated Pressure Transducer Data for Figures 14 and 15 - Polyisobutylene Solution

Recess Hole Diam.; inches	Q sec^{-1}	Axial Position	Pressure; psi									P^*_{RL}
			0.00	2.25	3.75	5.25	7.25	11.00	16.00	22.00	29.00	31.50
0.020	23.2		149.	131.	121.	115.	106.	92.	69.	42.	11.	---
	40.1		158.	139.	134.	126.	116.	102.	76.	48.	15.	1.25
	170.		179.	155.	146.	139.	127.	109.	83.	52.	16.	3.00
	600.		203.	168.	158.	152.	140.	121.	93.	60.	21.	7.25
	1220		228.	178.	166.	160.	147.	126.	97.	63.	23.	8.75
	1840		255.	189.	175.	165.	153.	131.	100.	66.	24.	9.50
0.029	.104		46.	43.	41.	39.	34.	28.	21.	14.	4.	---
	.501		77.	73.	71.	64.	60.	50.	38.	24.	7.	---
	4.75		130.	121.	117.	109.	99.	86.	64.	40.	11.	---
	37.8		158.	144.	137.	130.	121.	103.	78.	47.	14.	1.00
	88.0		167.	152.	146.	137.	127.	109.	81.	48.	15.	1.50
	203.		180.	163.	152.	143.	132.	113.	85.	53.	16.	2.75
	380.		194.	169.	157.	149.	139.	119.	90.	56.	18.	4.50
	600.		200.	169.	160.	150.	139.	119.	90.	57.	18.	5.00
	813.		208.	177.	165.	155.	143.	124.	94.	56.	21.	6.50
	1260		228.	181.	168.	158.	146.	124.	96.	58.	21.	7.00
	1690		251.	193.	178.	164.	150.	129.	99.	64.	22.	8.25
0.040	37.0		158.	142.	135.	128.	120.	102.	76.	47.	14.	1.25
	108.		171.	156.	148.	145.	131.	112.	84.	53.	16.	2.50
	281.		187.	166.	156.	148.	136.	116.	91.	57.	18.	4.00
	653.		204.	170.	161.	154.	141.	122.	96.	60.	19.	6.50
	1780		252.	192.	177.	167.	151.	131.	102.	66.	25.	10.50

cont.

* Obtained by extrapolation of the profile to the tube exit

Table 6 (cont.). Tabulated Pressure Transducer Data for Figures 14 and 15 - Polyisobutylene Solution

Recess Hole Diam.; inches	Q sec^{-1}	Axial Position	Pressure; psi									P^*_{RL}
			0.00	2.25	3.75	5.25	7.25	11.00	16.00	22.00	29.00	31.50
0.052	.029		23.	22.	20.	19.	18.	14.	10.	7.	--	--
	62.1		163.	148.	140.	135.	124.	104.	81.	51.	15.	1.75
	168.		176.	161.	153.	144.	133.	114.	89.	54.	17.	3.50
	203.		180.	161.	153.	147.	136.	116.	89.	57.	18.	4.00
	506.		200.	171.	162.	156.	144.	125.	96.	62.	20.	5.50
	1210		228.	186.	172.	164.	152.	132.	102.	67.	23.	8.50
	1730		250.	190.	177.	168.	155.	136.	104.	68.	24.	10.00
0.063	.052		32.	30.	29.	26.	24.	19.	15.	9.	3.	--
	16.9		148.	137.	131.	125.	115.	100.	74.	46.	13.	1.00
	52.4		162.	152.	143.	135.	124.	106.	81.	49.	15.	2.00
	196.		179.	159.	150.	144.	132.	113.	88.	54.	16.	3.00
	405.		193.	170.	159.	150.	140.	120.	91.	57.	17.	4.50
	838.		211.	186.	170.	160.	149.	126.	97.	60.	20.	6.00
	1770		253.	194.	180.	166.	152.	129.	100.	63.	22.	7.50

* Obtained by extrapolation of the profile to the tube exit

Table 7. Tabulated Pressure Transducer Data - Silicone Fluid (30,000 cs)

Tube Diam.; inches	Q sec^{-1}	Pressure; psi								
		Axial Position	0.00	2.25	3.75	5.25	7.25	11.00	16.00	22.00	29.00
0.312	– SEE TABLE 5										
		Axial Position	0.00	2.25	3.75	5.25	7.00	9.50	13.00	17.00	22.00
0.242	134.		187.	179.	165.	154.	139.	120.	93.	58.	19.
	284.		355.	322.	300.	279.	253.	218.	167.	106.	35.
	468.		515.	461.	429.	394.	361.	309.	237.	151.	50.
	687.		657.	594.	555.	512.	470.	399.	306.	196.	65.
	1415		1055.	958.	880.	813.	736.	628.	481.	306.	102.
		Axial Position	0.00	2.25	3.75	5.25	6.75	8.50	10.50	13.50	16.50
0.186	121.		164.	143.	130.	115.	102.	89.	71.	42.	17.
	219.		271.	234.	211.	188.	170.	140.	115.	71.	31.
	406.		457.	390.	351.	316.	282.	241.	192.	121.	50.
	823.		740.	651.	585.	523.	461.	396.	315.	199.	83.
	1435		1055.	939.	846.	744.	657.	556.	445.	279.	116.

Table 8. Tabulated Pressure Transducer Data for Figures 16 and 18 - Polyisobutylene Solution

Tube Diam.; inches	Q sec^{-1}	Axial Position	Pressure; psi									P_{RL}
			0.00	2.25	3.75	5.25	7.25	11.00	16.00	22.00	29.00	31.50
0.312*	16.7		151.	138.0	133.5	122.0	113.0	98.0	75.5	45.5	12.5	1.00
	61.1		170.	158.5	148.0	139.0	129.0	110.0	82.0	51.0	15.5	2.25
	188.		183.	163.0	156.0	144.0	134.0	114.0	87.5	53.0	16.0	3.25
	530.		208.	178.0	166.0	157.0	146.0	125.0	96.0	60.0	19.5	5.25
	1390		253.	195.0	183.0	169.5	154.5	132.5	102.0	65.5	22.0	7.50
		Axial Position	0.00	2.25	3.75	5.25	7.00	9.50	13.00	17.00	22.00	24.50
0.242	.657		79.	71.5	67.5	61.5	55.5	48.0	37.5	23.0	8.5	--
	16.4		151.	140.0	132.0	122.0	112.0	97.0	73.0	49.5	17.0	1.00
	138.		181.	166.0	155.5	145.5	133.0	115.0	88.0	59.0	20.0	2.75
	380.		198.	172.0	160.0	151.0	140.0	119.5	92.5	62.0	22.0	5.00
	669.		210.	182.5	171.0	157.0	146.5	125.0	97.0	63.0	24.0	5.50
	1615		248.	199.0	182.0	168.0	154.0	133.0	105.0	68.0	27.5	7.50
	2345		273.	210.0	191.0	173.0	159.0	137.0	108.0	69.0	29.0	8.50
	2750		296.	214.0	193.0	176.0	160.0	138.0	109.5	72.5	30.5	9.00

cont.

* See Table 6 for additional runs with the 0.312 inch diameter tube

Table 8 (cont.). Tabulated Pressure Transducer Data for Figures 16 and 18 - Polyisobutylene Solution

Tube Diam.; inches	Q sec^{-1}	Axial Position	Pressure; psi									P** RL
			0.00	2.25	3.75	5.25	6.75	8.50	10.50	13.50	16.50	18.50
0.186	.230		56.	50.0	44.0	40.0	36.0	31.0	25.0	15.0	5.0	---
	1.00		91.	78.5	73.0	66.0	59.0	51.0	41.0	25.0	9.5	---
	4.06		129.	117.0	106.5	96.5	86.0	74.0	58.0	37.5	15.0	---
	29.0		165.	147.0	131.0	119.0	107.0	91.0	72.5	45.5	18.0	1.00
	97.6		172.	156.0	142.0	128.5	115.0	97.5	79.5	50.5	20.5	2.50
	240.		185.	167.0	150.0	135.0	122.0	103.0	85.0	55.0	22.5	4.00
	278.		188.	168.5	150.5	136.5	123.5	102.0	85.0	54.0	22.5	4.00
	517.		198.	172.0	156.0	140.0	127.0	109.0	89.0	56.5	24.5	5.75
	680.		209.	176.0	162.0	146.5	130.5	114.5	92.0	60.0	27.0	6.25
	983.		219.	181.0	165.0	151.0	133.0	115.0	95.0	59.5	27.5	7.00
	1465		240.	188.0	173.0	148.5*	139.0	118.5	98.5	64.0	31.0	8.50
	2180		258.	188.0*	178.5	156.5	138.0	124.5	101.5	63.5	30.0	9.50
	2610		271.	201.5	181.0	159.0	142.5	123.0	103.0	64.0	32.0	9.00
	3380		291.	215.0	188.0	165.5	146.0	127.0	104.0	69.0	33.5	9.75
	4045		310.	229.0	192.0	170.0	151.0	132.0	106.0	69.0	34.0	10.50

* These values are noticeably in error
** Obtained by extrapolation of the profile to the tube exit

Table 9. Tabulated Swell Data for Figure 17 - Polyisobutylene Solution

Length to Diameter Ratio									
2.00		4.00		8.00		16.00		64.00	
Q sec^{-1}	δ	Q sec^{-1}	δ	Q sec^{-1}	δ	Q sec^{-1}	δ	Q sec^{-1}	δ
6.50	1.20	12.2	1.22	1.96	1.23	5.62	1.14	5.10	1.15
41.4	1.45	13.8	1.14	15.8	1.24	78.0	1.30	7.00	1.13
175.	1.84	43.3	1.32	72.0	1.38	193.	1.49	30.1	1.18
299.	1.90	70.1	1.45	125.	1.59	203.	1.52	92.3	1.32
572.	2.34	152.	1.71	258.	1.81	374.	1.77	219.	1.43
1135	2.63	340.	1.94	500.	1.94	727.	2.15	440.	1.74
1205	2.63	355.	2.03	695.	2.23	1460	2.41	800.	1.97
1615	2.79	503.	2.22	908.	2.29	1750	2.57	1080	2.13
1670	2.79	661.	2.38	1070	2.29	2960	2.76	1725	2.44
2290	2.92	850.	2.41	1275	2.44			2810	2.69
		1205	2.57	1620	2.60			4940	2.94
		2670	2.86	2140	2.66			10900	3.44
		3885	3.12	2500	2.73				

Table 10. Tabulated Pressure Drop Data for the Bagley Entrance Correction Analysis for Figures 19,AV-2,AV-3 and AV-4 - Polyisobutylene Solution

Length to Diameter Ratio											
2		4		8		16		64		100	
ΔP psi	Q sec^{-1}	ΔP psi	Q sec^{-1}	ΔP psi	Q sec^{-1}	ΔP psi	Q sec^{-1}	ΔP psi	Q sec^{-1}	ΔP psi	Q sec^{-1}
5.5	6.55	3.0	.211	5.0	.240	11.0	.415	31.0	.193	47.0	.150
10.5	35.1	5.0	.702	10.5	1.81	17.5	1.25	50.0	.755	55.0	.232
16.0	176.	6.8	2.41	16.5	17.6	22.5	3.02	67.0	1.52	61.0	.304
20.5	298.	8.3	5.67	21.5	56.5	25.0	5.81	81.0	2.97	68.0	.398
21.0	327.	10.0	12.2	22.5	70.2	25.5	6.88	90.0	7.12	76.0	.538
31.5	842.	10.0	13.8	26.0	126.	28.0	12.8	99.0	30.2	80.0	.679
39.0	1210	15.0	43.3	29.5	255.	32.0	38.0	111.0	101.	92.0	1.04
47.0	1660	15.5	70.2	31.0	252.	35.5	71.2	119.0	199.	98.0	1.19
60.0	2280	20.0	150.	37.5	503.	42.0	192.	130.0	373.	105.0	1.61
75.0	3390	26.0	342.	38.5	480.	42.0	203.	139.0	598.	122.0	2.57
85.0	3860	26.0	351.	43.0	679.	47.0	356.	144.0	723.	133.0	4.21
		30.0	497.	51.0	889.	49.0	380.	153.0	1010	141.0	7.02
		35.0	749.	55.0	1100	60.0	735.	162.0	1275	148.0	13.0
		45.0	1190	57.0	1250	70.0	1125	186.0	1950	153.0	21.5
		55.0	1520	65.0	1580	90.0	2065	214.0	3200	158.0	27.7
		65.0	2200	75.0	2160	109.0	3010			160.0	40.8
		74.0	2620	85.0	2460					166.0	58.6
		87.0	3600	99.0	3510					172.0	96.2
										181.0	178.
										185.0	252.
										190.0	271.
										195.0	370.
										200.0	516.
										210.0	714.
										222.0	975.
										247.0	1430
										263.0	2110
										278.0	2550
										297.0	3220
										310.0	3980

Table 11. Tabulated Pressure Drop Data for the Bagley Entrance Correction Analysis for Figures 20, AV-2, AV-3 and AV-4 - Polyisobutylene Solution

Q	Length to Diameter Ratio						N
sec^{-1}	2	4	8	16	64	100	
1.00	3.10	3.70	8.70	15.4	59.0	92.0	1.0
2.00	3.85	6.40	10.8	19.6	73.0	113.	1.3
5.00	5.10	8.00	13.4	24.5	87.0	135.	2.0
10.0	6.40	9.50	15.2	27.3	94.0	143.	2.5
20.0	8.00	11.2	17.2	30.0	98.0	151.	3.5
50.0	10.5	14.3	20.8	33.5	104.	163.	5.0
100.	13.5	17.5	24.0	37.0	111.	172.	6.5
200.	17.5	22.0	28.5	42.0	120.	183.	9.0
500.	25.8	30.5	39.5	53.0	136.	200.	13.5
800.	32.0	38.0	47.0	61.0	146.	213.	17.0
1000	36.0	43.0	52.0	67.0	152.	223.	19.0
2000	54.0	63.0	71.0	89.0	182.	259.	27.0
3000	71.0	80.0	89.0	108.	210.	290.	32.5
4000	87.0	96.0	106.	128.	240.	313.	37.0

Table 12. Tabulated Data for the Three Material Functions of Figure 21 - Polyisobutylene Solution

Q sec^{-1}	$\tau_w \cdot 10^{-4}$ $dynes/cm^2$	$P_{RL} \cdot 10^{-4}$ $dynes/cm^2$	$\sigma_1 \cdot 10^{-4}$ $dynes/cm^2$	$\sigma_2 \cdot 10^{-4}$ $dynes/cm^2$	Excess Elastic Stress $\cdot 10^{-4}$ $dynes/cm^2$
1.00	1.69	----	----	----	----
2.00	2.13	----	----	----	----
5.00	2.40	2.76	2.76	17.3	----
10.0	2.52	4.83	4.83	34.8	----
20.0	2.64	7.11	7.11	79.7	----
50.0	2.76	12.08	12.08	163.7	----
100.	2.83	17.25	17.58	272.8	----
175.	2.87	----	----	281.3	----
200.	2.91	23.81	24.15	270.1	3.6
500.	3.07	35.88	37.11	177.1	25.5
800.	3.20	43.13	45.39	159.0	68.3
1000	3.29	46.58	49.56	152.7	102.1
2000	3.58	58.65	67.84	141.8	262.2
3000	3.76	65.55	84.21	138.4	400.2
4000	3.95	72.45	104.18	130.0	531.3

* Values of P_{RL} were obtained from Figure 18

Table 13. Tabulated Recoverable Shear Strain Values of Figure 22 - Polyisobutylene Solution

Q sec^{-1}	δ	S_R (Eq. 29)	σ_1/τ_w
5.00	1.10	2.40	1.15
10.0	1.13	3.00	1.92
20.0	1.15	3.30	2.69
50.0	1.25	4.85	4.38
100.	1.32	6.00	6.21
200.	1.44	8.10	8.30
500.	1.78	15.8	12.1
800.	1.93	20.4	14.2
1000	2.13	27.7	15.1
2000	2.50	44.3	19.0
3000	2.72	57.0	22.4
4000	2.88	68.0	26.4

Table 14. Recoverable Shear Strain at the Die Entrance Values for Figure 23 - Polyisobutylene Solution

Q sec^{-1}	$\delta\|_{z=0}$	Tanner	Bagley et al.	S_R(Eq.32)	S_R(Eq.33)
10.0	1.35	6.40	5.65	10.2	1.92
20.0	1.42	8.90	6.41	13.4	2.69
50.0	1.58	11.0	8.08	20.0	4.38
100.	1.72	14.3	9.67	26.4	6.51
200.	1.96	21.0	12.9	36.8	9.54
500.	2.35	37.5	18.7	56.0	20.4
800.	2.55	48.5	22.1	70.0	35.5
1000	2.70	57.0	24.7	77.4	46.2
2000	3.00	77.0	30.5	108.	92.2
3000	3.20	93.0	34.7	130.	129.
4000	3.37	108.	38.6	150.	161.

Table 15. Tabulated Material Relaxation Time Values of Figure 24 - Polyisobutylene Solution

Q sec^{-1}	Material Relaxation Times; sec	
	Excess Elastic Stress Relaxation	Swell Ratio Decay
10.0	----	4.70
20.0	----	3.00
50.0	----	1.26
100.	----	.677
200.	----	.423
500.	----	.145
515.	.0966	----
680.	.0780	----
983.	.0420	----
1000	----	.0571
1465	.0287	----
2000	----	.0288
2180	.0198	----
2610	.0193	----
3000	----	.0196
3380	.0202	----
4000	----	.0136
4045	.0159	----

BIBLIOGRAPHY

1. Bagley, E.B. and Schreiber, H. P., Trans. Soc. Rheol. 5, 355 (1961).
2. Bagley, E.B. and Birks, A.M., J. Appl. Phys. 31, 556 (1960).
3. Ballenger, T.F. and White, J.L., Trans. Soc. Rheol. 15(2), 195 (1971).
4. Gaskins, F.H. and Philippoff, W., Trans. Soc. Rheol 3, 181 (1959).
5. Schlichting, H., "Boundary Layer Theory", pp. 400-429, McGraw-Hill (1955).
6. Dodge, D.W., Ph.D. Theses, University of Delaware, 1957.
7. Metzner, A.B. and Reed, J.C., A.I.Ch.E. J. 1, 434 (1955).
8. Philippoff, W. and Gaskins, F.H., Trans. Soc. Rheol 2, 263 (1958).
9. Boger, D.V. and Ramamurthy, A.V., A.I.Ch.E. J. 16, 6, 1089 (1970).
10. Kowalski, R.C., Proc. 4th Intl. Congr. Rheol. (1963).
11. Han. D.H. and Charles, M., A.I.Ch.E. J. 16, 3, 499 (1970)
12. Han. D.H., Charles, M., and Philippoff, W., Trans, Soc. Rheol., 14, 3, 393 (1970).
13. Middleman, S., "The Flow of High Polymers", Interscience, p. 46 (1968).
14. Sakiadis, B.C., A.I.Ch.E. J. 8, 317 (1962).
15. Sakiadis, B.C., A.I.Ch.E. J. 9, 706 (1962).

cont.

16. Han, C.D., Charles, M., Philippoff, W., Trans. Soc. Rheol. 13, 4, 455 (1969).

17. Eswaren, R., Janeschitz-Kriegl, H., and Schiff, J., Rheol. Acta, 3, 83 (1963).

18. Noll, W., Arch. Rat. Mech. Anal. 2, 197 (1956).

19. Coleman, B.D. and Noll, W., Arch. Rat. Mech. Anal. 3, 239 (1959).

20. Coleman, B.D. and Noll, W., J. Appl. Phys. 30, 1508 (1959).

21. Coleman, B.D., Markovitz, H., and Noll, W., "Viscometric Flows of Non-Newtonian Fluids", Springer-Verlag (1964).

22. Schertzer, C.R. and Metzner, A.B., Proc. 4th Intl. Congr. Rheol., p. 603 (1963).

23. Schertzer, C.R., Ph.D. Thesis, University of Delaware, June 1965.

24. Ginn, R.F. and Metzner, A.B., Proc. Intl. Congr. Rheol. (1963).

25. Han, C.D. and Charles, M., Trans. Soc. Rheol. 14, 3, 409 (1970).

26. Broadbent, J.M., Kaye, A., Lodge, A.S., and Vale, D.G., Nature, 217, 55 (1968).

27. Lipson, S.M. and Lodge, A.S., Rheol. Acta, 7, 364 (1968).

28. Kaye, A., Lodge, A.S., and Vale, D.G., ibid., p. 368.

29. Tanner, R.I. and Pipkin, A.C., Trans. Soc. Rheol., 13, 471 (1969).

cont.

30. Metzner, A.B., Houghton, W.T., Sailor, R.A., and White, J.L., Trans. Soc. Rheol. 5, 133 (1961).

31. Tanner, R.I., Trans. Soc. Rheol., 14, 4, 483 (1970).

32. Graessley, W.W., Glasscock, S.D., and Crawley, R.L., ibid. p. 519.

33. Bagley, E.B. and Duffey, H.J., ibid., p. 545.

34. Tanner, R.I., "A Theory of Die-Swell" (to appear in J. Poly. Sci. (A2)).

35. Bagley, E.B., J. Appl. Pol. Sci. 7, 1661 (1963).

36. White. J.L., A.I.Ch.E. J. 9, 559 (1962).

37. Skelland, A.H.P., "Non-Newtonian Flow and Heat Transfer", pp. 53-59, J. Wiley & Sons (1967).

38. Schertzer. C.R., Master Thesis, University of Delaware, Newark, Delaware, 1964.

39. Metzner, A.B., Houghton, W.T., Sailor, R.A., and White, J.L., Trans. Soc. Rheol. 5, 133 (1961).

40. Bagley, E.B., J. Appl. Phys., 28, 624 (1957).

41. Skelland, A.H.P., "Non-Newtonian Flow and Heat Transfer", pp. 35-36, 73-75, J. Wiley & Sons (1967).

42. Powell, R., and Middleman, S., Trans. Soc. Rheol., 13, 1, 111 (1969).

43. Powell, R. and Middleman, S., Trans. Soc. Rheol., 13, 2, 241 (1969).

cont.

44. Brodnyan, J.G., Gaskins, F.H., and Philippoff, W., Trans. Soc. Rheol., 1, 109 (1967).

45. Lund, J.K., and Pohl, H.A., Can. J. Ch. Eng., 231, (10/65).

46. Pearson. J.R.A., "Mechanical Properties of Polymer Melts", p. 37, Pergamon Press (1966).

47. Williams, D.J., "Polymer Science and Engineering", pp. 343-345, Prentice Hall (1971).

VITA

David Blum is a lecturer in the Chemical Engineering Department of The City College of New York. He received his B.Ch.E. and M.Ch.E. degrees from The City College. He has worked for the Shell Chemical and Shell Oil Companies on the research and development of improved polymer processing methods and on the application of analog and digital computers to process engineering calculations. Upon graduation, he will be employed by Chem Systems, Inc., working at their laboratory in Hackensack, New Jersey